Immune and peripheral endogenous opioid mechanisms of electroacupuncture analgesia

Immunologische und periphere endogene Opioidmechanismen bei Analgesie durch Elektroakupunktur

Doctoral thesis for a doctoral degree
at the Graduate School of Life Sciences,
Julius-Maximilians-Universität Würzburg,

Section …**Neuroscience**……..

Submitted by

……Ying Wang…….

from

……Xi'an, China……

Würzburg**……2014……..**

Submitted on: ……..……..

Office stamp

Members of the *Promotionskomitee*:

Chairperson: Prof. Dr. Paul Pauli

Primary Supervisor: Priv.-Doz. Dr. Heike Rittner

Supervisor (Second): Prof. Dr. Claudia Sommer

Supervisor (Third): Prof. Dr. Erhard Wischmeyer

Date of Public Defence: ……..……

Date of Receipt of Certificates: …….

AFFIDAVIT

I hereby confirm that my Ph.D. thesis entitled "**Immune and peripheral endogenous opioid mechanisms of electroacupuncture analgesia**" is the result of my own work. I did not receive any help or support from commercial consultants. All sources and/or materials applied are listed and specified in the thesis.

Furthermore, I confirm that this thesis has not yet been submitted as part of another examination process neither in identical nor in similar form.

Würzburg, 12-3-2014

(Ying Wang)

ACKNOWLEDGEMENT

I started my second Ph.D. project about acupuncture analgesia in August 2011 and completed all the experiments for the paper revision in October 2013. I would not have been be able to finish my major Ph.D. project and dissertation within this time frame without the encouragement and support of my thesis committee members, help from colleagues and friends, and support from my husband and parents.

I would like to express my deepest gratitude to my primary advisor, Priv.-Doz. Dr. Heike Rittner, for her excellent guidance on molecular pain research, as well as Professor Dr. Erhard Wischmeyer, who provided me with superb advice and support for my project. I would also like to express my profound appreciation to Professor Dr. Claudia Sommer, who gave me tremendous encouragement for my research. I am grateful to Priv.-Doz. Dr. Heike Rittner, Professor Dr. Erhard Wischmeyer and Professor Dr. Claudia Sommer for being my thesis committee and taking significant time and making significant efforts to support me for the duration of my thesis project. I would also like to thank Professor Dr. Alexander Brack for his huge efforts together with Priv.-Doz. Dr. Heike Rittner on leading the molecular pain research group, from which I was fortunate enough to benefit from the extensive knowledge and existing expertise on pain research.

I am so grateful for the help of Dr. Dagmar Hackel and Dr. Winfried Neuhaus, who turned out to be my friends, for their considerable patient and helpful cooperation on analyzing and solving problems hampering my research in the past few years.

I want to thank Dr. Shaaban Mousa for the excellent work he did for my second paper as a helpful advisor and cordial friend, as well as medical student Rebekka Gehringer,

who as a good friend contributed her wonderful cooperation and work on my acupuncture project.

Many thanks to Dr. Malgorzata Burek, Dr. Solange Sauer, Diana Pflüke, Egle Mambretti, Kirsten Langenbrink, Judith Bosten, Katerina Pech, Anja Neuhoff, Judith Skirde and all my other colleagues from the lab for their kind assistance and useful suggestions for my research and general concern and care for me.

I would also like to especially express my cordial gratefulness to Dr. Gabriele Blum-Oehler, Dr. Franz-Xaver Kober and Bianca Putz from Graduate School of Life Science (GSLS), for their wonderful help and great efforts in organizing abundant activities including symposia, seminars, workshops and trips. In particular I would especially like to thank Dr. Gabriele Blum-Oehler and Jennifer Braysher, who assisted me greatly with different questions and problems during my Ph.D. period.

Last but not least, I am very grateful to Jennifer Braysher for her warm help in polishing the whole thesis with her proof reading work in her native language of English.

After years of learning and experiencing many setbacks and problems from research design and execution, I have grown from these experiences in such a way that I will have more confidence to confront such challenges and frustrations in my future career. I am truly and deeply grateful for this precious learning opportunity I have experienced in the Department of Anesthesiology and the GSLS in Würzburg with all my supervisors, colleagues and friends. I wish them all the best for the future.

Contents

Abbreviations

Ab	antibody
AA	acupuncture analgesia
ANOVA	analysis of variance
BL	baseline
CB2	cannabinoid B2
CCL2	monocyte chemoattractant protein-1/MCP-1
CCL3	macrophage inflammatory protein-1alpha/ MIP-1alpha
CCR2	C-C-chemokine receptor type 2
CNS	central nervous system
BCA	bicinchoninic acid
CCL7	monocyte chemoattractant protein-3/MCP-3
CFA	complete Freund's adjuvant
CRH/CRF	corticotropin-releasing hormone/factor
CTOP	Cys2, Tyr3, Orn5, Pen7-amide
CXCL8	interleukin-8/IL-8
CXCL9	monokine induced by interferon-gamma/MIG
CXCL10	interferon-gamma inducible protein 10/IP-10

DAPI	4',6-diamidino-2-phenylindole
DNA	deoxyribonucleic acid
DNTPs	deoxynucleoside triphosphates
DOR	delta opioid receptor
DYN	dynorphin A
EA	electroacupuncture
ELISA	enzyme-linked immunosorbent assay
EM	endomorphin
END	beta-endorphin
ENK	met-enkephalin
ER	endoplasmic reticulum
FACS	fluoresce-activated cell sorting
Fig.	figure
FITC	fluorescein isothiocyanate
FSC	forward scatter
FPR	formyl peptide receptor
GB	the Gallbladder Meridian of Foot-Shaoyang
IDV	integrated density value
IFN	interferon
Ig	immunoglobulin

IHC	immunohistochemistry staining
i.p.	intraperitoneal
i.pl.	intraplantar
IP3	inositol 1, 4, 5-triphosphate
IL	interleukin
KOR	kappa opioid receptor
LPS	lipopolysaccharide
LSM	laser scanning microscope
MARK	mitogen-activated protein kinase
MOR	mu opioid receptor
mRNA	messenger ribonucleic acid
NLX	naloxone
Nor-BNI	nor-binaltorphimine
NTI	naltrindole
NURBs	non-uniform rational B-spline
O.D.	optical density
PE	phycoerythrin
PI3K	phosphoinositol-3-kinase
PLC	phospholipase C
PMN	polymorphonuclear cells (neutrophils)

PPT	paw pressure threshold
PWL	paw withdrawal latency
RM	repeated measurements
RNase	ribonuclease
RQ	relative quantification
RT	room temperature
RT-PCR	reverse transcription-polymerase chain reaction
SA-HRP	streptavidin-horseradish peroxidase
SDS-PAGE	sodium dodecyl sulfate-polyacrylamide gel electrophoresis
SEM	standard error of mean
SSC	sideward scatter
T_h	T helper
TLR	toll like receptor
TNF	tumor necrosis factor
UV/Vis	ultraviolet/visible
WB	western blot

Summary

A precious treasure in traditional Chinese medicine (TCM), acupuncture played a vital and irreplaceable role in contributing to people's health in the thousands of years of Chinese history, and in 2010 was officially added to the "Representative List of the Intangible Cultural Heritage of Humanity" by the United Nations. Because of the side-effects of long-term drug therapy for pain, and the risks of dependency, acupuncture has been widely accepted as one of the most important alternative choice therapies for treating varieties of acute and chronic pain-related disorders. The clinical application and scientific mechanism research of acupuncture have therefore increased intensively in the last few decades. Besides hand acupuncture, other treatment approaches e.g. electroacupuncture (EA) have been widely accepted and applied as an important acupuncture-related technique for acupuncture analgesia (AA) research. The involvement of opioid peptides and receptors in acute AA has been shown via pre-EA application of opioid receptor/peptide antagonists. However, existing publications still cannot illuminate the answer to the following question: how does sustained antinociception happen by EA treatment? The hypothesis of opioid peptide-mediated tonic AA might be able to answer the question.

In the first part of this thesis, the institution of a reproducible acupuncture treatment model as well as the endogenous opioid-related mechanisms was demonstrated. An anatomically-based three-dimensional (3D) rat model was established to exhibit a digital true-to-life organism, accurate acupoint position and EA treatment protocol on bilateral acupoint GB-30 Huantiao. The optimal EA treatment protocol (100 Hz, 2-3 mA, 0.1 ms, 20 min) at 0 and 24 h after induction of inflammatory pain by complete Freund's adjuvant (CFA) on conscious free-moving rats was then established. EA elicited significant sustained mechanical and thermal antinociception up to 144 h. Post-EA application of opioid receptors (mu opioid receptor, MOR; delta opioid receptor, DOR) antagonists naloxone (NLX) and naltrindole (NTI), or opioid peptide antibodies anti-beta-endorphin (anti-END), met-enkephalin (anti-ENK) or -dynorphin

A (anti-DYN) could also block this effect at a late phase (96 h) of CFA post-EA, which suggested opioid-dependent tonic analgesia was produced by EA. Meanwhile, EA also reduced paw temperature and volume at 72-144 h post CFA indicating anti-inflammatory effects. Nociceptive thresholds were assessed by paw pressure threshold (Randall-Sellito) or paw withdrawal latency (Hargreaves) and an anti-inflammatory effect was evaluated by measurement of plantar temperature and volume of inflamed paw.

The second part of the thesis further suggests the correlation between the chemokine CXCL10 (= interferon-gamma inducible protein 10, IP-10) and opioid peptides in EA-induced antinociception. Based on a comprehensive Cytokine Array of 29 cytokines, targeted cytokines interleukin (IL)-1alpha, interleukin (IL)-1beta, tumor necrosis factor (TNF)-alpha, interleukin (IL)-4, interleukin (IL)-13, interferon (IFN)-gamma as well as CXCL10 were selected and quantified by enzyme-linked immunosorbent assay (ELISA), and real time reverse transcription-polymerase chain reaction (RT-PCR) quantification confirmed upregulation of CXCL10 mRNA at both 72 and 96 h. The following hyperalgesic assessment suggested the antinociceptive effect of CXCL10. The double immunostaining localizing opioid peptides with macrophages expressed the evident upregulation of CXCR3-receptor of CXCL10 in EA treated samples as well as the significant upregulation or downregulation of opioid peptides by repeated treatment of CXCL10 or antibody of CXCL10 via behavioral tests and immune staining. Subsequent immunoblotting measurements showed non-alteration of opioid receptor level by EA, indicating that the opioid receptors did not apparently contribute to AA in the present studies. *In vitro*, CXCL10 did not directly trigger opioid peptide END release from freshly isolated rat macrophages. This might implicate an indirect property of CXCL10 in *vitro* stimulating the opioid peptide-containing macrophages by requiring additional mediators in inflammatory tissue.

In summary, this project intended to explore the peripheral opioid-dependent analgesic mechanisms of acupuncture with a novel 3D treatment rat model and put

forward new information to support the pivot role of chemokine CXCL10 in mediating EA-induced tonic antinociception via peripheral opioid peptides.

Zusammenfassung

Als wertvoller Schatz in der traditionellen chinesischen Medizin (TCM) spielt die Akupunktur eine wichtige und unersetzliche Rolle für die Gesundheit der Menschen in der über tausendjährigen Geschichte von China und wurde im Jahr 2010 offiziell in das "Weltkulturerbe" der Vereinten Nationen aufgenommen. Aufgrund der Nebenwirkungen von Langzeittherapien zur Schmerzbehandlung und dem Risiko der Abhängigkeit wird Akupunktur weithin als eine wichtigste Alternative für die Behandlung von akuten und chronischen Schmerzen eingesetzt. Die klinische Anwendung und Forschung in der Akupunktur wurden in den letzten Jahrzehnten intensiv vorangetrieben. Neben Handakupunktur gibt es noch andere Behandlungsmöglichkeiten, wie z.B. die Elektroakupunktur (EA). EA ist vor allem eine allgemein akzeptierte und wichtige akupunkturbezogene Technik für die Akupunkturanalgesie (AA) in der Forschung. Die Beteiligung von Opioidpeptiden und Opioidrezeptoren in der akuten AA wurde mittels Anwendung von Opioidrezeptorantagonisten/Opioidpeptidantikörpern appliziert vor EA gezeigt. Nach dem aktuellen Forschungsstand kann man jedoch nicht die Frage beantworten, wie die längerfristige (tonische) Antinozizeption nach EA-Behandlung funktioniert. Mit einer Hypothese zur Opioidpeptid vermittelten tonischen AA könnte man die Frage hierzu beantworten.

In der vorliegenden Arbeit wurden in einem Modell der Akupunktur zum ersten Mal endogene Opioid-vermittelte Mechanismen reproduzierbar nachgewiesen. Es wurde ein dreidimensionales (3D) anatomisch-basiertes Rattenmodell entworfen, um am wachen Tier ein genaue Akupunkturbehandlung (EA) an den Akupunkten GB-30 Huantiao beidseitig durchzuführen. Darüber hinaus wurde ein optimiertes Behandlungsprotokoll von EA (100 Hz, 2-3 mA, 0.1 ms, 20 min) bei Ratten 0 und 24 h nach intraplantarer Injektion von komplettem Freunds Adjuvans (CFA) etabliert.

Nozizeptive Schwellen wurden mittels Pfotendruckschwelle (Randall-Sellito) oder Pfotenrückzugslatenzzeit (Hargreaves) gemessen und die entzündungshemmende Wirkung durch Messung der Pfotentemperatur und Volumen der entzündeten Pfote ausgewertet. EA bewirkte eine signifikante mechanische und thermische Antinozizeption, welche bis zu 144 h anhielt. Die antinozizeptive Wirkung durch EA war nach Injektion von Opioidrezeptorantagonisten (mu opioid receptor, MOR; delta opioid receptor, DOR) Naloxon (NLX) und Naltrindol (NTI) oder Antikörpern gegen die Opioidpeptide beta-Endorphin (anti-END), Met-Enkephalin (anti-ENK) oder Dynorphin A (anti-DYN) während der späten Entzündungsphase (96 h) mit CFA blockierbar. Dies lässt auf eine durch EA induzierte tonische Analgesie schließen. Darüber hinaus reduzierte EA auch die erhöhte Pfotentemperatur und das erhöhte Pfotenvolumen, welche sehr typisch ist für eine 96-144 h Entzündung mit CFA. Dies spricht für eine entzündungshemmende Wirkung von EA.

Nachfolgend wurde die Beteiligung von Opioidpeptiden und dem Chemokin CXCL10 (= Interferon-gamma induziertes Protein 10, IP-10) sowie die Korrelationen zwischen beiden geklärt. Basierend auf umfangreichenden Zytokinarrays mit 29 Zytokinen, wurden die Zytokine Interleukin (IL)-1alpha, Interleukin (IL)-1beta, Tumornekrosefaktor (TNF)-alpha, Interleukin (IL)-4, Interleukin (IL)-13, Interferon (IFN)-gamma und CXCL10 gezielt ausgewählt und im Enzym Immunoassay (ELISA) sowie durch eine Echtzeit Reverse Transkription-Polymerase Kettenreaktion (RT-PCR) quantifiziert. Die Quantifizierung auf mRNA-Ebene zeigte eine Hochregulation von CXCL10 bei 96 h und zum früheren Zeitpunkt von 72 h. Nachfolgende Schmerzschwellenmessungen wiesen auf eine antinozizeptive Wirkung von CXCL10 hin. Eine Doppelimmunfärbung zeigte die Lokalisation von Opioidpeptiden in Makrophagen. Nachweislich wurde die Expression des CXCR3-Rezeptor von CXCL10 in EA behandelten Pfoten erhöht. Ebenso kam es zu einer signifikanten Hochregulation von Opioidpeptiden durch wiederholte Behandlung mit CXCL10 bzw. Herunterregulation der Opioidpeptide nach wiederholter Behandlung mit

anti-CXCL10 Antikörper. Dies wurde sowohl in Verhaltenstests als auch in der Immunfärbung zu beobachtet. Immunoblotting zeigte keine Veränderung der Expression von Opioidrezeptoren nach EA, was schließen lässt, dass die Menge an Opioidrezeptoren in den vorliegenden Untersuchungen keine Rolle spielen. Da CXCL10 *in vitro* keine direkten Effekt auf die Freisetzung des Opioidpeptides beta-END aus frisch isolierten Rattenmakrophagen hat, liegt die Vermutung nahe, dass CXCL10 *in vitro* eine indirekte Rolle als Mediator zukommt und indirekt die Opioidpeptidfreisetzung aus Makrophagen in entzündlichen Gewebe stimuliert wird.

Zusammenfassend wurden in dem hier vorgestellten Projekt die Opioidpeptid-abhängigen analgetischen und peripheren Mechanismen der Akupunktur mit einem neuartigem 3D-Behandlungsmodell der Ratte untersucht und eine Schlüsselrolle des Chemokins CXCL10 bei der Vermittlung der EA-induzierten tonischen Antinozizeption in Abhändigkeit von peripheren Opioidpeptiden.

(Translated by Dr. Dagmar Hackel and revised by Priv.-Doz. Dr. Heike Rittner)

1. Introduction

1.1 Opioid-dependent acupuncture analgesia (AA)

Acupuncture, a traditional Chinese medicine (TCM)-related therapy, is broadly accepted as an important alternative medical therapy for treating varieties of acute and chronic pain-related disorders. Clinical application and scientific mechanism research of acupuncture has intensively increased in the last few decades by means of acupuncture-related techniques, especially electroacupuncture (EA) as one of the main substitutes for manual acupuncture. A great quantity studies employed EA to explore the mechanisms underlying acupuncture analgesia (AA). According to TCM theory, the fundamental basis of acupuncture treatment is considered as the regulation and balance of Yin and Yang [1], in contrast, scientific research in the past few decades discovered multiple molecular signaling pathways involved in AA including adenosine A1 receptor [2], cannabinoid B2 (CB2) receptor [3] as well as other multiple, distinctive neurobiological mechanisms summarized by Zhao [4]. Additionally, anti-inflammatory effects of EA were also demonstrated by previous researchers [5-10] by assessing the increased circumference of paw with inflammation as well as quantification of pro-inflammatory cytokines. Endogenous opioid-dependent analgesia at spinal cord level was initially associated with mechanisms of AA [11-14]. Subsequent studies extended the investigations on pivotal role of endogenous opioids in mediating the AA via application of antibodies (Abs) of opioid peptides or opioid receptor antagonists at central [15-16] or peripheral level [17-19]. In particular, the intensive studies on analgesic mechanism of EA at central level indicated the frequency-dependent opioid release by EA, among which an alternative frequency mode 2/100 Hz was speculated and found to be significantly more effective than the pure low- (2 Hz) or pure high-frequency (100 Hz) therapy [15] (**Fig. 1**). By comparison, the correlative mechanisms between AA and peripheral opioid-mediated analgesia are still largely unknown.

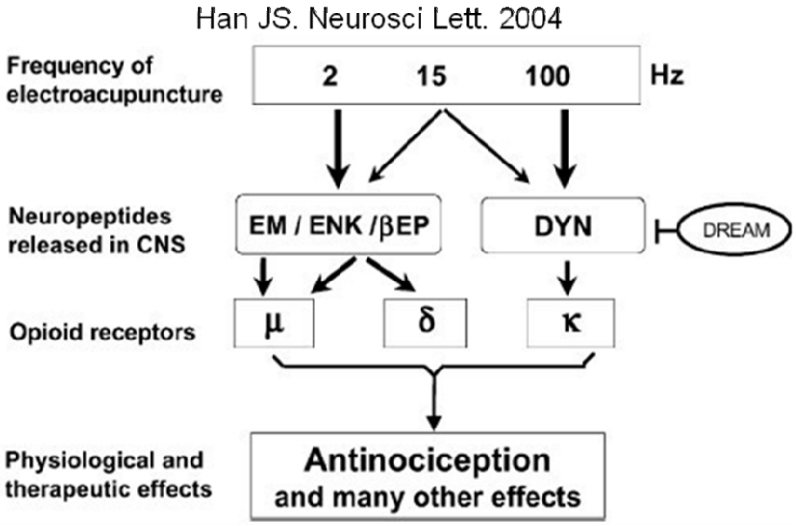

Fig. 1: Frequency-dependent opioid mechanisms of electroacupuncture-induced analgesia in central nervous system (CNS). Representatives (2, 15 and 100 Hz) of three different frequencies (low, middle and high frequencies) were compared. The neuropeptides (opioid peptides) release was measured by radioimmunoassay on perfusate of subarachnoid space of spinal cord. There was a sharp difference exists between the 2 and 100 Hz frequency. In a chart with a log scale, 15 Hz is in the middle point between 2 and 100 Hz, which can partially activate both sides, leading to antinociceptive and other therapeutic effects (EM: endomorphin, ENK: met-enkephalin, βEP: beta-endorphin, DYN: dynorphin, μ/δ/κ: mu/delta/kappa opioid receptor) (Figure and legend were modified from **Fig. 2** in [15]).

1.2 Comparison of different modes of electroacupuncture (EA) treatment

In order to obtain the ideal effect from acupuncture treatment, a clear and correct acupoint positioning approach and needling techniques are the most important factors. This is in line with the acupuncture-induced sensation 'De Qi' majorly referring to subjective responses to needling including soreness, numbness, distension and aching (dull pain in deep tissue) [1]. Addressing these issues requires relatively precise localization and the effects can be felt best on conscious subjects. Nevertheless, needling on conscious subjects, especially animals, is considered to be stressful. An

anesthetic or restrainer was therefore often utilized on animals during needling in order to mitigate the treatment discomfort [2,20-22] (**Fig. 2 and 3**). However, the effects from either anesthetics or restrainers are difficult to estimate and would probably impair treatment effect or biological and psychological conditions.

As one of the frequently used acupoints in clinical settings, GB-30 Huantiao (GB: the Gallbladder Meridian of Foot-Shaoyang; Chinese name in pinyin: Huantiao) is thought to be effective in treating symptoms or disease referenced to lower limbs- and lower back-related pain and thus frequently employed in scientific investigations [3,16,22-24]. The precise anatomical location of GB-30 Huantiao on humans is clearly known and easy to find, however the exact procedures to accurately locate the corresponding point in rats has not been very well described by pervious researchers [3,16,22-24].

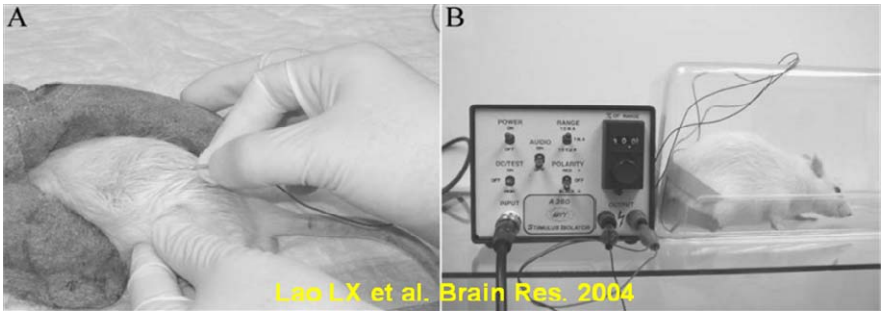

Fig. 2: Acupuncture procedure by two experimenters and EA treatment on rat in semi-free restrainer. The animals were gently handled for 30 min each day for 2-3 days and habituated to the acupuncture treatment before the experiment. [**A**] After cleaning the skin with alcohol swabs, disposable acupuncture needles with electrodes soldered to their handles were swiftly inserted bilaterally, approximately 1/2 in deep, into GB-30 Huantiao by one investigator while the other gently held the animal. The needles and the electrodes were stabilized with adhesive tape. The procedure typically lasted less than 20 s and caused little distress to the animal. [**B**] The EA stimulation was delivered by an electrical stimulator via an isolator to convert electrical voltage into constant electrical current (Figure and legend were modified from **Fig. 1** in [16]).

Fig. 3: EA treatment was performed on fully restrainer-stabilized rats. Rats were kept in a special transparent Lucite barrel with tails and hind-legs left out naturally. The Lucite barrels were designed to restrict rats and ensure the successful EA operations to these clearheaded rats. In order to minimize the bias effect induced by barrel restraint, rats were placed quietly for 15 min to be stabilized and were given different EA treatments in groups (Figure and legend were modified from **Fig. 3** in [21]).

1.3 Tonic analgesia mediated by peripheral opioid peptides containing-immune cells

"In the local inflammatory pain model induced by CFA, opioid peptide-containing leukocytes migrate into the inflamed tissue and release opioid peptides. Opioid peptides bind to opioid receptors on peripheral nociceptive neurons and mediate a peripheral analgesic effect. This analgesic effect elicited by exogenous triggers e.g. cold-water swim stress or local injection of certain cytokines (e.g. tumor necrosis factor (TNF)-alpha, interleukin (IL)-1beta), chemokines (CXCL2/3) (**Fig. 4**), corticotrophin-releasing hormone/factor (CRH/CRF), or formyl peptides (**Fig. 5**) [25-28] could only last for a short period (10-20 min), which partly hampers clinical application" [5].

However, previous studies indicated that opioid peptides were continuously released from opioid peptide-containing leukocytes at the inflammatory site and attenuate inflammatory pain via formyl peptide receptors on neutrophils in an early phase (2 h) of CFA [29] (**Fig. 5**) which partially answered clinical and experimental postulations for tonic analgesia [30,31]. As illustrated before, accumulating evidences have supported acupuncture elicited analgesia via opioid receptors/peptides. Nevertheless, in all publications to date the pre-EA application mode of antagonists/Abs of opioid receptors/peptides could only manifest opioid-dependent acute analgesia of acupuncture. The question of how sustained (tonic) analgesia of acupuncture can exist remains, illustrated through the large number of publications in this area.

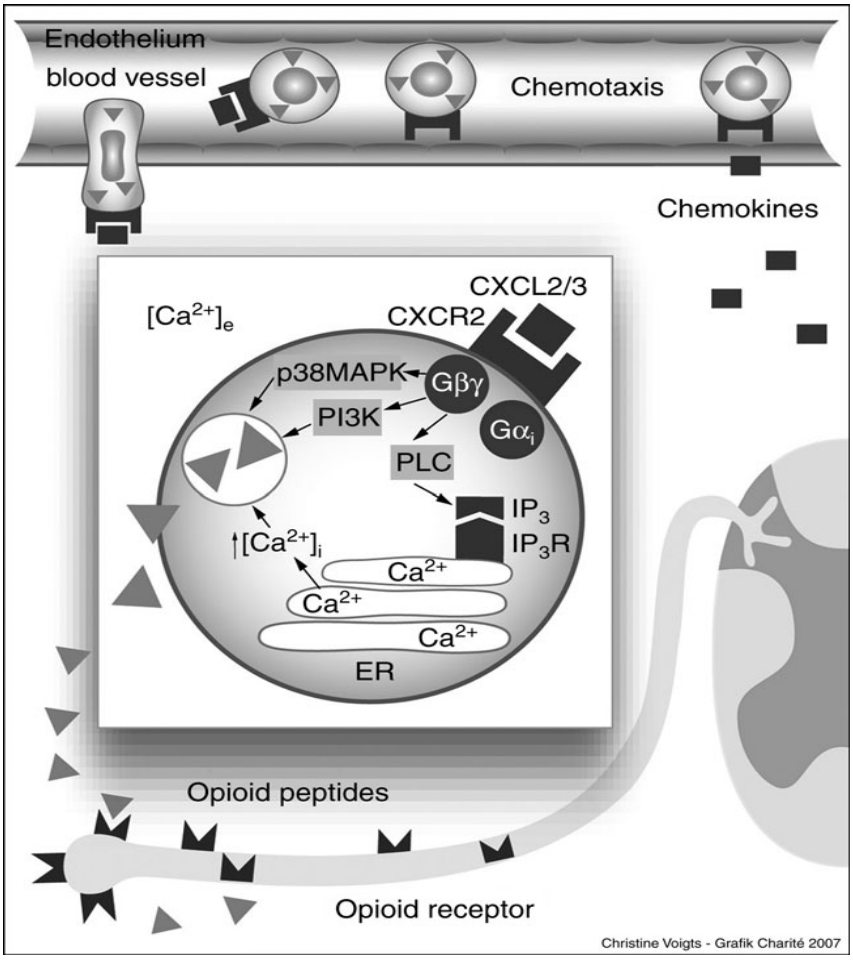

Fig. 4: Chemokine receptor CXCR2 and ligand CXCL2/3 attenuates peripheral inflammatory pain via opioid peptide-containing polymorphonuclear cells (PMNs, neutrophils) at early phase (2 h) of CFA. Chemokine CXCL2/3 released

from endothelium blood vessel binds to CXCR2 expressed on neutrophils, leading to Ca^{2+} influx from the endoplasmic reticulum (ER) of neutrophils via activating p38 mitogen-activated protein kinase (MARK) and phosphoinositol-3-kinase (PI3K). The increased intracellular level of Ca^{2+} leads to opioid peptides release from neutrophils. Opioid peptides binding to opioid receptors on nociceptor of peripheral sensory neurons induces peripheral antinociception (PLC: phospholipase C, IP3: inositol 1, 4, 5-triphosphate) (Figure and modified legend were cited from [27]).

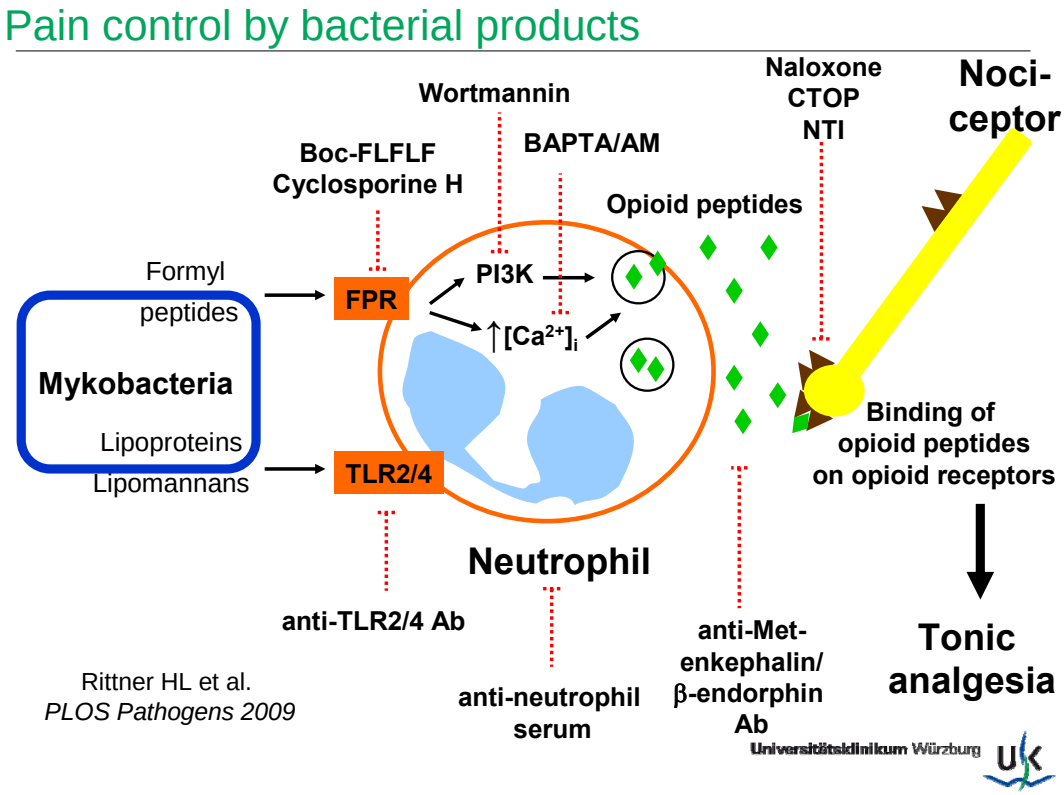

Fig. 5: Opioid peptide-containing neutrophils mediate tonic analgesia at early phase (2 h) of CFA. Mycobacterial components (**blue** square) formyl peptides and lipoproteins /lipomannans respectively bind to formyl peptide receptor (FPR, **orange**) and toll like receptor (TLR) 2/4 (**orange**) on neutrophils (with **light blue** segmented cell nucleus). Formyl peptides-FPR binding activated PI3K and Ca^{2+} influx, leading to continuous secretion of opioid peptides (**green** rhomboids) from neutrophils. The continuous released opioid peptides binding to opioid receptors (**brown**) on nociceptor of peripheral sensory neurons (**yellow**) thereby produces tonic analgesia continuously attenuating peripheral inflammatory pain (Boc-FLFLF/Cyclosporine H: antagonists of FPR, Wortmannin: inhibitor of PI3K, BAPTA/AM: intracellular Ca^{2+} level inhibitor (chelator highly selective for Ca^{2+} over Mg^{2+}), Naloxone/CTOP (Cys2, Tyr3, Orn5,

Pen7-amide)/NTI (naltrindole): antagonists of mu/delta receptor, Ab: antibody) (Figure and modified legend were cited from [29]).

1.4 Cytokine-mediated hyperalgesic and anti-hyperalgesic responses in pain

A broad set of publications in the last few decades supported the hyperalgesic role of pro-inflammatory cytokines and anti-hyperalgesic property of anti-inflammatory cytokines during inflammation. Since SH Ferreira and his colleagues first reported the potent nociceptive effect IL-1beta in non-inflamed paw [32], they produced subsequent studies which expanded this cytokine spectrum that deteriorates the inflammatory hyperalgesia to TNF-alpha and IL-6 [33]. TNF-alpha also evoked mechanical allodynia in a neuropathic pain model [34]. The anti-hyperalgesic action of anti-inflammatory cytokines including IL-4, IL-10 and IL-13 were separately investigated in carrageenan or bradykinin – induced hyperalgesia via application of inhibitory Abs of cytokines *in vivo* and *in vitro*, which notably decreased the nociceptive intensity *in vivo* and suppressed the production of IL-1beta and TNF-alpha *in vitro* [35-37]. It was also demonstrated that IL-13 induced MOR expression in lymph nodes from patients with T cell lymphoma, which might be beneficial for down-modulating immune response [38].

Apart from the large body of references emphasizing the hyperalgesic role of pro-inflammatory cytokines, notably, some pro-inflammatory cytokines were also recognized as antinociceptive. TNF-alpha as well as IL-1beta was indicated to opioid-dependently elicit transient but potent mechanical antinociception *in vivo* [25,28]. Intracerebroventricular administration of IL-1alpha could inhibit thermal hyperalgesia, which might be mediated by CRH and the noradrenergic system [39]. Generally speaking, the current knowledge referring to the hyperalgesic or

anti-hyperalgesic role of cytokines might be considerably reliant on specific circumstances and inflammatory phases in different models.

1.5 Aims

The current existing, intriguing conclusions of opioid-dependent AA and cytokine-mediated roles in pain inspired the initial aims of this thesis with discovering:

1. Which parameter setting of EA is beneficial for achieving optimal EA-induced sustained (tonic) antinociception and whether the EA treatment could be accomplished under free-moving rats.
2. Whether EA produced tonic antinociception is peripheral opioid receptor/peptide-dependent.
3. Whether EA could regulate local cytokines, and of regulated cytokines, which key cytokine contributes to tonic AA as well as the possible immune and peripheral opioid-correlated mechanism.

2. Materials and Methods

2.1 Materials

2.1.1 Chemicals

Table 1: Abbreviations and companies of applied chemicals

Chemicals	Companies
Acrylamide/Bis (30:2)	Carl Roth GmbH, Karlsruhe, Germany
Agarose	Sigma-Aldrich, Munich, Germany
Albumine from bovine serum (BSA)	Sigma-Aldrich, Munich Germany
Ammonium persulfate (APS)	Sigma-Aldrich, Munich, Germany
Aprotinin	Sigma-Aldrich, Munich, Germany
Bestatin	Sigma-Aldrich, Munich, Germany
Beta-Mercaptoethanol	Carl Roth GmbH, Karlsruhe, Germany
Bromophenol Blue	Sigma-Aldrich, Munich, Germany
Chloroform	Roche Diagnostics, Mannheim, Germany
Collagenase	Sigma-Aldrich, Munich, Germany
Complete Protease Inhibitor Cocktail	Roche Diagnostics, Mannheim, Germany
Cytochalasin B	Sigma-Aldrich, Munich, Germany
DAPI (4',6-diamidino-2-phenylindole)	Sigma-Aldrich, Munich, Germany
Enhanced chemiluminescence solution (ECL) detection reagent	Roche Diagnostics, Mannheim, Germany
Ethanol	Merck, Darmstadt, Germany
Ethylenediaminetetraacetic acid (EDTA)	Sigma-Aldrich, Munich, Germany
Ethylene glycol tetraacetic acid (EGTA)	Sigma-Aldrich, Munich, Germany
Glycerol	Sigma-Aldrich, Munich, Germany
Hank's Balanced Salt Solution (HBSS)	Sigma-Aldrich, Munich, Germany
HEPES (4-(2-hydroxyethyl)-1-piperazineethanesulfonic acid)	Sigma-Aldrich, Munich, Germany
Heparin	Rotexmedica GmbH, Trittau, Germany
Hyaluronidase	Sigma-Aldrich, Munich, Germany

Imidazole hydrochloride	Carl Roth GmbH, Karlsruhe, Germany
Isopropanol	Merck, Darmstadt, Germany
Magnesium chloride (MgCl2)	Sigma-Aldrich, Munich, Germany
Nonfat-Dried Milk bovine	Sigma-Aldrich, Munich, Germany
Paraformaldehyde (PFA)	Sigma-Aldrich, Munich, Germany
Phenylmethanesulfonyl fluoride (PMSF)	Sigma-Aldrich, Munich, Germany
Phosphate buffered saline (PBS, sterile, 0,1M, pH 7.4)	Biochrom AG Biotechnologie, Berlin, Germany
Potassium chloride (KCl)	Carl Roth GmbH, Karlsruhe, Germany
Roswell Park Memorial Institute (RPMI) 1640	Invitrogen/Life Technologies, Darmstadt, Germany
Saponin	Sigma-Aldrich, Munich, Germany
Sodium azide (NaN3)	Sigma-Aldrich, Munich, Germany
Sodium chloride (NaCl)	Sigma-Aldrich, Munich, Germany
Sodium dodecyl sulphate (SDS)	Sigma-Aldrich, Munich, Germany
Sodium fluoride (NaF)	Merck, Darmstadt, Germany
Sodium molybdate (Na2MoO4)	Carl Roth GmbH, Karlsruhe, Germany
Sucrose	Sigma-Aldrich, Munich, Germany
Tetramethylethylenediamine (TEMED)	Sigma-Aldrich, Munich, Germany
Thioglycolate	Sigma-Aldrich, Munich, Germany
Thiorphan	Sigma-Aldrich, Munich, Germany
Tissue-Tek compound	OCT, Miles, Elkhart, Indiana, USA
Tris hydroxymethyl aminomethane (Tris)	Sigma-Aldrich, Munich, Germany
Triton X-100	Sigma-Aldrich, Munich, German
Trypan Blue	Sigma-Aldrich, Munich, German
TRIzol®	Invitrogen/Life Technologies, Darmstadt, Germany
Tween20	Sigma-Aldrich, Munich, Germany

2.1.2 Antibodies (Abs)

Table 2: Suppliers and doses of primary Abs (Behavior: behavioral assays, WB: western blot, FACS: fluoresces-activated cell sorting, IHC: immunohistochemistry staining, BD Pharmingen™: Pharmingen/Becton Dickinson, KOR: kappa opioid receptor)

Primary Abs	Companies	Concentrations	Applications			
			Behavior	WB	FACS	IHC
Rabbit anti-END Rabbit anti-ENK Rabbit anti-DYN	Peninsula Laboratories Merseyside, UK	2 µg/100 µl 1.25 µg/100 µl 1 µg/100 µl	X X X			
Rabbit anti-CXCL10	Peprotech Hamburg Germany	2 µg/100 µl	X			
Rabbit anti-END Rabbit anti-ENK Rabbit anti-DYN	Peninsula Laboratories Merseyside, UK	1:1000				X X X
Mouse anti-CD68 Rabbit anti-macrophages antiserum Mouse anti-CXCR3	Serotec Düsseldorf, Germany Cedarlane Laboratories, Ontario Canada My Biosource, San Diego, USA	1:400 1:200 1:500				X X X
Mouse anti-CD45 Mouse anti-CD3	BD Pharmingen™, Heidelberg, Germany	0.2 µg/µl 0.5 µg/µl			X X	
Mouse anti-CD68	Serotec Düsseldorf, Germany	0.1 µg/µl			X	
Mouse anti-MOR Rabbit anti-KOR	Abcam, Cambridge, UK	1:500 1:1000		X X		
Rabbit anti-DOR	Neuromics, MN, USA	1:250		X		

Table 3: Suppliers and doses of secondary and control Abs

Secondary or control Abs	Companies	Concentrations	Applications			
			Behavior	WB	FACS	IHC
Rabbit IgG (IgG control)	Peninsula Laboratories Merseyside, UK	2 μg/100 μl	X			
Donkey anti-mouse Ab (both secondary Abs) Goat anti-rabbit Ab	Vector Laboratories, Burlingame, CA	1:250				X
Mouse IgG1 (both isotype controls) Mouse IgG3	BD Pharmingen™	0.5 μg/μl			X	
Anti-mouse Ab (both secondary Abs)	GE Healthcare, München, Germany	1:5000		X		
Anti-rabbit Ab	Roche, Mannheim, Germany	1:3000		X		
Mouse anti-GAPDH (control Ab)	Millipore, Schwalbach, Germany	1:2000		X		

2.1.3 Additional drugs for peripheral administration

Table 4: Doses and suppliers of other drugs for intraplantar (i.pl.) administration

Drugs	Doses (i.pl.)	Suppliers
Complete Freund's adjuvant (CFA)	150 µl	Calbiochem, San Diego, CA, USA
Naloxone hydrochloride dehydrate (NLX)	0.56 ng/100 µl	Sigma-Aldrich, Munich, Germany
Naltrindole hydrochloride (NTI)	25 µg/100 µl	Sigma-Aldrich, Munich, Germany
Recombinant rat IP-10 (CXCL10)	0.2 ng/100 µl	Peprotech, Hamburg, Germany
Sodium chloride (0.9% NaCl solution)	100 µl	B. Braun Melsungen AG, Melsungen Germany

2.1.4 Kits

Table 5: Suppliers of all kits

Kits (application)	Companies
Rat TNF-alpha kit (ELISA) Rat IL-4 kit (ELISA) High-Capacity cDNA Reverse Transcription Kit (RT-PCR)	Invitrogen/Life Technologies, Darmstadt, Germany
Rat Cytokine Array kit (Cytokine Array) Rat IL-1beta kit (ELISA) Rat IL-1alpha kit (ELISA) Rat IFN-gamma kit (ELISA)	R&D systems, London, UK
Rat IL-13 kit (ELISA)	Abcam, Cambridge, UK
Rat IP-10 (CXCL10) kit (ELISA)	Peprotech, Hamburg, Germany
Pierce BCA protein assay kit (WB)	Thermo Fisher Scientific, Ulm, Germany

Rat beta-END kit (ELISA)	Phoenix Pharmaceuticals, Inc., Karlsruhe, Germany

2.1.5 Experimental software and hardware

Table 6: Suppliers and application of software for experimental analysis

Software	Companies	Application
Sigma plot 11.0	Systat Software GmbH, Erkrath, Germany	Statistical analysis and graphing
EndNote X6	Thomson Reuters GmbH, Philadelphia, PA, USA	References managing
Sunrise® Tecan	Tecan Deutschland GmbH, Crailsheim, Germany	ELISA plate reader and data analysis; WB (Pierce BCA protein assay kit)
7300 System Sequence Detection Software v1.4.0	Applied Biosystems GmbH, Darmstadt, Germany	PCR amplification and analysis
FluorChem FC2 MultiImage II	Alpha-InnoTech, Kasendorf, Germany	WB image scanning and densitometric analysis
NIH Image J software	Bethesda, MD, USA	IHC image analysis
CellQuest	BD Pharmingen™	FACS staining analysis and graphing

Table 7: Suppliers and application of hardware for experiment performance

Hardware	Companies	Application
AS Super_4_digital electrical stimulator	Schwa-medico, Ehringshausen, Germany	Electric stimulation
Randall-Sellito Analgesiemeter (Modified Randall-Sellito test)	Ugo Basile, Comerio, Italy	Mechanical nociceptive test
IITC Plantar (Hargreaves Method)	IITC Inc/Life Science, Woodland Hills, CA, USA	Thermal nociceptive test
Thermometer (TM99A)	Cooper-aktins, FL, USA	Paw temperature measurement
Plethysmometer (37140)	Ugo Basile, Comerio, Italy	Paw volume measurement
Sunrise® Tecan	Tecan Deutschland GmbH, Crailsheim, Germany	ELISA plate reader
7300 System Sequence Detection hardware	Applied Biosystems GmbH, Darmstadt, Germany	RT-PCR amplification
GeneAmp® PCR System 9600 thermal cycler	Applied Biosystems GmbH, Darmstadt, Germany	cDNA transcription
Eppendorf Thermalmixer®	Eppendorf AG, Hamburg, Germany	RNA isolation
peqPOWER 300 Volt Power Supply	PEQLAB Biotechnologie GmbH, Erlangen, Germany	Electrophoresis (WB)
FluorChem FC2 MultiImage II	Alpha-InnoTech, Kasendorf, Germany	WB image scanner
Tissuelyser (and sterilized stainless steel beads)	Qiagen, Düsseldorf, Germany	Paw tissue homogenization (WB and RT-PCR)
Cryostat (Micro™ HM 525)	Thermo Fisher Scientific, Ulm, Germany	Tissue slice preparation for IHC
Zeiss 510META laser scanning microscope	Zeiss AIM, Jena, Germany	IHC image obtaining and graphing
FACS Scan	BD Pharmingen™	FACS staining analysis

2.2 Experimental methods

2.2.1 Peripheral inflammatory pain model on animals

Male adult Wistar rats weighing 280-350 g were housed collectively in rat cages (6 per cage) under controlled experimental conditions with free access to food and drink. All research schemes were approved by the University of Würzburg associated animal care committee. Experimental procedures were conducted strictly in accordance with the recommendations of the International Association for the Study of Pain [40]. Isoflurane was applied as an anesthesia for all pharmacological interventions. Inflammatory pain was triggered by administration (i.pl.) of 150 µl CFA in the plantar of right paw of all rats in accordance with previous investigations [41]. Rats were required to be sacrificed by an overdose of CO_2 or T61 (a veterinary euthanasia drug made with embutramide) up to 144 h post CFA injection according to animal ethical committee.

2.2.2 Establishment of EA treatment

In order to ease the rats during treatment, repeated handling work for 3-4 days prior to the experiments was performed on rats 3 times per day. Experimental rats were gently handled within a man-made covering which was formed from a piece of pre-disinfected paper (same handling approach as showed in **Fig. 7A, B**).

Before experiments, all properly handled and randomly selected rats were divided into three experimental groups including CFA + EA (CFA rats with EA treatment), CFA + sham (CFA rats with sham-EA treatment) and CFA control (CFA). The adjacent hair of the lower back area close to GB-30 Huantiao was cleanly removed by a shaver. Before needle insertion, adjacent skin upon acupoint GB-30 Huantiao was completely

disinfected to avoid infection; GB-30 Huantiao was anatomically located in accordance with the established 3D modeled position. The hiatus sacral of rats is comparable to the last sacral vertebra on the human body. The bony landmarks to position GB-30 Huantiao consisting of the last sacral vertebrae and the great trochanter, were firstly palpated and marked up (bilateral black circles and last vertical black circle in **Fig. 6A, B**). Commercially purchased disposable acupuncture needles with a diameter of 0.20 mm and needle body length of 25 mm were used (Schwa-medico, Ehringshausen, Germany) and connected with an electrical stimulator. The depth and direction of the needle had to be carefully regulated in case the rat was irritated by the unbearable stimulus from the insertion as well as the electricity. During the first 1 min, the electrical current was quickly turned up to 1 mA, which induced a minor twitching of the limbs (**Fig. 6C**). At this point, tiny adjustments were still necessary if the rat was agitated by the treatment. To guarantee the complete freedom of movement of the rats during this stage of the experiment, the electrical current needed to be appropriately and slowly increased from 2 up to 3 mA in a pattern of 0.1 mA (**Fig. 6D**). Precise values of electrical intensity were variable according to individual tolerance, however normally within a range of 2-3 mA. In most cases, indication of correct performance on the GB-30 Huantiao could be described as gentle twitching of the entire hind limb including the paw due to an indirect stimulus on the sciatic nerve lying the underneath the GB-30 Huantiao. Sham EA rats received same treatment, with the exception of the electrical current being omitted. It is of worth to be noted that needling performance requires repeated practice with a premise to tame the rats through a correct handling method within the paper covering. The possibility to move freely has to be guaranteed to each rat to exclude bias from unequal treatment conditions in all the experiments.

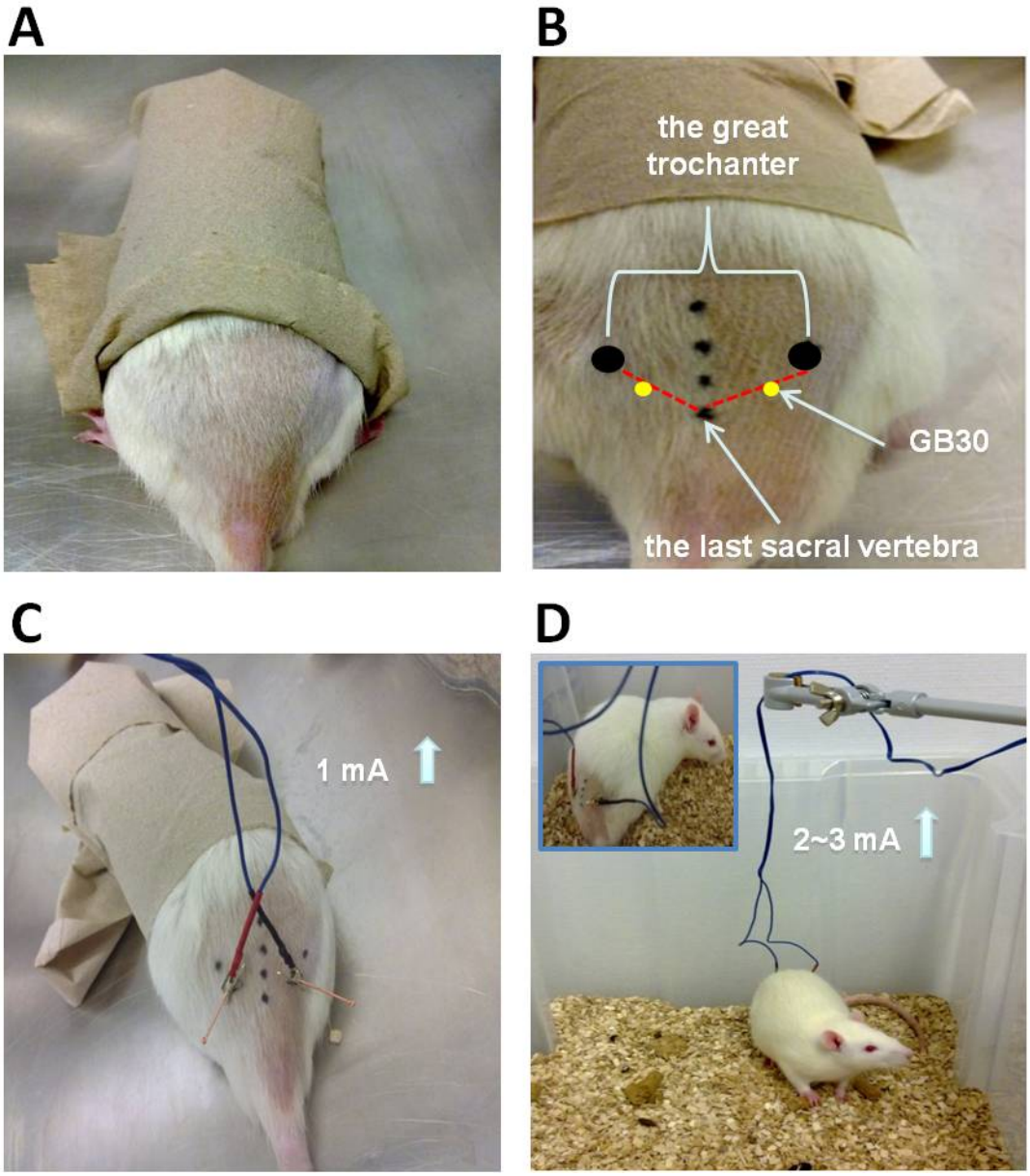

Fig. 6: Acupoint position and EA treatment on fully conscious free-moving rats. [**A**] Rat was gently handled in a pre-disinfected paper covering at least three days before the experiments and needling area was shaved and disinfected. [**B**] The bony marker of last four lumbar vertebral spinous processes (four black dots in a row) and the great trochanter (bilateral black dots) were palpated as marked on the graph. The accurate anatomical position of GB-30 Huantiao (bilateral yellow dots) on rats was located at the junction of lateral 1/3 and medial 2/3 of the distance between the great trochanter and the last sacral vertebra. [**C**] A pair of cables connected acupuncture needles was quickly penetrated through the surface skin. Entire needles were vertically inserted underneath skin adjacent subcutaneous tissue. Electrical intensity was adjusted to 1 mA within first 1 min. [**D**] Rat was allowed free mobility in the cage

following needle insertion. During the next 4 min, electrical intensity was gradually increased to 2 mA, with a maximal intensity at 3 mA (Figure and legend were modified from **Supplementary Fig. 1** in [5]).

2.2.3 Institution of computer-based three-dimensional (3D) rat model

Based on the anatomical features of Wistar rats, an accurate and reproducible 3D rat model was created by Maya 2012 (Autodesk, San Raphael, CA, USA) in aim of vividly exhibiting acupoint positioning methods and EA performance on the GB-30 Huantiao. An initial photograph of a Wistar rat was firstly edited in Adobe Photoshop 7.0 with an manual transformation into professional 3D image using computer programmer-based software Maya 2012. The image was based on the skeleton's shape, relative locations and size of each section exhibited in the original rat photo and was then automatically generated and used as a reference point for the following procedures. The creation of a digital 3D rat model was based on node-based theory in addition to NURBs (non-uniform rational B-spline) and polygon [5].

In the following procedures, based on the reference image, each section of the rat model was re-generated according to node-based theory composing NURBs and polygon. The NURBs and polygon were employed to sketch the shape and size of each section, e.g. the principle part of the rat model was initially generated from a polygon sphere and a column, which was then appropriately reshaped to four limbs. For the sketching of each section, the precise mathematical parameters of each node (the term "node" is considered as a "unit composing the entire model") from width (X axis) to height (Y axis) as well as depth (Z axis) were appropriately and proportionally defined in accordance with the size, skeleton and the angle of each individual section of the photographed rat in original picture. Subdivisions of each section were then accurately constructed within the given 3D space and this developed into a pilot 3D rat model.

In line with its anatomical location and bilateral acupuncture needles, the sciatic nerve underneath the GB-30 Huantiao was precisely mapped on the junction of lateral 2/3

and medial 1/3 on the line between the great trochanter and last sacral vertebrae. With this, an entire rat model was ultimately displayed in a 3D perspective.

(Patent application is on the review)

2.2.4 Drug delivery

A volume of 150 µl complete Freund's adjuvant (CFA) was i.pl. administered on the right plantar of all rats in order to trigger local inflammatory pain. Following drugs were injected with a volume of 100 µl dissolved in solvent. Naloxone hydrochloride dehydrate (NLX, MOR antagonist), naltrindole hydrochloride (NTI, DOR antagonist) as well as Abs against opioid peptides (anti-END, -ENK, or -DYN) were i.pl. administered in post-EA at late phase of CFA (96 h). Recombinant rat CXCL10 or rabbit anti-rat CXCL10 was either singly (96 h) or daily (day 0 to 4) i.pl. administered. Dose ranges of NLX and NTI were selected according to the previous studies [29]. Optimal doses of opioid peptide Abs (anti-END, -ENK and -DYN) were based on previous studies as well as pilot experiments [29,42]. Selected doses of CXCL10 and anti-CXCL10 were established in preliminary experiments. The same amount of solvent saline (0.9% NaCl solution) or an identical dose of rabbit IgG was used as a control for all experimental groups.

2.2.5 Measurement of nociceptive thresholds (Behavioral assays)

Paw withdrawal latency (PWL, Hargreaves method) indicating thermal nociceptive thresholds were measured in accordance with earlier publications [29]. To describe the method: at least three days before the experiments, rats were placed and habituated in independent plastic-made containers, situated upon a glass plate. A beam of yellow light was emitted from a mobilized light producing beamer pointing at the plantar of the rats. The intensity of the light and cut-off point could be properly adjusted. Time

(s) was automatically recorded during the measurement. The tolerable time (s) before the rat withdrew the paw was considered as the thermal nociceptive threshold. The bearable time for non-inflamed paw was established as 20 s as a baseline threshold. The cut-off point was set 30 s to avoid tissue damage. The average of raw values of two measurements (with 20 s intervals) was calculated for statistical analysis.

Paw pressure threshold (PPT, modified Randall-Sellito test) indicating mechanical nociceptive threshold was measured according to previous studies [29]). For at least three days prior to the experiment, experimental rats were repeatedly handled in a man-made paper covering as photographed in **Fig. 7A, B,** the same handling method that was utilized when nociceptive assessment was performed (**Fig. 7C, D**). The manually generated pressure was continually increased on a randomly chosen point on the dorsal surface of hind paw. The pressure (g) that caused the rat to retract its paw suggested the mechanical nociceptive threshold. 250 g was set up as the cut-off point in order to prevent tissue damage. There was a 10 s interval between each measurement to ensure the accuracy of the values. The average of raw values of three nociceptive thresholds was calculated and applied for statistical analysis.

A statistically decreased value of the nociceptive threshold normally indicates hyperalgesia (increased sensitivity to pain) and statistically increased values normally suggest anti-hyperalgesia (= antinociception or analgesia, decreased sensitivity to pain). The differences between the pain-related terms are illustrated further in **Table 8**.

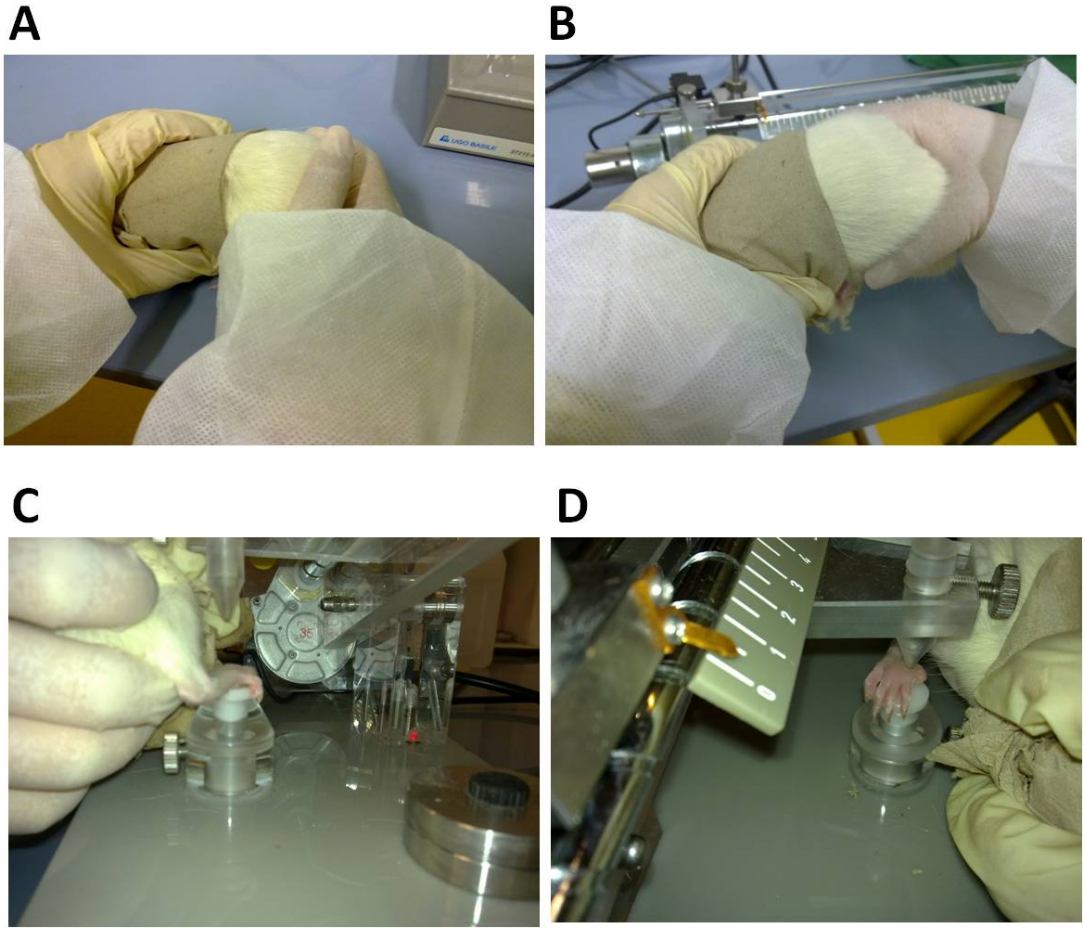

Fig. 7: Measurement of paw pressure threshold (PPT). [**A**] Healthy male Wistar rats were used. Handling was repeatedly performed at least three days prior to behavior experiments to guarantee the rats used to the experimenter. [**B**] Rats were hold in the hand softly by using a natural and comfortable position for them. [**C**] For evaluation of the withdrawal response to pressure, a modified Randall and Sellito apparatus was used. One of its hind paws was placed on the test pad slowly and then the plastic piston was placed on the dorsal surface of the paw softly. [**D**] An incremental pressure was continuously applied by a blunt piston of surface area 1.75 mm^2 until the rat withdrew its paw, the weight (g) recorded was the mechanical nociceptive threshold. The pressure test was applied on three different points on the dorsal surface of each paw and with 10 s interval between each test. The mean value was then determined from three tests (Modified from mini-thesis of Ying Wang "Effect of Resolvin D1 and chemerin upon nociception in local inflammation induced by complete Freund's adjuvant").

Table 8: Definitions of pain-related terms (Modified from Table 1 in [43])

Terms	Definition
Nociception	The neural processes of encoding and processing noxious stimuli
Antinociception (Applied on animals)	An increase in pain threshold to a stimulus that is normally painful
Hyperalgesia	A decrease in pain threshold to a stimulus that is normally painful
Anti-hyperalgesia	An increase in pain threshold to a stimulus that is normally painful
Analgesia (Applied on human)	An increase in pain threshold to a stimulus that is normally painful
Allodynia	Pain evoked by a stimulus that does not normally provoke pain
Nociceptive/hyperalgesic behavior test	Behavioral responses to noxious stimuli

2.2.6 Measurement of paw temperature and volume

The surface temperature of the plantar skin was measured with a contact Thermometer sensor before (0 h) and 6 d (144 h) post CFA injection. The volume of the hind paw was measured by submerging the entire hind paw to the tibiotarsal joint inside a water-filled Perspex cell of a Plethysmometer, and the connected professional volume reader displayed the exact value in mm^2. The measured values of temperature and volume divided baseline values were multiplied by 100 (values ÷ baseline × 100); the average value of two measurements was manually calculated and used for statistical analysis. Experimental procedures measuring paw volume and temperature were conducted referring to previous research [44,45].

2.2.7 Cytokine Array and enzyme-linked immunosorbent assay (ELISA)

Sample preparation: At 96 h post CFA, rat subcutaneous paw tissue was collected by a sharp scalpel and immediately minced in cold lysis buffer containing a complete Protease Inhibitor Cocktail (dissolved in PBS, pH 7.4, one tablet/10 ml lysis buffer) (**Table 9**). Homogenate samples were kept on ice until being transferred into a -80°C freezer. One day before further usage for cytokine detection, the frozen homogenate was taken out from the freezer and transferred into a 4°C fridge and left overnight, allowing complete cytokine release from incubated cells in tissue lysates. Tissue lysates were centrifuged at 14×1000 g for 10 min to remove the debris, and the supernatant was aliquoted and prepared for further application on Cytokine Array to detect relative expression levels of individual cytokine analytes, or ELISA in order to assess the quantified concentrations of individual cytokines. Procedures for sample preparation were conducted according to [45].

Rat Cytokine Array: Cognate immobilized capture Ab was pre-coated on the membrane of the Rat Cytokine Array kit. The sample supernatant and detection Ab mixture was then incubated. Cytokine antigen and detection Ab complex were bound. After removing the unbounded capture Ab on the membrane, Streptavidin-horseradish peroxidase (SA-HRP) was then subsequently added. The membrane was visualized using enhanced chemiluminescence solution (ECL) by FluorChem FC2 MultiImage II. Integrated density value (IDV) of duplicated spots (representing individual cytokine according to the datasheet) was analyzed with FluorChem FC2 MultiImage II. The percentage of intensity of each cytokine level relative to the positive control was calculated and analyzed by statistical software.

Individual ELISA kits: Each kit for measuring IL-1alpha, IL-1beta, IFN-gamma, CXCL10, TNF-alpha, IL-4 or IL-13 was used according to the manufacturer's instructions. A general summary for the principles of ELISA including all applied kits in this thesis: a specific capture Ab of one cytokine was pre-coated on the wells of the microplate provided in each kit and nonspecific binding sites were blocked. Standards, controls and samples were pipetted into the wells sequentially, and any cytokine antigen presented would simultaneously bind to the immobilized pre-coated captured Ab. Unbound reagents were removed by a wash buffer after a specific enzyme-linked Ab was added. Following the addition of subtract solution, which acted on the bound enzyme to produce color; the intensity of the color was proportionally determined by the level of the targeted cytokine bound complex. The addition of sulfuric acid stopped the solution changing the color, enabling accurate measurement of the intensity of the targeted cytokine bound complex at 450 nm using an ultraviolet/visible (UV/Vis) spectrophotometry (Sunrise® Tecan). A standard curve was automatically drawn from a serial dilution of known-concentration solution of the target molecule. The concentration for each sample was automatically calculated referring to the optical density (O.D.) values that were compared to standard curve. The measured concentration of each sample was multiplied by its respective dilution factors if

samples have been diluted prior to the assay and then further applied for statistical analysis.

Table 9: Ingredients of tissue lysis buffer

20 mM Imidazole hydrochloride
100 mM KCL
1 mM MgCl2
10 mM EGTA
1 mM EDTA
10 mM NaF
1 mM Na2MoO4
1.0% Triton X-100
0.1 M PBS, pH 7.4

2.2.8 RNA extraction, cDNA transcription and reverse transcription-polymerase chain reaction (RT-PCR)

RNA extraction: At 72 and 96 h post CFA, rat subcutaneous paw tissues were collected, following an immediate translocation into a -80°C freezer until proceeding with RNA extraction. Before RNA isolation, the tissue samples were thawed on ice after adding 1ml TRIzol® and were subsequently homogenized with sterilized stainless steel beads (5 mm) from Tissuelyser (frequency: 20 Hz, time: 4 min) [45], and then kept on ice for 6 min in order to completely release the protein, DNA and RNA. 200 µl of chloroform was added in order to form the detached phases. The upper phase containing the RNA was collected and transferred into a fresh tube with 500 µl isopropanol (100%) inside. Following complete vortex, RNA was kept in isopropanol at -20°C overnight (maximal 4 days). On the second day, RNA was centrifuged (13.6×1000 rpm, 5 min, 4°C), the obtained RNA enriched supernatant was washed with 75% ethanol. It was subsequently spun down and centrifuged (5.2×1000 rpm, 5min, 4°C) in order to get a RNA pellet loaded tube, which was further dried at 37°C for 10 min and resuspended in 100 µl nuclease free water. The final suspension was

incubated in Eppendorf Thermalmixer® (1.4×1000 rpm, 57°C) for 10 min, and then aliquoted and stored in -80°C before cDNA transcription.

cDNA transcription: 10 µl cDNA of a mixture volume of cDNA reagent was aliquoted into a 96-well reaction template. Components from High-Capacity cDNA Reverse Transcription Kit for the reaction plate were described in **Table 10**. After calculating the extracted RNA concentration, an equal volume of 10 µl master mix as well as a corresponding volume (µl) of 1 µg purified RNA was sequentially added and reversely transcribed into cDNA according to a well established program with the Thermal cycler (25°C for 10 min, 37°C for 120 min, 85°C for 5 min) and was held at 4°C. cDNA products were aliquoted and kept at -80°C before PCR amplification.

RT-PCR: 25 µl of PCR reaction mixture were shown in **Table 11** amplified by RT-PCR with Taqman gene expression assays for rat CXCL10 (labeled with FAM; Assay ID: Rn01413889_g1) and GAPDH (glyceraldhyde-3-phosphate dehydrogenase, labeled with VIC) as a housekeeping gene. FAM or VIC refers to specific compatible fluorescein-based 5' end reporter dye. Sequences of FAM/VIC labeled primers were kept confidential from Invitrogen/Life Technologies. Thermal cycling conditions were established according to the manufacturer's instructions: 50 cycles of melting for 15 s at 95°C and followed annealing and extension for 1 min at 60°C. Two different RT-negative controls were conducted: all the reagents were added with either 1) replacement of cDNA by sterilized water or 2) replacement of enzyme mix "ABsolute QPCR ROX Mix" (Thermo Fisher Scientific, Ulm, Germany) with sterilized water in order to evaluate the contamination from genomic DNA or other sources which would lead to artificial positive amplification in reverse transcription reaction. As a result of the relatively uniform expression in inflamed and non-inflamed paw tissue compared to beta-actin and 18SrRNA in preliminary trials (data not shown), GAPDH was chosen as an optimal housekeeping gene control.

Data analysis: C_T values were calculated using the $2^{\Delta\Delta C_T}$ method ($^{\Delta\Delta C_T} = {}^{\Delta C_T}$ sample – $^{\Delta C_T}$ calibrator) for relative quantification (RQ). C_T values of inflamed paw normalized

to non-inflamed paw were used. ΔC_T was calculated by normalized C_T values of samples minus C_T values of GAPDH (calibrator). The relative quantification values $2^{\Delta\Delta C_T}$ were obtained by individual $2^{\Delta C_T}$ dividing the average $2^{\Delta C_T}$ values, and further applied for statistical analysis.

Table 10: Pipetting scheme of cDNA reaction plate

Reagent	Volume
Reverse Transcription buffer (10 ×)	2 µL
Deoxynucleoside triphosphates (DNTPs, 25 ×)	0.8 µL
MultiScripe™ Reverse Transcriptase	1 µL
Random primers (10 ×)	2 µL
Ribonuclease (RNase) Inhibitor	1 µL
Nuclease-free H2O	3.2 µL

Table 11: Pipetting scheme of PCR reaction template

Reagent	Volume
ABsolute QPCR ROX mix	12.5 µL
Taqman gene expression assay (20 ×)	1.25 µL
Nuclease-free H2O	6.25 µL
cDNA (1:10 diluted)	5 µL

2.2.9 Immunohistochemistry staining (IHC)

Tissue preparation: At 96 h CFA, rats were anesthetized with isoflurane and fixed in supine position. Right before recovering from anesthesia, rats were transcardially perfused with PBS (0.1 M, pH 7.4) containing heparin (0.66 ml heparin in 100 ml PBS, 20 ml/rat) to prevent coagulation and then continuously perfused with 4% paraformaldehyde (PFA, dissolved in PBS, pH 7.4, 150 ml/rat) (fixative solution) in order to remove the blood from circulatory vessels. Procedures were referring to

previous investigations [46]. The subcutaneous tissues adjacent to the plantar skin were collected from both inflamed and non-inflamed hind paws, post-fixed in the same fixative solution for 1.5-2 hours, and then cryoprotected in 10% sucrose solution at 4°C overnight. All solutions were freshly prepared prior to experiments. The tissue samples were embedded in tissue-Tek compound, and kept frozen in -80°C. 7 μm thick sections were obtained using Cryostat and mounted on gelatin-coated glass slides.

Double immunoflourescence staining: The tissue sections mounted on slices were incubated for 60 min in PBS containing 0.3% Triton X-100, 1% BSA, 10% goat serum (Vector Laboratories, CA, USA) as blocking solution to prevent nonspecific binding. The slices were then incubated overnight with the following primary Abs: 1) polyclonal rabbit anti-rat END or -ENK or -DYN (all diluted in 1:1000) in combination with monoclonal mouse anti-CD68 (ED1, 1:400) or 2) mouse anti-CXCR3 (1:500) in combination with polyclonal rabbit anti-rat macrophage antiserum (1:200). After incubation with primary Abs, the tissue slices were washed with PBS (3×20 min) and then incubated with Texas red conjugated goat anti-rabbit Ab (1:250) in combination with fluorescein isothiocyanate (FITC) conjugated donkey anti-mouse Ab (1:250). Thereafter, the tissue sections were washed with PBS, and the nuclei were stained bright blue with 4',6-diamidino-2-phenylindole (DAPI) (0.1 μg/ml in PBS). Finally, the tissue slices were washed in PBS and mounted in Vectashield (Vector Laboratories). To demonstrate specificity of the staining, omission of either the primary or the secondary Abs was performed.

Image obtaining and analyzing: After staining, selected sections of all samples were scanned and imaged with a confocal laser scanning microscope (LSM). Three fields from three samples within one group were pictured and further applied for image analysis by NIH Image J software. The percentage of double-labeled macrophages

found in all single stained macrophages was calculated for all images. The average of three percentage values within one group was used for statistical analysis. Analyzer for percentage calculation and statistical analysis was blinded.

2.2.10 Fluorescence-activated cell sorting (FACS)

Tissue digestion: At the time point of 96 h CFA, rat subcutaneous paw tissues were collected. Cellular staining was performed by using the supernatant of homogenized tissue fraction for flow cytometry analysis in accordance with previous descriptions [26]. Freshly obtained rat subcutaneous inflamed and non-inflamed paw tissues were firstly homogenized into 1-2 mm fragments and digested for 1 h in 37°C with a digestive solution of 10 ml RPMI 1640 medium containing 30 mg collagenase, 10 mg hyaluronidase, and 0.5 ml 1M HEPES (3 ml digestive solution/sample, freshly prepared). The digested fragments were then pressed through a 70 μm nylon filter (BD Pharmingen^{TM}) to isolate pure cell suspension from tissue debris. Purified cell suspensions were washed with PBS and centrifuged (1.2×1000 rpm, 10 min), supernatant was discarded and cell pellet was resuspended in PBS and aliquoted into FACS tubes. After centrifuge (1.2×1000 rpm, 10 min), cells were coated on the bottom of FACS tube and resuspended in PBS.

Double staining:

All solutions were freshly prepared prior to experiment.

1) **For extracellular staining**: Pure cell suspensions were simultaneously incubated with a pre-tested optimal volume of 10 μl mouse anti-rat-CD3-FITC (recognizing T cells, 0.5 μg/μl) and 5 μl mouse anti-rat-CD45-phycoerythrin (PE)-Cy5 Ab (identifying all hematopoietic cells, 0.2 μg/μl) for 30 min in dark at room temperature (RT), stained cell suspensions were washed by PBS and centrifuged (1.2×1000 rpm, 10 min).

2) **For intracellular staining**: Cells were firstly fixed in 1% PFA (30 min, 250 µl/tube) and cell membrane was permeabilized by saponin (0.5% saponin, 0.5% BSA, 0.05% NaN3 in PBS). After centrifuge, supernatant was discarded and the left 50 µl cell suspensions were simultaneously stained with 10 µl mouse anti-rat-ED1-FITC (marking the CD68 antigen expressed on monocytes/macrophages, 0.1 µg/µl) and 5 µl mouse anti-rat-CD45-PE-Cy5 Ab for 30 min in dark (RT). Saponin and PBS were sequentially used to wash the cells. Stained cell suspensions were washed by PBS and centrifuged (1.2×1000rpm, 10 min).

Following centrifuge, supernatant was discarded and stained samples were resuspended in PBS and freshly analyzed within 24 h; for later analysis: cells were fixed by 1% PFA (30 min, 250 µl/tube), resuspended in PBS (2 ml/tube) and then stored at 4°C prior to application.

Flow cytometry analysis: 10.000 events were set up and acquired by the FACS Scan (BD Pharmingen™). Data analysis was performed by using CellQuest software (BD Pharmingen™). Multicolor was applied for identifying subpopulations of stained cell suspensions that were grouped by forward scatter (FSC) and sideward scatter (SSC). Percentage of subgroup cells were shown in Dot Plot graphics.

2.2.11 Western blot (WB)

Sample preparation: Subcutaneous paw tissues of the rat at 96 h post CFA were immersed in radioimmunoprecipitation lysis buffer (RIPA) (**Table 12**) containing complete protease inhibitor cocktail (one tablet/10 ml RIPA) and were homogenized with sterilized stainless steel beads (5 mm) by Tissuelyser (frequency: 20 Hz, time: 10 min). Sample supernatant was diluted (5:1) in Laemmli buffer (5×, **Table 13**) and kept

in -20°C before use.

BCA (bicinchoninic acid) protein assay: The protein level of the inflamed paw tissue lysate was determined using Pierce BCA protein assay kit. Standards test tube protocol and 96-well microplate procedure were used in accordance with the manufacturer's instructions. Albumin standard dilutions were prepared in the range from 20 to 2000 µg/ml in RIPA buffer (without complete protease inhibitor) and measured in triplicate (25 µl/well). 10-fold diluted samples (in RIPA buffer) were also measured in triplicate (25 µl/well). Reagent A and B were mixed (50:1) and used as a working reagent (200 µl/well), followed by a thorough mixture for the microplate on the shaker (30 s). The plate was covered and incubated at 37°C for 30 min. The plate was then cooled down to RT and the absorption at 540 nm was measured using an UV/Vis spectrophotometry (Sunrise® Tecan) after incubation. The concentration of each sample was calculated referring to the O.D. values that were interacted with the values on a linear standard curve.

Western blot: 25 µg of protein of inflamed paw tissue lysate diluted in Laemmli buffer was separated on a 10% sodium dodecyl sulfate-polyacrylamide gel electrophoresis (SDS-PAGE, 50 V for 30 min and then 150 V for 80 min) (**Table 14**) by Volt POWER Supply and then immobilized onto nitrocellulose membranes (15 V, 90 min). The extracted membranes were blocked at RT for 1 h with 5% nonfat milk in Tris-buffered saline with 0.05% Tween20 (TBS-Tween), and the incubation was performed at 4°C overnight (with agitation of 50 rpm) with mouse-monoclonal-anti-MOR (1:500), rabbit-polyclonal-anti-DOR (1:250) or rabbit-polyclonal-anti-KOR (1:1000). Mouse-monoclonal-anti-GAPDH (1:2000) was loaded as a control. Following washing with TBS-Tween (3×10 min), the membranes were continuously incubated at RT (with agitation of 50 rpm) for 1 h with anti-mouse secondary Ab (1:5000) or anti-rabbit secondary Ab (1:3000) conjugated to horseradish peroxidase, dissolved in TBS-Tween with 2.5% nonfat milk and 2.5%

BSA. Blots were washed repeatedly with TBS-Tween (3×10 min) prior to detection.

Image obtaining and densitometric analysis: Protein bands-loaded membranes were visualized using ECL for 1 min and were then immediately exposed to the autoradiography camera for 3-10 min. IDV of each protein band was determined. Analysis was performed within the same blot. The differences of raw IDV values of the target protein and GAPDH were firstly calculated. Then relative IDV values of target protein to the average IDV of GAPDH were calculated. The individual relative value was normalized to the average value of all samples and further applied for statistical analysis. Both scanning and densitometric analyzing were performed using FluorChem FC2 MultiImage II system.

Table 12: Recipe of RIPA buffer

25 mM HEPES, pH 7.6
2 mM EDTA
25 mM NaF
1% SDS ultrapure

Table 13: Recipe of Laemmli buffer

250 mM Tris, pH 6.8
2% SDS ultrapure
10% Glycerol
1% Beta-Mercaptoethanol
2 mM EGTA
1 mM PMSF
0.2% Bromophenol Blue

Table 14: Components of 10% SDS-PAGE

H_2O
Acrylamide/Bis (30:2)
3M Tris, pH 8.8
10% SDS
10% APS
TEMED

2.2.12 Rat macrophages harvest and stimulation by CXCL10 (Release)

Rat macrophages harvest and isolation: Inflammatory peritoneal rat macrophages were harvest and obtained at 96 h post intraperitoneal (i.p.) injection of 3% thioglycolate [46]. Rats were intracardially sacrificed by an overdose of potent sedative drug T61 (300 µl/rat) [47]. Peritoneum lavage was performed (i.p.) with EDTA (0.2 M, 100 µl) containing PBS (20 ml). Macrophages enriched peritoneal fluid was collected and diluted in EDTA/PBS (400 µl 0.2 M EDTA in 30 ml PBS) on ice. Freshly isolated macrophages suspension was purified by sequential addition of 0.2% and 1.6% hypotonic NaCl to lyse the debris of red blood cells. Cell suspensions were spun down (1.2×1000 rpm, 10 min) and resuspended in PBS. Cell numbers were counted 1:20 in Trypan Blue. Following centrifuge (1.2×1000 rpm, 10 min), cells were resuspended in HBSS containing the proteinase inhibitors bestatin (40 µg/ml), aprotinin (1 µg/ml) and thiorphan (25.33 µg/ml), and concentration of resuspended cells was adjusted to 0.5×10^6 cells/100 µl.

Release: Before stimulation, the concentrations of all reagents were adjusted in proteinase inhibitor containing-HBSS as diluent. Purified rat macrophages co-incubated with selected doses of recombinant rat CXCL10 (0.01, 0.1 and 1 ng) were agitated on a shaker (700 rpm, 37°C) following a pre-incubation with

cytochalasin B (5 mg/ml) for 5 min [29]. The dose range of CXCL10 was adjusted in accordance with behavioral and pilot experiments. HBSS and ionomycin (10 μM) were used as a solvent control and a positive control. Supernatants were obtained after 15 min stimulation. Acquired cellular suspension was centrifuged (4×1000 rpm, 5 min) and supernatants were then stored at -20°C until further analysis was conducted by ELISA using commercially available kits for rat END detection.

2.3 Experimental design

Before experiments, all animals were randomly divided to CFA + EA (CFA rats with EA treatment), CFA + sham (CFA rats with sham EA treatment) as well as CFA (CFA rats without treatment).

1. Changes of nociceptive threshold were daily measured from day 0 to day 6 (0-144 h) and paw volume and temperature were simultaneously assessed. Antagonists of opioid receptors (NLX, NTI) or Abs against opioid peptides (anti-END, -ENK and -DYN) were respectively applied (i.pl.) at 96 h post CFA; nociceptive threshold changes were assessed 5 min post injection.
2. Rat Cytokine Array for 29 cytokines was performed at 96 h CFA to firstly discover the positively expressed cytokines/chemokines in the inflamed paw by EA treatment, and then ELISA was conducted to quantify the protein level of selected cytokines/chemokines from Cytokine Array and to recognize targeted cytokine/chemokine. The following RT-PCR experiments were performed to detect mRNA level of targeted chemokine CXCL10 by CFA + EA treatment in the inflamed paw tissue taken at both 72 and 96 h post CFA. Subsequent double immunostaining of the inflamed paw tissue (96 h CFA) for macrophages (ED1 or anti-macrophages serum) with either each opioid peptide (END, ENK and DYN) or CXCR3 (CXCL10 receptor) were performed.

3. CFA rats were administered (i.pl.) with CXCL10 (0.2 ng) or CFA + EA rats were injected (i.pl.) with the CXCL10 blocking Ab (2 μg) either at 96 h CFA or daily performed (0-4 day, 5 times). Nociceptive thresholds were correspondingly assessed. Double immunostaining with monocytes/macrophages (ED1) and opioid peptides for inflamed tissue daily (0-4 day, 5 times) treated with CXCL10, or the Ab against CXCL10, was applied.
4. Opioid receptor levels were evaluated by WB at 96 h CFA. Opioid peptide release (END) from CXCL10 stimulated rat macrophages *in vitro* was detected by ELISA.

2.4 Statistical analysis

All data were presented as mean ± SEM. Multiple measurements at one time point between two or more than two groups were analyzed by t-test or one way analysis of variance (ANOVA), respectively. Multiple measurements at different time points between two or more than two groups were analyzed by two way repeated measurements (RM) ANOVA. The Holm-Sidak method was used for one way ANOVA and the Student-Newman-Keuls Method was used for two way RM ANOVA. * $P < 0.05$ or ** $P < 0.01$ was regarded as statistically significant (Significance between CFA + EA and CFA + sham was represented by $^{\$}p < 0.05$, and significance between CFA + sham and CFA was represented by $^{\#}p < 0.05$, showed in **Fig. 10 and 11**).

3. Results

3.1 Acupoint positioning and needling were modeled by computer-based 3D rat model

As illustrated before, accurate position of acupoint is the premise of achieving "De Qi" sensation, however, unclear acupoint location on animals in previous studies hampered the reproducible application by subsequent researchers. An anatomically accurate skeleton based rat model created by Maya 2012 clearly displayed essential acupoint positioning for GB-30 Huantiao in a 3D space. Acupuncture needles were inserted bilaterally into the GB-30 Huantiao. Needling angle, depth and relative location to bony marks could be distinctly visualized by rotating the model from all perspectives, although the visualized perspectives were restricted by two-dimensional image shown in **Fig. 8**.

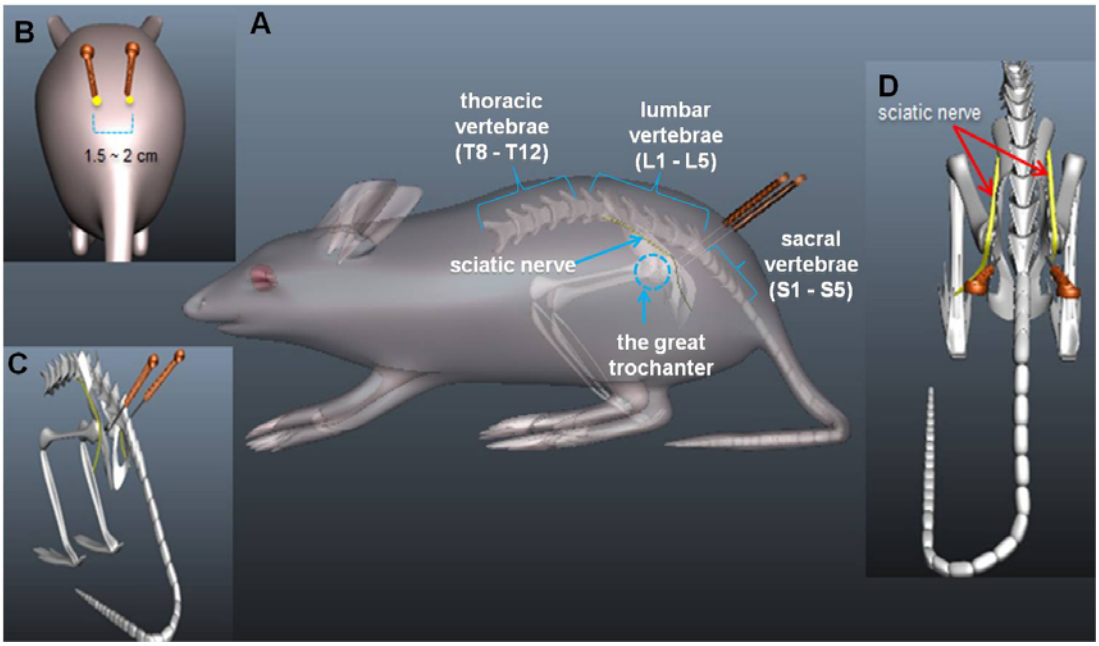

Fig. 8: GB-30 Huantiao needling essential exhibited by computer-based three-dimensional (3D) rat model. The needles were inserted perpendicularly into

GB-30 Huantiao. [**A**] Acupoint location and needling on GB-30 Huantiao was modeled by 3D computer-based rat model. [**B**] Distance between bilateral needles inserted on GB-30 Huantiao (yellow dots) was approximately 1.5-2 cm from rear perspective. [**C, D**] Needle tips perpendicularly inserted underneath GB-30 Huantiao reached nearby tissues of sciatic nerve from side or vertical view (Figure and legend were modified from **Fig. 1** in [5]).

3.2 Optimal parameter selection for EA by comparison of different frequencies

EA-induced antinociception in the central nervous system (CNS) was validly attributed as frequency-dependent (**Fig. 1**). However, which frequency and treatment setting could produce optimal sustained analgesia has not been very well examined. Rather than testing multiple parameters and examining their effects on antinociception, this thesis initially focused on evaluating the potential different nociceptive effects between multiple frequencies, with other pre-established parameters including intensity (2-3 mA), pulse width (0.1 ms) and duration (20 min) on acupoint GB-30 Huantiao according to early researcher [16]. This allowed us to evaluate differences in the frequencies (including 10, 2/100, 120 and 100 Hz) and timing of the EA application (One EA treatment at 0 h CFA or two EA treatments at both 0 and 24 h CFA). The frequencies were selected according to pilot experiments (data not shown). Thermal nociceptive thresholds changes (paw withdrawal latency, PWL) were assessed. Treatment of 2/100, 120 and 100 Hz displayed distinctive features of nociception (**Fig. 9B-D**) whereas 10 Hz produced a small anti-hyperalgesia effect without significance (**Fig. 9A**). Since the purpose of this study was principally concerned with tonic analgesia at a late phase of CFA (72-96 h), it was manifest that high frequency 100 Hz (**Fig. 9D**) and an alternatively changed frequency 2/100 Hz (**Fig. 9B**) showed comparable postponed antinociception at 72 and 96 h CFA, and obviously that one treatment of each frequency potentiated the maximal effect obtained at 72 h. Due to the mechanisms for high frequency 100 Hz were scantly

understood from previously restricted investigations, this frequency was thereby selected for following study. Two treatments of 100 Hz further extended the maximal effect from 72 to 96 h, which exactly matched the initial assumption (**Fig. 9E**).

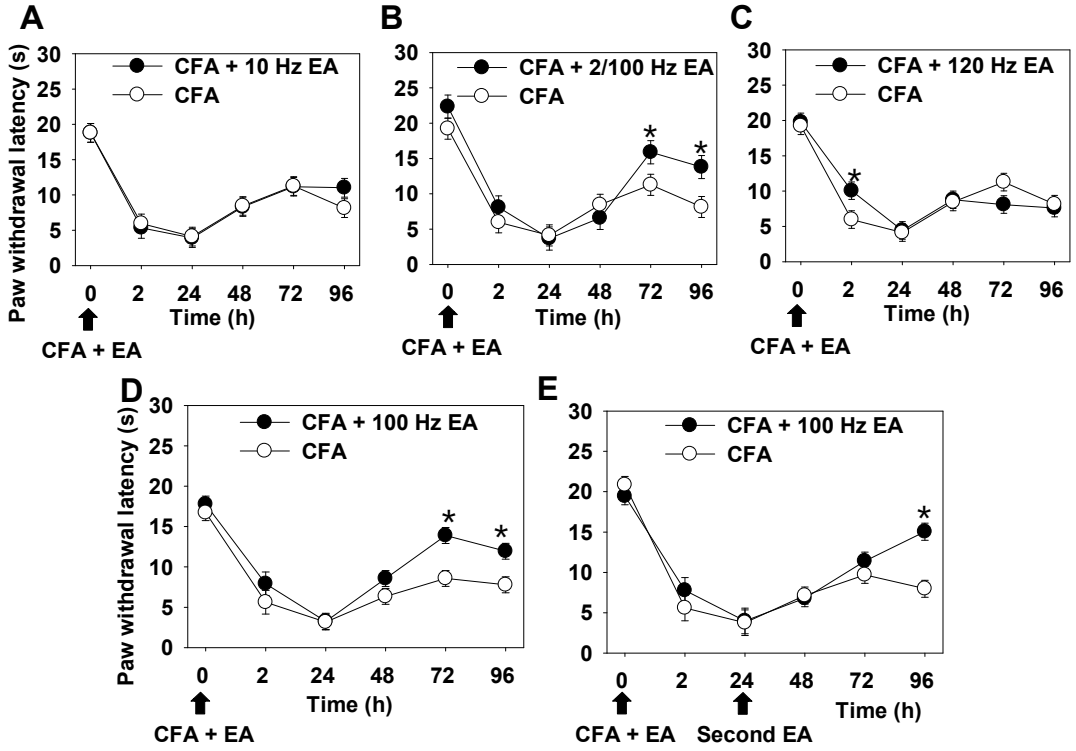

Fig. 9: EA produced thermal antinociception was frequency-dependent. EA treatments (0.1 ms, 2-3 mA, 20 min) with different frequencies (10, 120, 2/100 or 100 Hz) on bilaterally GB-30 Huantiao were performed on rats with CFA inflammation. [**A-D**] One EA treatment with selected frequencies was applied. Thermal nociceptive thresholds (paw withdrawal latency, PWL) were measured at given time points (0, 2, 24, 48, 72 and 96 h). [**E**] Two treatments (0 and 24 h) of 100 Hz EA (0.1 ms, 2-3 mA, 20 min) were performed. PWL was assessed at same time points. Data were shown as mean ± SEM (n = 6 per group, *p < 0.05, CFA + EA versus CFA; two way RM ANOVA, Student-Newman-Keuls, n = 6 per group). (Figure and legend were modified from **Fig. 2** in [5]).

3.3 EA produced sustained antinociception and anti-inflammation

Optimal EA settings (two treatments at 0 and 24 h, frequency: 100 Hz, intensity: 2-3 mA, pulse wide: 0.1 ms, duration: 20 min) was established by thermal nociceptive assessment in **Fig. 9**. The further question was asked whether the same setting could also produce comparable mechanical antinociception. To suggest the specificity of EA-produced antinociception, sham-EA treatment was applied as an additional control. Two treatments of optimal EA settings reversed mechanical (PPT) and thermal hyperalgesia (PWL) respectively at different time points (**Fig. 10A, B**). The mechanical antinociception started at 48 h (**Fig. 10B**), earlier than thermal antinociception (**Fig. 10A**) and sustained until 144 h post CFA (**Fig. 10C**). There was a reversal effect on PPT at 96 h by sham EA treatment compared to the CFA control (**Fig. 10B**).

The anti-inflammatory effect was considered by early researchers to be frequency -dependent [48] whereas other researchers provided conflicting information [8]. For the purpose of distinguishing the current discrepant conclusions, inflammatory indicators including volume and temperature of inflamed paw from either EA, sham-EA or CFA treatment were selected and compared to evaluate the inflammation elicited by CFA. The daily assessment of changes of paw volume and temperature from 0 to 144 h CFA demonstrated that EA could significantly decrease the inflamed paw temperature at both 72 and 144 h compared to CFA control, whereas the significance between EA and sham-EA occurred only at 72 h (**Fig. 11A**). Paw volume was attenuated by EA in comparison with sham-EA and CFA control at 72 and 144 h respectively (**Fig. 11B**). No difference between sham-EA and CFA control was observed at each time point.

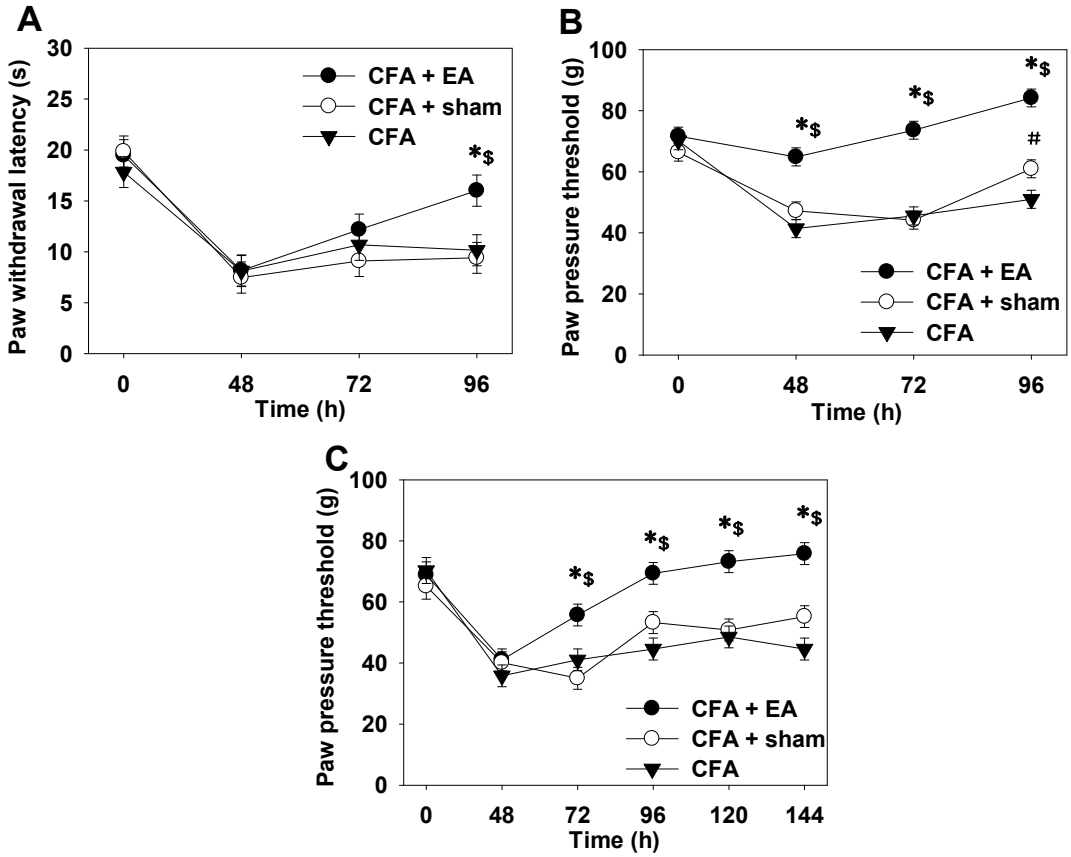

Fig. 10: Sustained mechanical and thermal antinociception were produced by two applications of EA. Optimal EA settings (frequency: 100 Hz, intensity: 2-3 mA, pulse wide: 0.1 ms, duration: 20 min) was applied at 0 and 24 h on rat treated (i.pl.) with CFA. [**A, B**] Paw pressure threshold (PPT) and paw withdrawal latency (PWL) were daily assessed at 0, 48, 72 and 96 h (n = 6 per group). [**C**] Changes of PPT were measured up to 144 h post CFA (n = 8 per group). Data were shown as mean ± SEM (*$p < 0.05$, CFA + EA versus CFA; $^{\$}p < 0.05$, CFA + EA versus CFA + sham; $^{\#}p < 0.05$, CFA + sham versus CFA; two way RM ANOVA, Student-Newman-Keuls). (Figure and legend were modified from **Fig. 3** in [5]).

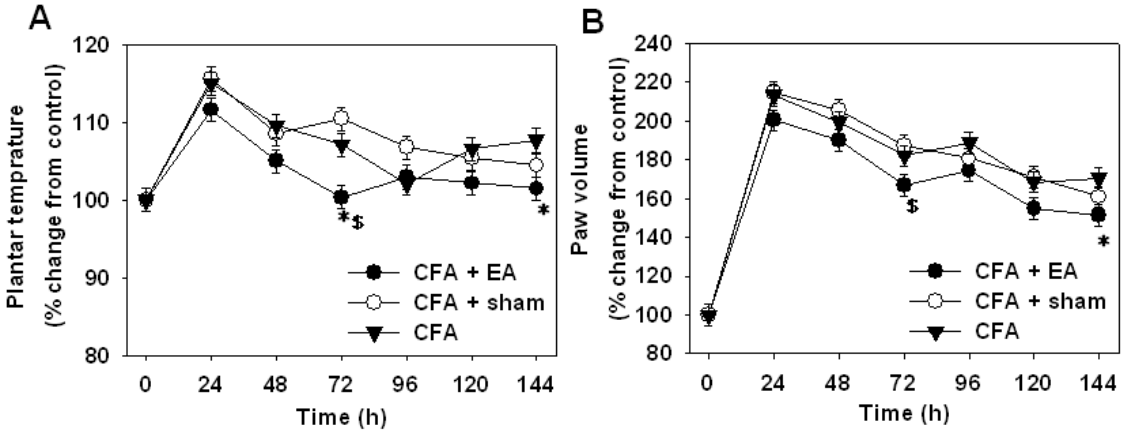

Fig. 11: EA reduced CFA-evoked paw swelling and increased temperature. Rats injected (i.pl.) with CFA received two EA treatments at 0 and 24 h as described before. [**A**] Skin temperature of inflamed plantar was repeatedly assessed (7 times, daily, 0 to144 h post CFA). [**B**] Inflamed paw volume was evaluated at same time points. Data were shown as mean ± SEM (n = 8 per group, *$p < 0.05$, CFA + EA versus CFA; $^{\$}p < 0.05$, CFA + EA versus CFA + sham; two way RM ANOVA, Student-Newman-Keuls). (Figure and legend were modified from **Fig. 5** in [5]).

3.4 Peripheral endogenous opioids contributed to tonic antinociception of EA

Opioid receptors in past decades were thought to play a role in EA-produced analgesia from both clinical and experimental studies majorly via pre-EA application of antagonists of opioid receptors [4,11,14,16,49], frequently referring to MOR antagonist NLX or Cys2, Tyr3, Orn5, Pen7-amide (CTOP), DOR antagonist NTI as well as KOR antagonist nor-binaltorphimine (Nor-BNI).

In a previous study, we illustrated that MOR and DOR as well as opioid peptide END and ENK were involved in tonic analgesia at an early phase (2 h) of CFA by post-CFA administration of NLX, NTI or Abs of each opioid peptide [29] (**Fig. 5**). In order to explore whether opioid receptor MOR and DOR mediated tonic antinociception produced by current EA settings at a late phase (96 h) of CFA,

optimal doses of NLX (0.56 ng) and NTI (25 μg), determined by pilot experiments (**Fig. 12A, B**) and early studies [29] were injected (i.pl.) and distinctly showed reversal of EA-induced antinociception at 96 h CFA (**Fig. 12C, D**). Of note, the mechanical threshold of sham-EA was not affected by an identical dose of NLX (**Fig. 12C**).

Depending on the frequency used, opioid peptides were released from perfusate of subarachnoid space of spinal cord by EA [15] (**Fig. 1**). To understand the role of peripheral opioid peptides in tonic antinociceptive effects at high frequency (100 Hz) EA, optimal doses of blocking Abs against opioid peptides (anti-END, -ENK, -DYN) determined from preliminary experiments and the study mentioned above [29] were post-EA administered at 96 h CFA respectively. Increased mechanical hyperalgesic thresholds of EA were suppressed by each performance of the Abs (**Fig. 13D, E, G**) whereas thermal hyperalgesic thresholds of EA were only inhibited by anti-END and -ENK (**Fig. 13A, B**) 5 min post injection. Simultaneous injection of anti-END and anti-ENK Abs did not produce better effects than single injections of each Ab (**Fig. 13F**).

Depending on the comparison between all mechanical and thermal hyperalgesic tests, we discovered:

1. Mechanical antinociception of EA was evidently addressed earlier (starting from 48 h CFA (**Fig. 10B**) and in a more sustained manner (up to 144 h CFA, **Fig. 10C**) than thermal antinociception (**Fig. 10A**) which is also partially in line with former research demonstrating better mechanical than thermal hyperalgesic suppression by EA [50].

2. There was extensive involvement of opioid peptides (END, ENK and DYN) in mechanical anti-hyperalgesia (**Fig. 13D-G**) whereas only END and ENK were

involved in thermal anti-hyperalgesia (**Fig. 13A-C**).

Additionally, the mechanism of mechanical hyperalgesia was distinct from the thermal hyperalgesia, as reported by previous studies, therefore only mechanical nociceptive measurement was applied in subsequent investigations.

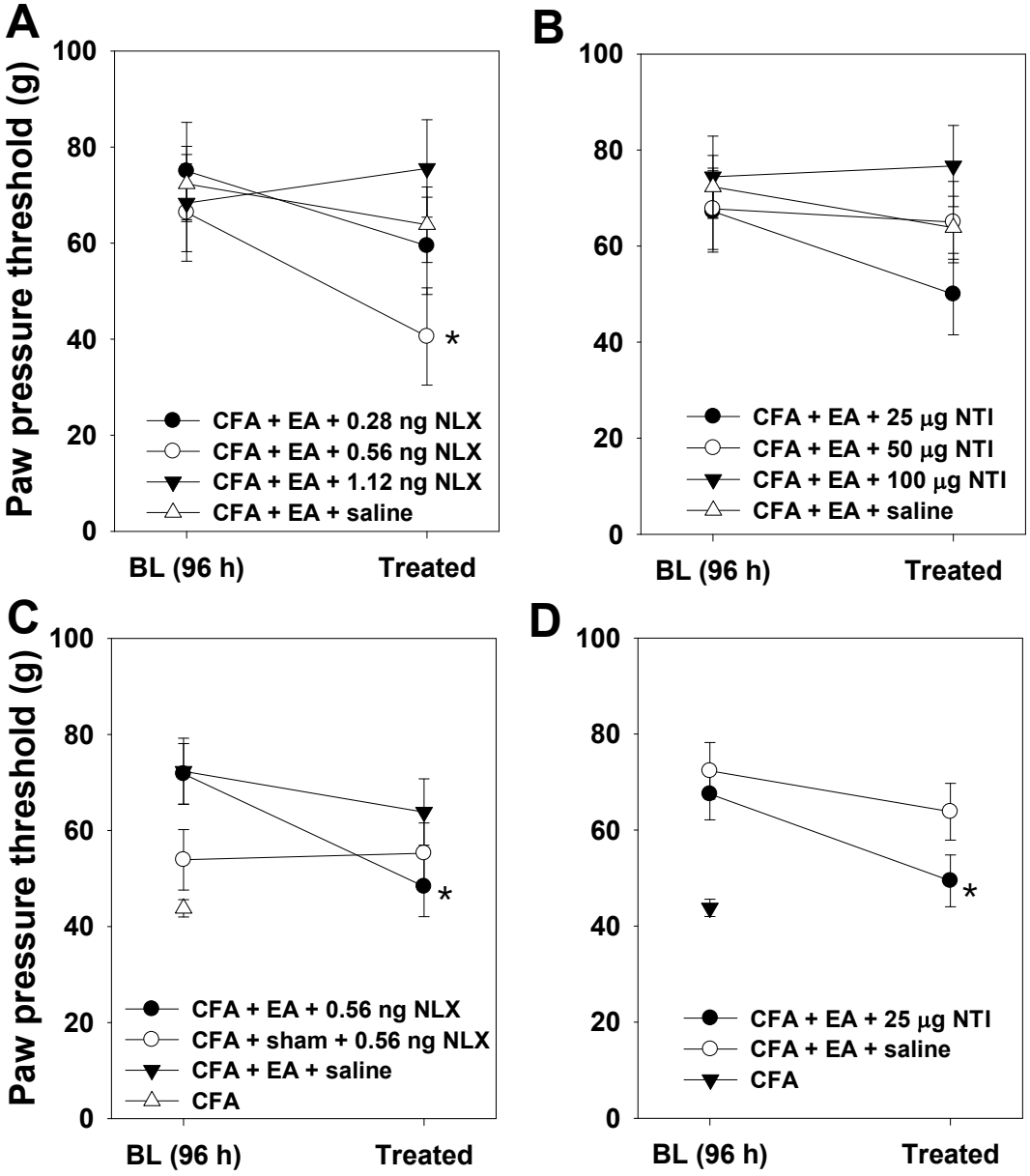

Fig. 12: Antagonists of MOR (naloxone, NLX) and DOR (naltrindole, NTI) reversed EA-induced mechanical antinociception at late phase (96 h) of CFA. Rats with CFA inflammation were treated with two EA treatments (at 0 and 24 h, 100

Hz, 2-3 mA, 0.1 ms, 20 min) or sham-EA. [**A, B**] Dose-response experiments were designed to establish the optimal dose of the opioid receptor antagonists, Paw pressure threshold (PPT) changes were assessed following administration (i.pl.) of selected doses of NLX (0.28, 0.56 and 1.12 ng) and NTI (25, 50 and 100 µg) in EA treated rats were measured before (baseline: BL) and 5 min after injection (Treated) (n = 3-5 per group). [**C, D**] Optimal doses of NLX (0.56 ng) and NTI (25 µg) were further applied (i.pl.) on EA or sham-EA treated rats, PPT were measured before (BL) and 5 min (Treated) post injection. Identical amount of solvent (saline) was administered (i.pl.) as control. Pain thresholds of CFA rats (CFA) at 96 h were only presented for comparison but not for statistical analysis (n = 6 per group). Data were shown as mean ± SEM (*p < 0.05, CFA + EA + NLX/NTI versus CFA + EA + saline, or, CFA + EA + NLX/NTI versus CFA + sham + NLX versus CFA + EA + saline; two way RM ANOVA, Student-Newman-Keuls). (Figure and legend were modified from [5]).

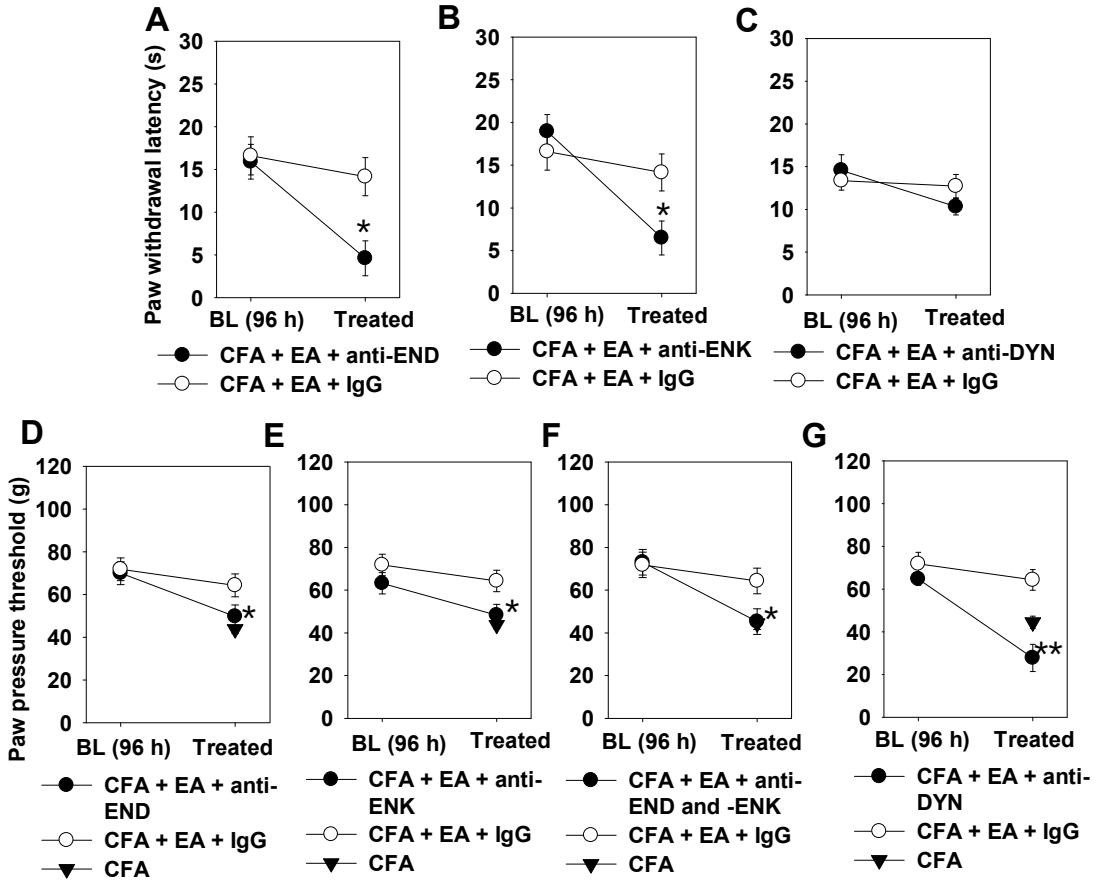

Fig. 13: EA attenuated CFA-induced hyperalgesia via peripheral opioid peptides at late stage (96 h) of CFA. Anti-END (2 µg [**A, D**]), anti-ENK (1.25 µg [**B, E**]), combination of anti-END and –ENK [**F**] or anti-DYN (1 µg [**C, G**]) was administered

(i.pl.) at 96 h CFA on rats with two EA treatments (at 0 and 24 h, 100 Hz, 0.1 ms, 20 min, 2-3 mA). Control animals were injected with identical doses of rabbit IgG or received CFA without EA treatment. Paw withdrawal latency [**A-C**] or paw pressure threshold [**D-G**] was determined before (BL: baseline) and 5 min after injection (Treated). CFA without EA treatment (CFA) was included as basal threshold of inflamed paw for comparison but not for statistical analysis. Data were shown as mean ± SEM (n = 6 per group, *p < 0.05, **p < 0.01, CFA + EA + anti-END/ENK/DYN versus CFA + EA + IgG; two way RM ANOVA, Student-Newman-Keuls). (Figure and legend were modified from [51]).

3.5 EA selectively regulated expressions of certain cytokines/chemokines

Aiming to find out whether local cytokines at inflammation site were modulated by EA at late phase (96 h) of CFA, relative levels of a total of 29 cytokines in inflamed or non-inflamed paw tissue from rats treated with CFA or CFA + EA were evaluated by Cytokine Array (**Fig. 14**).

In accordance with Cytokine Array, protein levels of seven cytokines/chemokines (CXCL10, IFN-gamma, TNF-alpha, IL-1alpha, IL-1beta, IL-4, IL-13) which displayed promising signals were further quantified by ELISA. Pro-inflammatory cytokines including TNF-alpha (**Fig. 15A**) and IL-1beta (**Fig. 15C**) were apparently downregulated by EA whereas IL-1alpha (**Fig. 15B**) was not affected. The anti-inflammatory cytokine IL-13 (**Fig. 15E**) was distinctly upregulated by EA whereas IL-4 (**Fig. 15D**) was barely regulated. Intriguingly, pro-inflammatory cytokine IFN-gamma was not commonly upregulated (**Fig. 15F**).

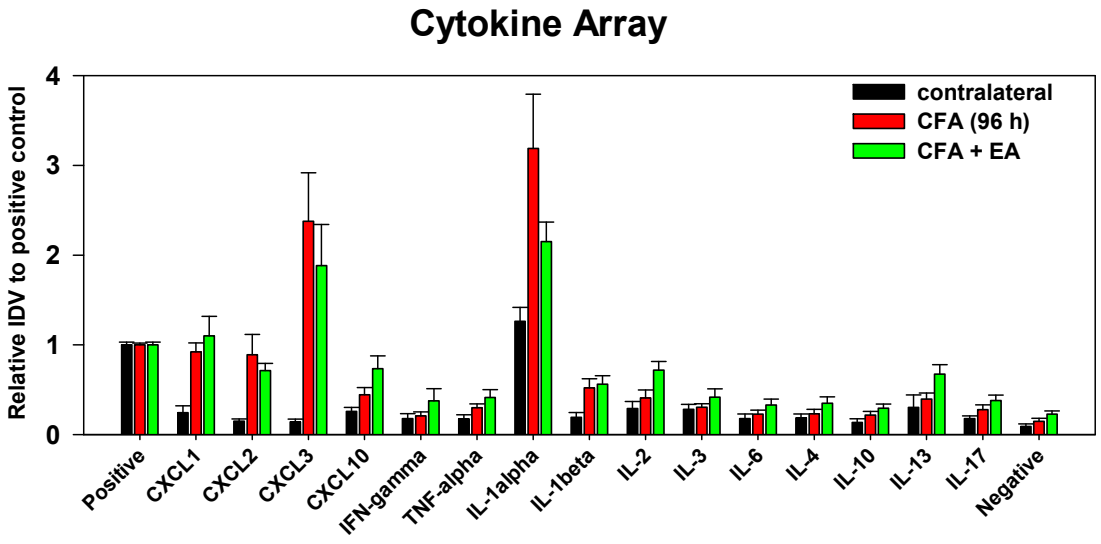

Fig. 14: Partial restoration of local cytokine profile by EA at late phase (96 h) of CFA. At 96 h CFA, rats with CFA inflammation were randomly treated with/without EA and grouped as CFA and CFA + EA. Inflamed and non-inflamed (contralateral) paw tissue were used for Cytokine Array. Local 29 cytokines signals (values were displayed as integrated density value (IDV) of each cytokine relative to positive control) were detected by Cytokine Array and selectively exhibited with 4 chemokines (CXCL1, CXCL2, CXCL3 and CXCL10) and 11 cytokines including IFN-gamma, TNF-alpha, IL-1alpha. IL-1beta, IL-2, IL-3, IL-6, IL-4, IL-10, IL-13, IL-17. Data were presented as mean ± SEM in all groups; non-inflamed (contralateral) paw tissue was included only for comparison but not for statistical analysis. No difference was observed between EA treatment and CFA control for each cytokine/chemokine (n = 5-6 per group, CFA + EA versus CFA, t-test).

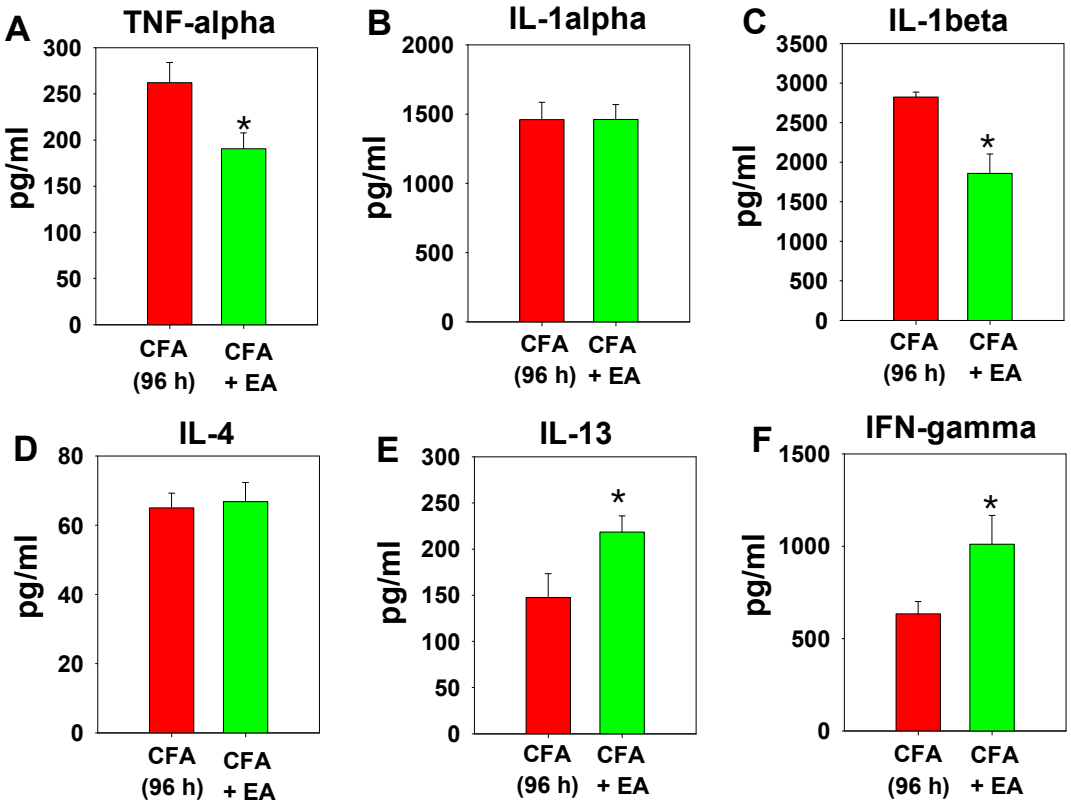

Fig. 15: EA alternatively regulated expressions of certain cytokines/chemokines at late phase (96 h) of CFA. Rats with CFA inflammation were randomly treated with/without EA and grouped as CFA and CFA + EA. At 96 h CFA, protein levels (pg/ml) of cytokines including IFN-gamma, TNF-alpha, IL-1alpha, IL-1beta, IL-4, IL-13 in inflamed paw were quantified by ELISA as a result of comparatively promising expression from Cytokine Array in **Fig. 14**. Data were shown as mean ± SEM (n = 5-6 per group, CFA + EA versus CFA, t-test). (Figure and legend were modified from [51]).

3.6 Upregulation of CXCL10 and CXCR3-expressing macrophages were associated with EA

IFN-gamma inducible chemokine CXCL10 was initially recognized as chemoattractant for T cells and monocytes [52]. Upregulation of IFN-gamma by EA potentiated subsequent experiments to concentrate on chemokine CXCL10, due to the former studies on antinociceptive property of CXC-chemokines in relieving CFA

inflammatory pain [27] (**Fig. 4**). EA remarkably promoted both the protein and mRNA level of CXCL10 (**Fig. 16A, B**). Since no change was seen on CXCL10 protein level in sham-treated animals (**Fig. 16A**), the sham-EA group was excluded from further mRNA analysis (**Fig. 16B**).

Peripheral opioid peptides secretion at the early stage of CFA (2 h) was mainly attributed to infiltrating neutrophils whereas inflammatory monocytes/macrophages (> 60%) were mainly the reason for opioid peptide secretion at the late phase (48-96 h) of CFA. At late phase (96 h) of CFA, only a small subpopulation of infiltrating T cells (< 5%) was identified, confirmed early conclusions [26] (**Fig. 17**).

Known from chemokine receptor CXCR3-unique receptor of CXCL10 [53], as well as the increased transcription and translation level of CXCL10 by EA in **Fig. 16**, the receptor availability for CXCL10 was evaluated by double staining for CXCR3 and macrophage in inflamed tissue. Co-expression content was analyzed. CXCR3 expression was observed on the vast majority of infiltrating macrophages (**Fig. 18A**). As expected, EA markedly enhanced the amount of $CXCR3^+$ expressing macrophages in all marked cells in comparison to CFA control (**Fig. 18B**).

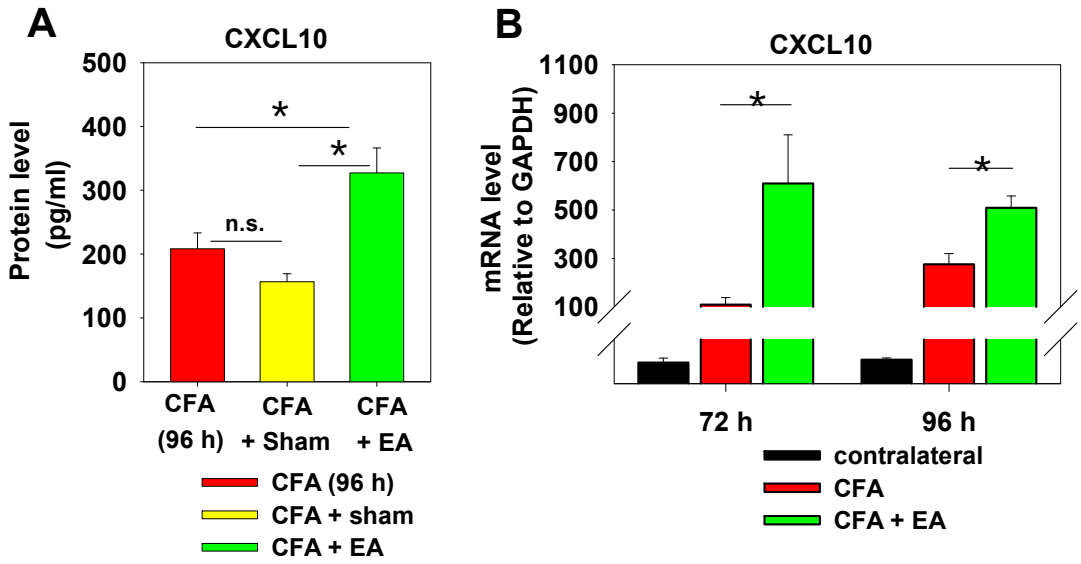

Fig. 16: Upregulation of CXCL10 by EA at late phase (72-96 h) of CFA. [**A**] All rats with CFA inflammation randomly received treatment with EA or sham-EA, and grouped as (CFA + EA), (CFA + sham) and CFA. At 96 h, ELISA was applied to quantify the level (pg/ml) of CXCL10 in subcutaneous paw tissue from each group; [**B**] mRNA level was detected by RT-PCR (tissue taken from 72 and 96 h), non-inflamed paw (contralateral) was only showing as a negative control instead of applying for statistical analysis. Data were shown as mean ± SEM (For ELISA: n = 6 per group, *p < 0.05, CFA + EA versus CFA + sham versus CFA, one way ANOVA, Holm-Sidak method; For RT-PCR: n = 6 per group, *p < 0.05, CFA + EA versus CFA; t-test). (Figure and legend were modified from [51]).

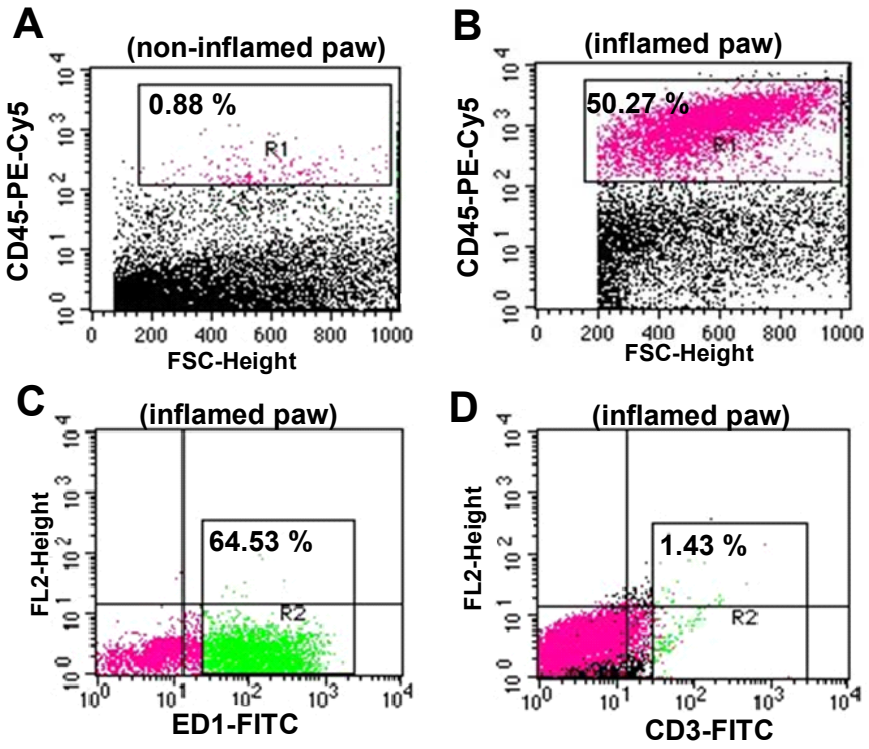

Fig. 17: ED1 positive tissue monocytes/macrophages constituted the major subtype of leukocytes at late phase (96 h) of CFA. Cells suspensions from subcutaneous non-inflamed **[A]** or inflamed **[B]** paw tissue were first stained. Dot Plot graphics showed the gate R1 on CD45-PE-Cy5 marked hematopoietic cells ratio in non-inflamed (0.88%) or inflammatory paw tissue (50.27%) (X-axis: forward scatter (FSC), Y-axis: CD45-PE-Cy5). $CD45^+$ cells were further stained for ED1-FITC identifying monocytes/macrophages [**C**] or CD3-FITC recognizing T cells [**D**]. Dot Plot graphics showed double stained hematopoietic cells gated on R2 for $CD45^+ED1^+$ (64.53%) or $CD45^+CD3^+$ (1.43%) cell group (X-axis: ED1/CD3-FITC, Y-axis: PE). Only representative samples are shown (n=4-5 for each staining).

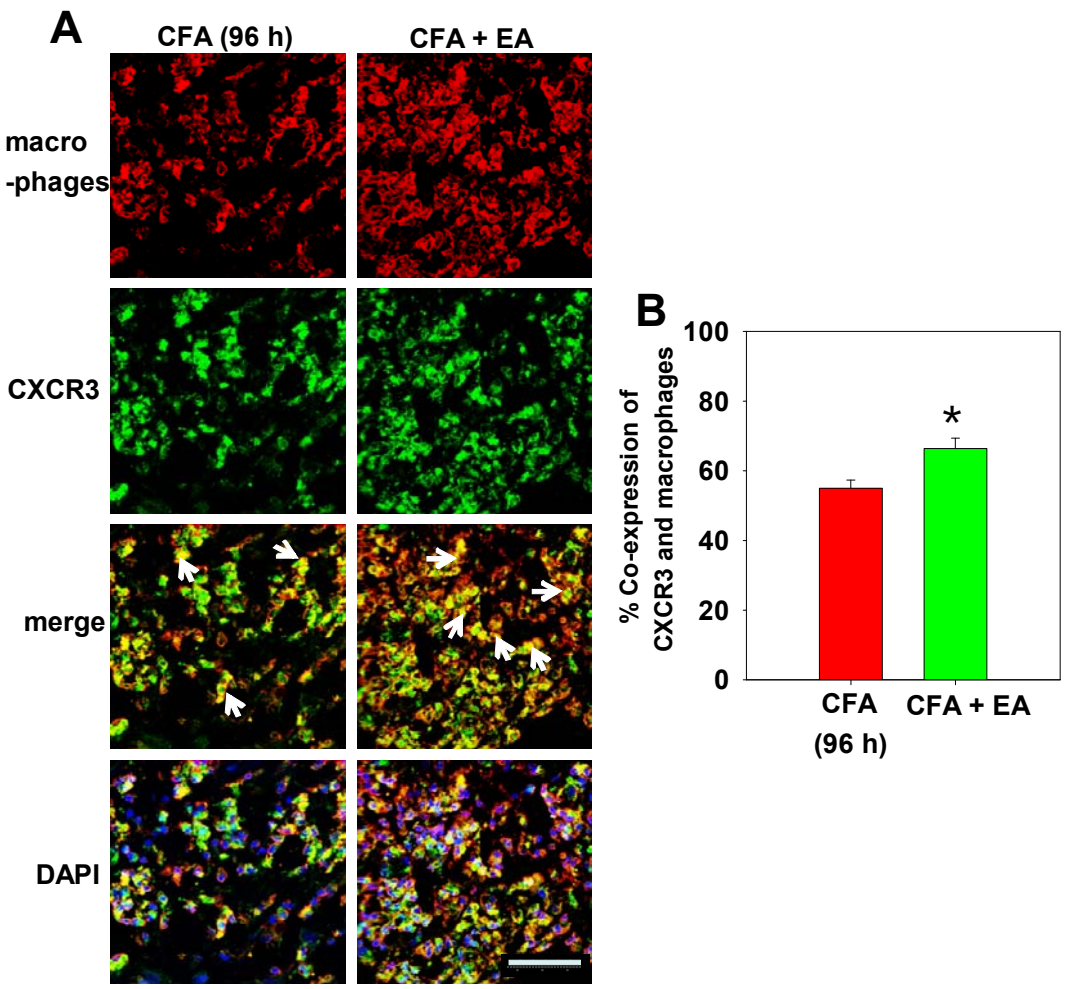

Fig. 18: Upregulation of CXCR3$^+$ macrophages in inflamed paw tissue by EA at late phase (96 h) of CFA. [**A**] At 96 h CFA, double staining on slices from inflamed tissue treated with/without EA was performed with rabbit anti-macrophage antiserum (red), mouse anti-CXCR3 (green). DAPI (blue) were stained to recognize cell nuclei. White arrows were pointing at double positive cells (Scale bar: 50 µm). [**B**] Quantification analysis displayed the ratio (%) for overlapping content of CXCR3 with macrophages in total amount of macrophages marked by antiserum. All data were presented as mean ± SEM (n = 3 per group, *$p < 0.05$, CFA + EA versus CFA; t-test). (Figure and legend were modified from [51]).

3.7 EA increased opioid peptides expression on recruited monocytes/macrophages

Not only central (**Fig. 1**) but also peripheral opioid peptides [17] contributed to EA induced antinociception. EA has been indicated to be responsible for robust upregulation of END expression on ED1 marked infiltrating monocytes/macrophages in inflamed paw at 6 days post CFA [3]. Since all three opioid peptides have been involved in EA-triggered antinociception (**Fig. 13**), we intended to figure out whether and how opioid peptide expression on monocytes/macrophages was regulated by current EA settings in the inflamed paw. Double staining on monocytes/macrophages (ED1 marked) with each opioid peptide (Abs against END, ENK and DYN) was performed (**Fig. 19A-C**). Quantification analysis showed EA increased expression ratio (approximately 75% for ENK, 65% for END and 60% for DYN) of all three opioid peptides on ED1 positive monocytes/macrophages compared to CFA rats, whilst no change was obtained between sham-EA and CFA treatment (**Fig. 19D**).

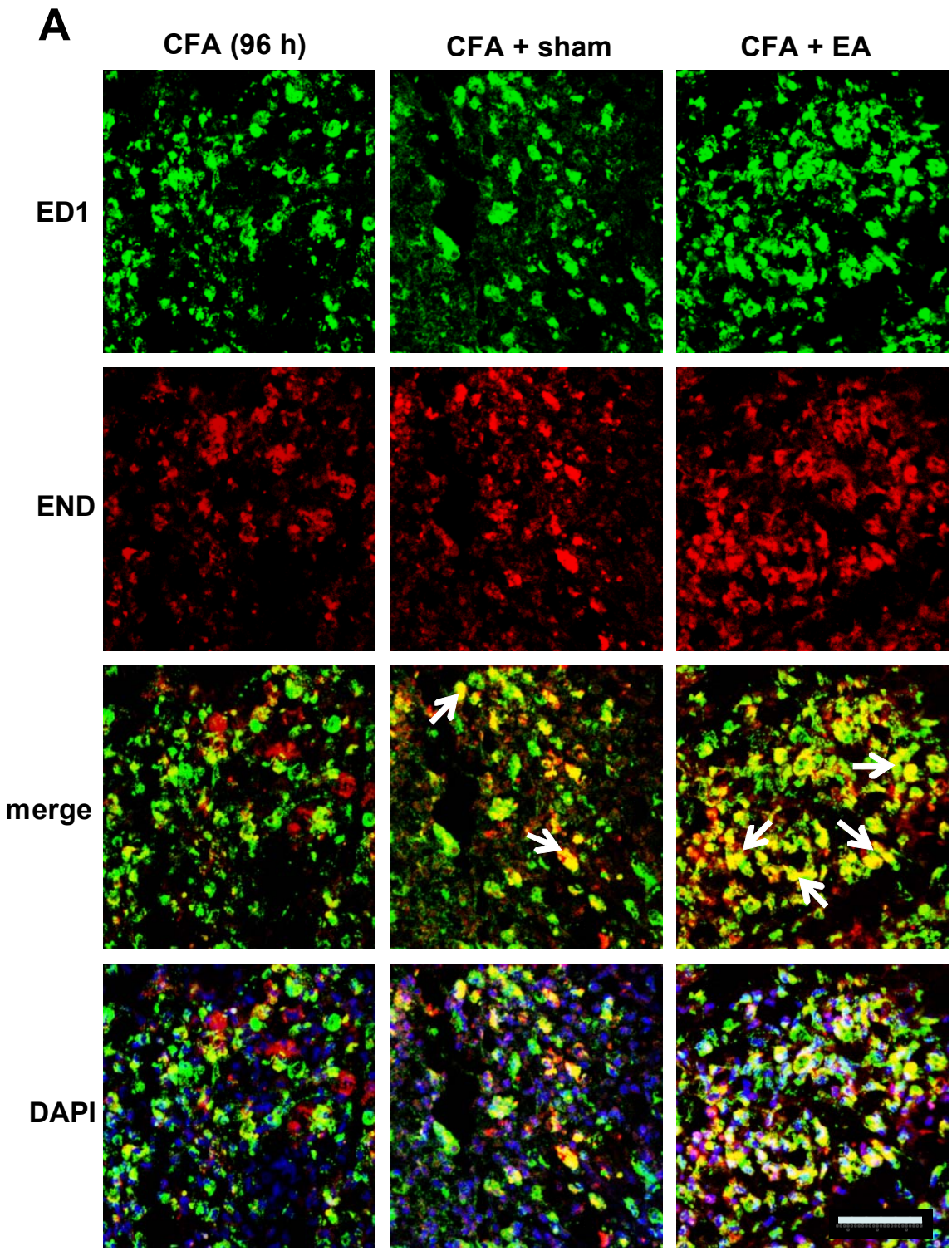
A
CFA (96 h)
CFA + sham
CFA + EA
ED1
END
merge
DAPI

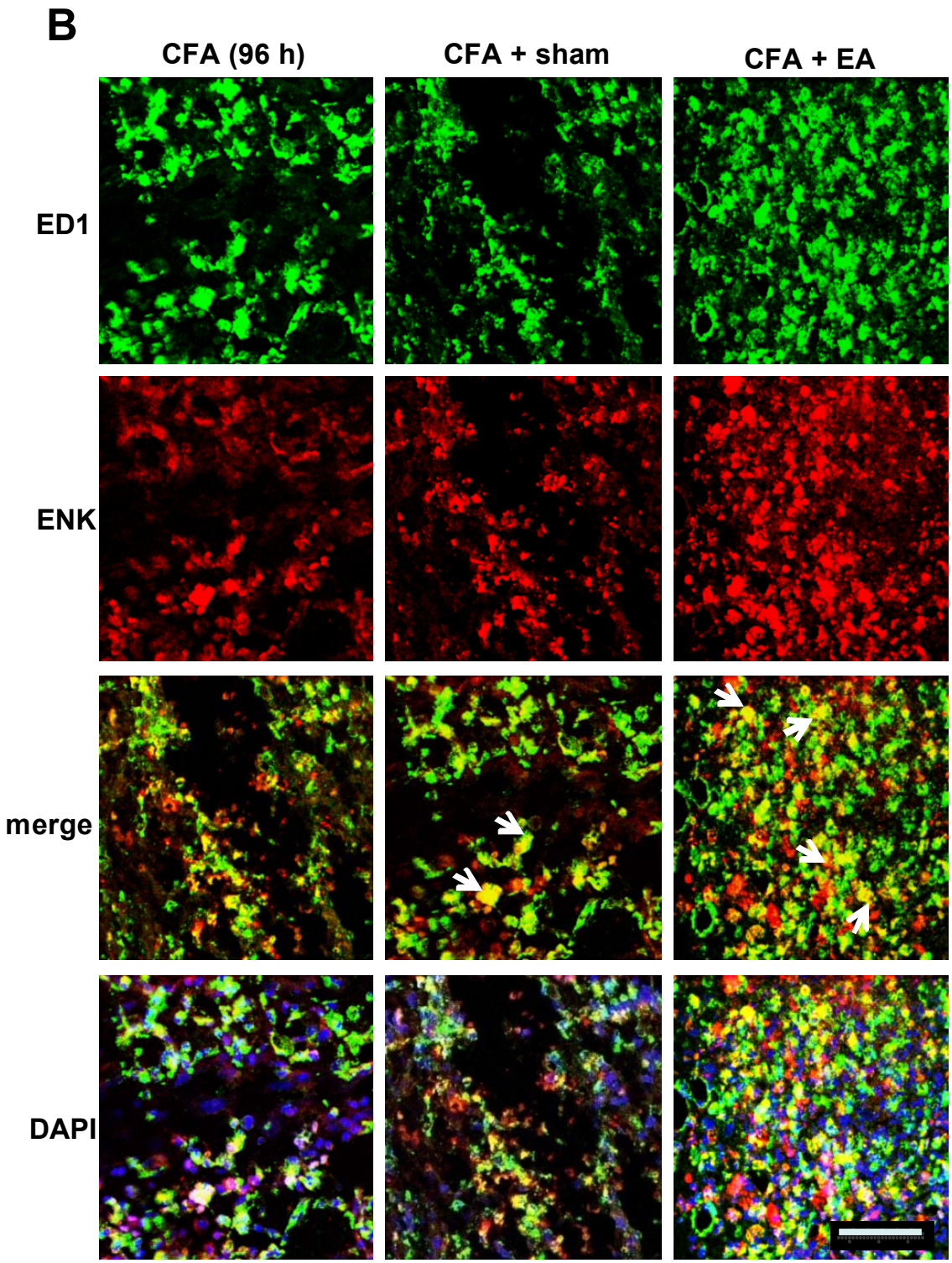
B
CFA (96 h)
CFA + sham
CFA + EA
ED1
ENK
merge
DAPI

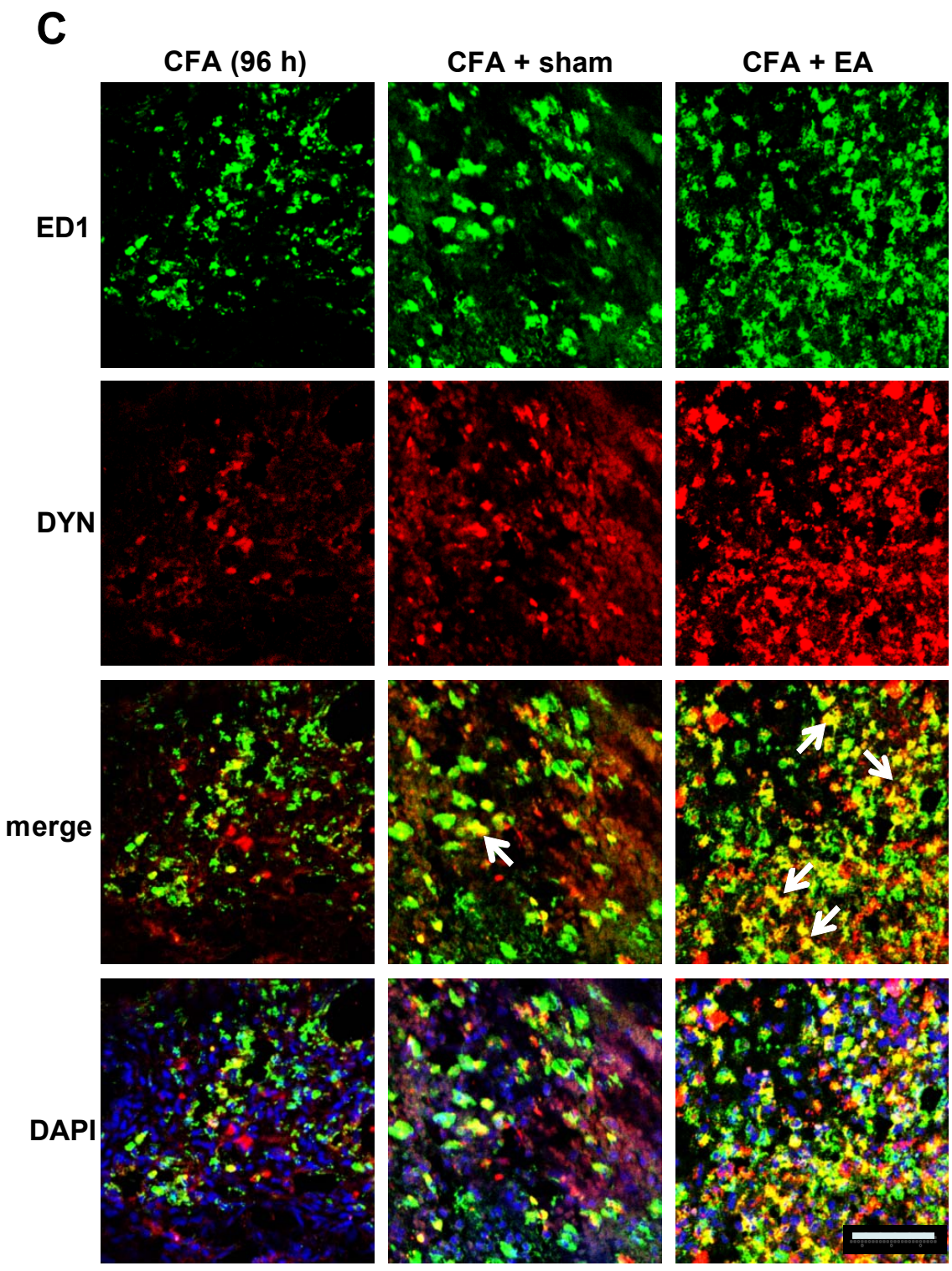
C
CFA (96 h)
CFA + sham
CFA + EA
ED1
DYN
merge
DAPI

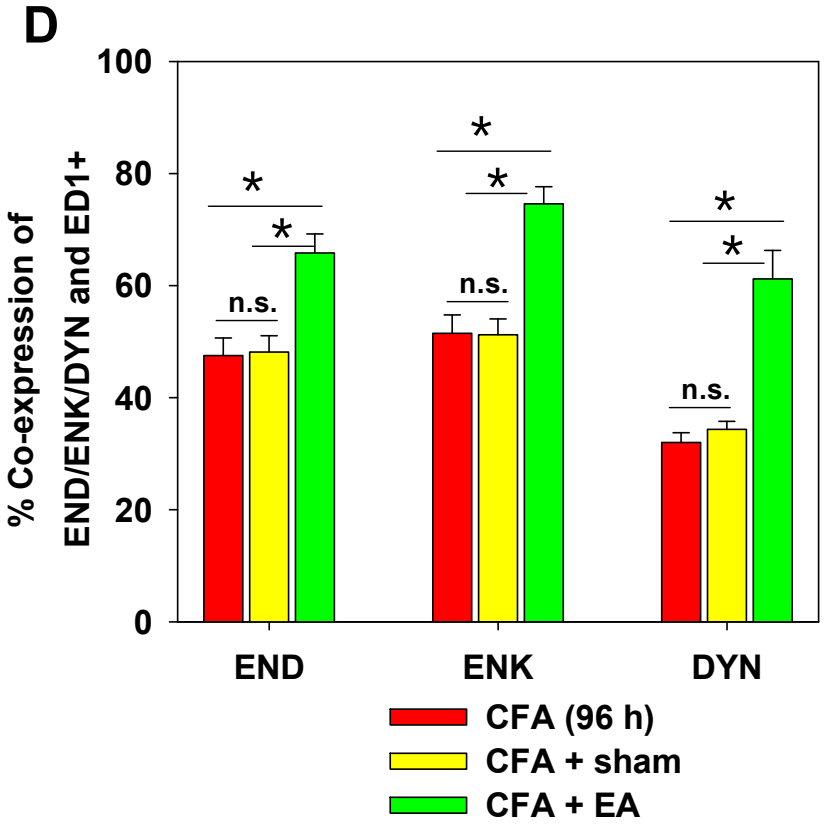

Fig. 19: EA promoted the opioid peptide expression on monocytes/macrophages at late phase (96 h) of CFA. All rats with CFA inflammation were randomly treated with EA or sham-EA, and grouped to (CFA), (CFA + EA), (CFA + sham). [**A-C**] Double immune staining with mouse anti-ED1 (CD68, identifying monocytes/macrophages, green) and rabbit anti-END/-ENK/-DYN respectively (All marked as red) was performed. Nuclei of cells were marked with DAPI (Blue). White arrows were pointing at double positive cells (Scale bar: 50 μm). [**D**] Quantification analysis displayed the ratio (%) of double positive ED1 marked monocytes/macrophages in total amount of $ED1^+$ cells. Data were shown as mean ± SEM (n = 3 per group, *$p < 0.05$, one way ANOVA, CFA + EA versus CFA + sham versus CFA, Holm-Sidak method) (Figure and legend were modified from [51]).

3.8 CXCL10 reversed CFA-induced mechanical hyperalgesia via peripheral opioid peptides

To our knowledge, certain chemokines were recognized as peripheral opioid-dependent antinociceptive in CFA induced inflammatory pain. At 2 h CFA, local administration (i.pl.) of chemokine CXCL2/3 dose-dependently attenuated mechanical hyperalgesia which was associated with promoted migration of neutrophils leading to opioid peptide (END and ENK) release regulated by intracellular Ca^{2+} level [27].

Since chemokine CXCL10 was markedly upregulated by CFA + EA treatment in former experiments (**Fig. 16)**, we then speculated that CXCL10 and CXCL2/3 might share common mechanisms. Mechanical threshold changes were assessed in pilot experiments after single local administration (i.pl.) of different doses of rat recombinant CXCL10 (0.2, 2, 20 and 200 ng; data not shown). 0.2 ng CXCL10 better suppressed mechanical hyperalgesia than other doses and was chosen for subsequent studies. Time-course experiment for single application (i.pl.) of 0.2 ng CXCL10 at 96 h displayed persistent anti-hyperalgesic effect until 3 h post injection (**Fig. 20A**) and daily application of an identical dose of CXCL10 fundamentally reversed mechanical pain threshold of CFA-elicited hyperalgesia (**Fig. 20B**). To further understand the mechanism, changes of nociceptive thresholds were evaluated following concomitant administration (i.pl.) of repeated CXCL10 (daily performance, from 0-4 day, 5 times) with each opioid peptide Ab (anti-END, -ENK, -DYN; acute performance, at 96 h). Complete reversed thresholds at 5 and 15 min post injection by anti-END, -ENK or -DYN suggested a peripheral opioid peptide-dependent feature of CXCL10 induced antinociception (**Fig. 20C-E**).

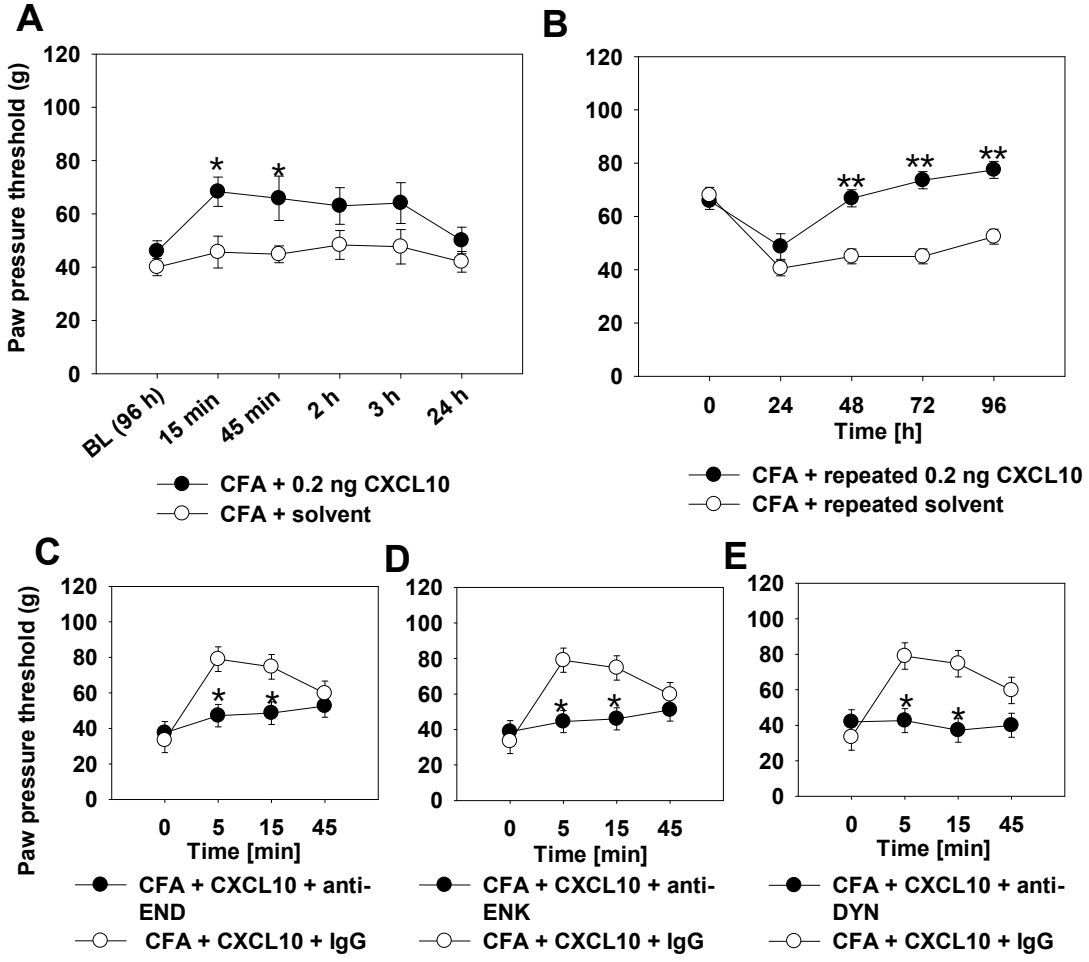

Fig. 20: Sustained mechanical antinociception elicited by CXCL10 was opioid peptide–dependent. Rats injected (i.pl.) with CFA received acute (at 96 h) or repeated (5 times, daily from 0 to 96 h) application with CXCL10 (0.2 ng) or solvent control. [**A**] 0.2 ng CXCL10 was i.pl. applied at 96 h CFA and paw pressure threshold (PPT) were was evaluated before (BL) and 5, 15, 45 min and 2, 3, 24 h after injection. [**B**] 0.2 ng CXCL10 was daily applied (i.pl.) and changes of PPT were daily determined at 0, 24, 48, 72 and 96 h before each injection. Data were shown as mean ± SEM (n = 6 per group, *p < 0.05, **p < 0.01, CFA + CXCL10 versus CFA + solvent; two way RM ANOVA, Student-Newman-Keuls). [**C-E**] At 96 h CFA, rabbit anti-END (2 µg), -ENK (1.25 µg) or -DYN (1 µg) was respectively administered (i.pl.) on rats with daily treatment of CXCL10 (0.2 ng). Changes of PPT were assessed until 45 min post injection. Rabbit IgG was applied (i.pl.) as control. Data were presented as mean ± SEM (n = 6 per group, *p < 0.05, **p < 0.01, CFA + CXCL10 + anti-END/ENK/DYN versus CFA + CXCL10 + IgG; two way RM ANOVA, Student-Newman-Keuls) (Figure and legend were modified from [51]).

3.9 CXCL10 enhanced opioid peptides expression on accumulated monocytes/macrophages *in vivo* instead of triggering opioid peptide release *in vitro*

Likewise, for the question raised whether the same mechanism accounts for this antinociceptive action of CXCL10, we performed identical staining with ED1 marked monocytes/macrophages and opioid peptides (END/ENK/DYN) respectively for the inflamed paw repeatedly treated with CXCL10. The expression of three opioid peptides on $ED1^+$ monocytes/macrophages was extensively enriched in CXCL10 treated tissue compared to solvent control treatment (**Fig. 21A-C**). CXCL10 increased the expression content of opioid peptides on $ED1^+$ monocytes/macrophages to 72% (ENK), 63% (END) and 55% (DYN) (**Fig. 21D**).

In view of the opioid-dependent antinociceptive effect of CXCL10 on rats, we further hypothesized CXCL10 might stimulate opioid peptide release from inflammatory rat macrophages *in vitro*. Thus far, incubation of human CD14+ monocytes and rat macrophages with ionomycin (10 μm) led to a significant release of END [29] theoretically due to elevated calcium intracellular level [54]. Ionomycin was thereby incubated as positive control in the present study. Isolated peritoneal rat macrophages were obtained 96 h following application (i.p.) of 3% thioglycolate. Three doses (1, 0.1 and 0.01 ng) of recombinant rat CXCL10 were chosen and 15 min was selected for incubation in accordance with preliminary experiments (data not shown). Short-term incubation (15 min) time was selected due to the optimal effect in pilot experiments in comparison with longer incubation times (60, 120 min and 24 h) (data not shown). Incubation of rat macrophages with ionomycin (10 μm) led to a remarkable END secretion whereas no difference was observed between each dose of CXCL10 and solvent control HBSS **(Fig. 22)**.

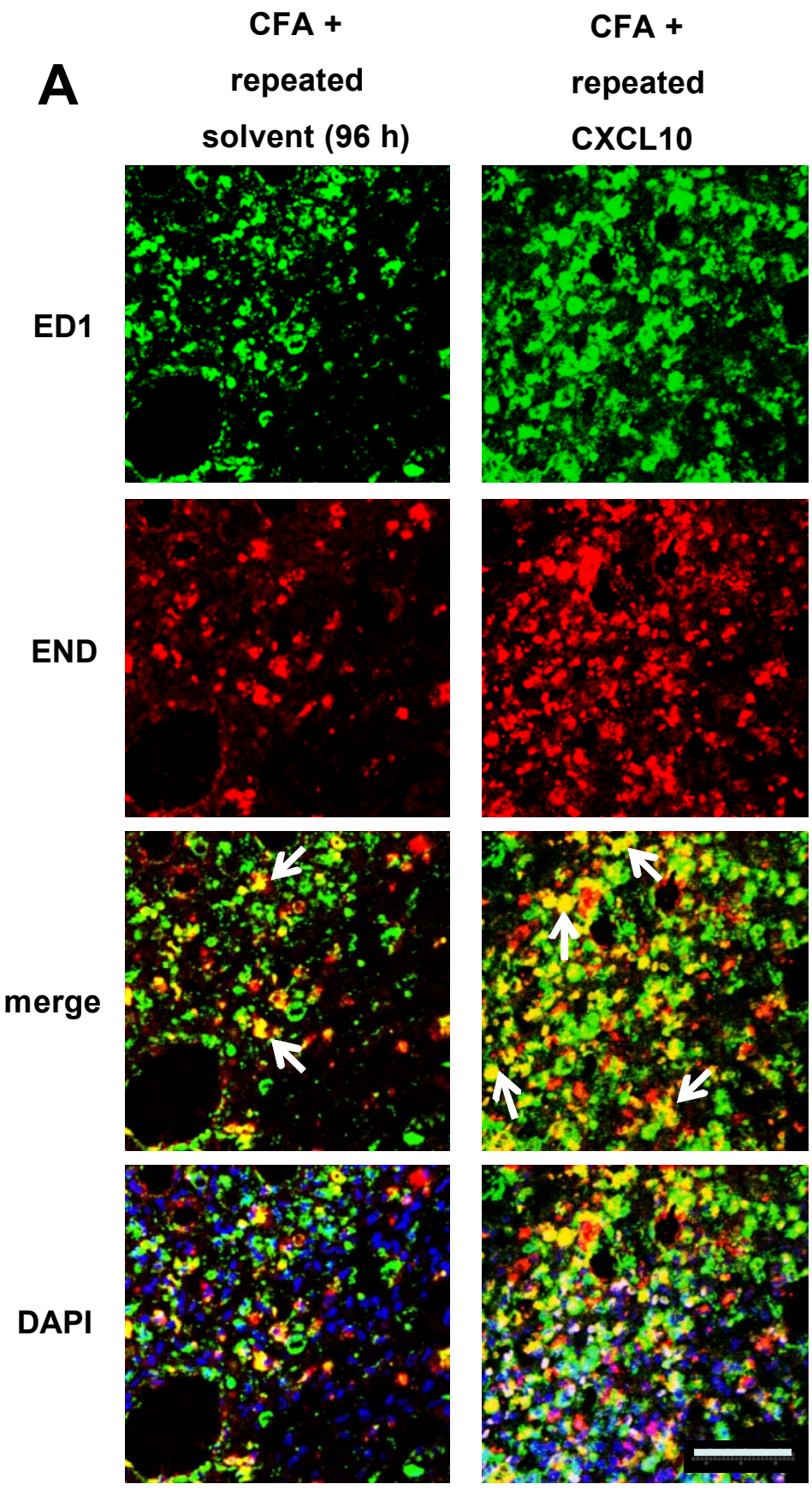
A
CFA + repeated solvent (96 h)
CFA + repeated CXCL10
ED1
END
merge
DAPI

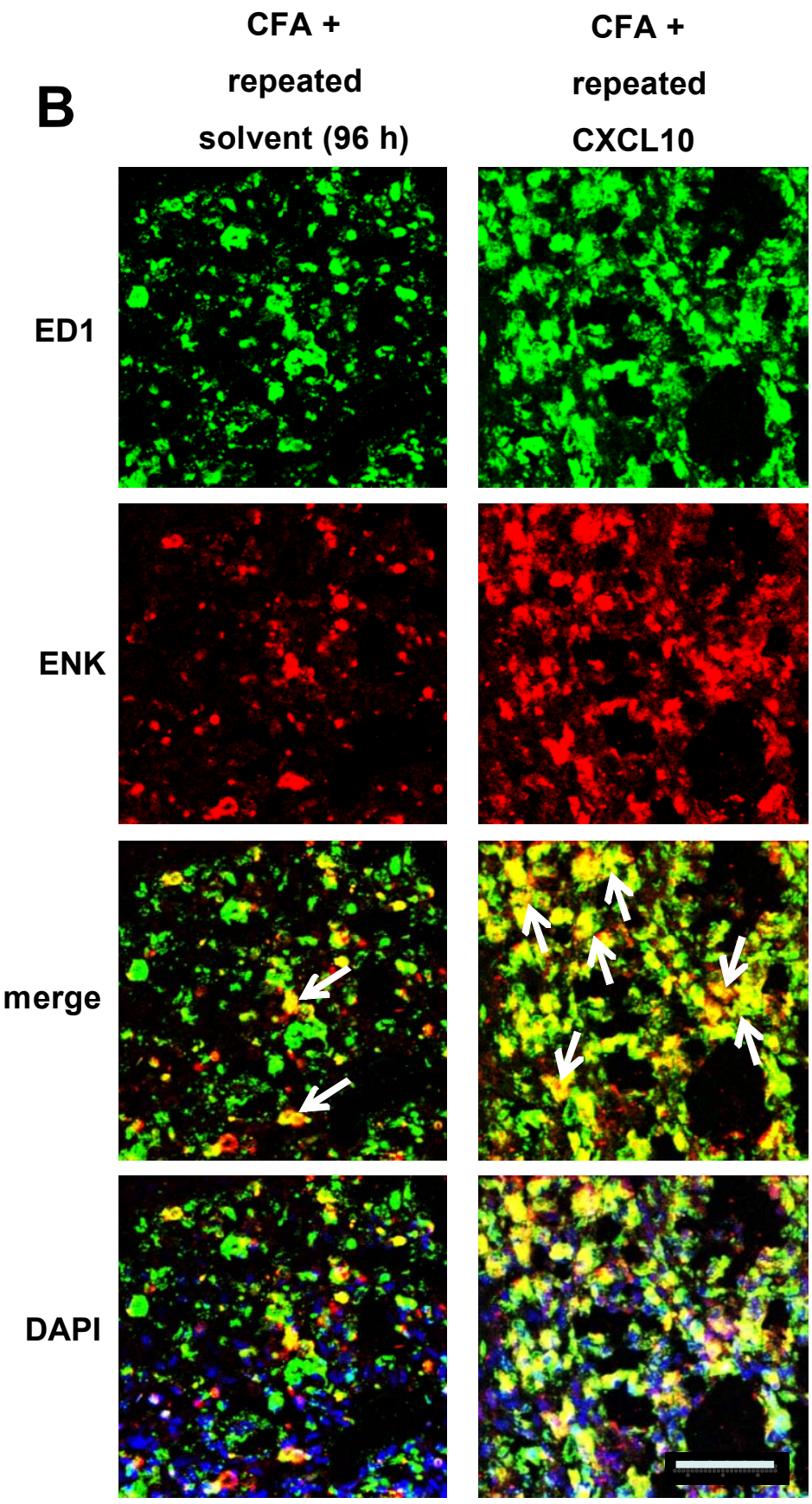
B
CFA +
repeated
solvent (96 h)
CFA +
repeated
CXCL10
ED1
ENK
merge
DAPI

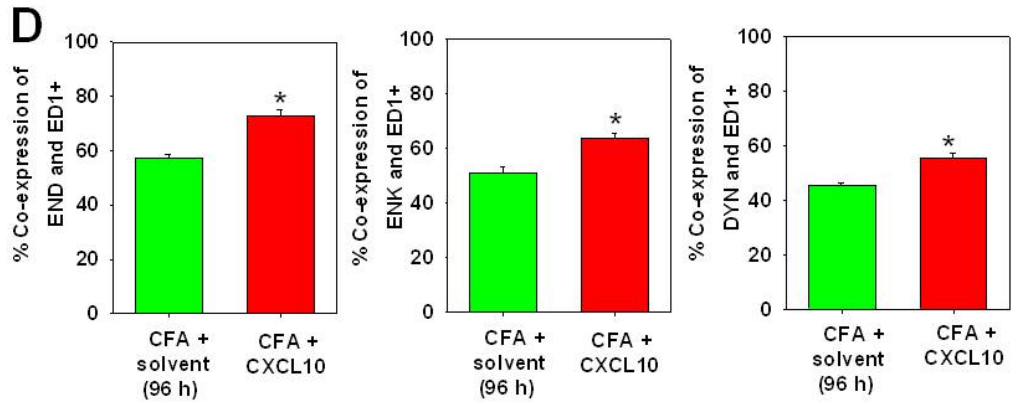

Fig. 21: Increased opioid peptide-expression on monocytes/macrophages by repeated CXCL10 injection. Rats with CFA inflammation were repeatedly administered (i.pl., 5 times, daily from 0-96 h) with CXCL10 or control solution. Slices from inflamed paw tissue sections were used for immune staining. [**A-C**] At 96 h CFA, specific section of paw tissue was double stained with a mouse anti-ED1 (CD68, recognizing monocytes/macrophages, green) and with rabbit anti-rat END, -ENK or -DYN Abs (red) and subsequently with DAPI (blue). White arrows were pointing at double positive cells (Scale bar: 50 µm). [**D**] Quantification analysis displayed the ratio (%) of double positive ED1 marked monocytes/macrophages in total amount of $ED1^+$ cells. Data were shown as mean ± SEM (n = 3 per group, *$p < 0.05$, CFA + CXCL10 versus CFA + solvent; t-test) (Figure and legend were modified from [51]).

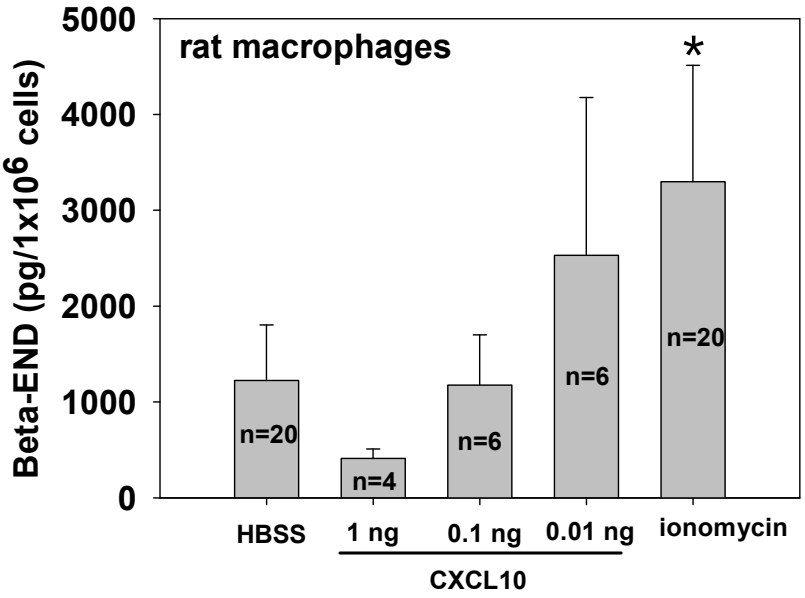

Fig. 22: CXCL10 could not trigger opioid peptide release from rat macrophages *in vitro*. Rat inflammatory peritoneal macrophages were isolated at 96 h following administration (i.p.) of 3% thioglycolate and then incubated with selected doses of CXCL10 (from 0.01 to 1 ng) for 15 min. HBSS buffer (HBSS) and ionomycin (10 μM) were used as control and positive control respectively. Beta-END (pg/1×10^6 cells) was quantified by ELISA from the stimulated cell suspension. Data were presented as means ± SEM. (n = 4-20, *$p<0.05$, one way ANOVA, Holm-Sidak method).

3.10 Blockage of CXCL10 impaired EA-induce antinociception and downregulated opioid peptide expression on monocytes/macrophages

Known from opioid peptide mediated antinociception of EA, we further asked whether an inhibitor of CXCL10 could dampen EA elicited antinociception. Anti-CXCL10 Ab was administered (i.pl.) on EA treated rats at 96 h post CFA. Antinociception induced by EA was time- and dose-dependently reversed by single i.pl. injection of 2 μg anti-CXCL10 (**Fig. 23A**). Multiple applications of an identical dose of anti-CXCL10 at daily time points completely reversed the pain threshold baseline of EA at 48 h and

reached the maximal effect at 96 h (**Fig. 23B**). The optimal dose 2 μg was selected from preliminary dose-response (2, 20 and 200 μg) experiments (data not shown).

Since repeated treatment of CXCL10 could promote expression of opioid peptides, the hypothesis was furthered by whether suppressant of CXCL10 would abolish the expression of opioid peptide enhanced by EA. In comparison to rabbit IgG control, repeated treatments of anti-CXCL10 blocking Ab markedly lowered the content of $ED1^+$ monocytes/macrophages co-expressing the opioid peptides END, ENK and DYN (**Fig. 24A-C**). EA decreased the ratio of opioid peptides expression on ED1 positive monocytes/macrophages to 53% (END), 43% (ENK) and 44% (DYN) (**Fig. 24D**).

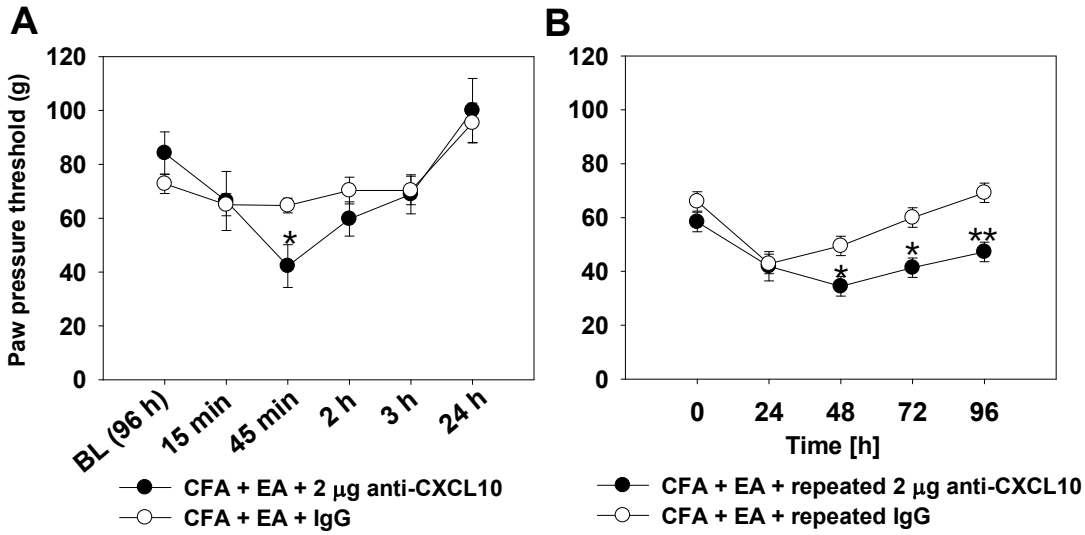

Fig. 23: Anti-CXCL10 blocking Ab dose- and time-dependently inhibited EA produced antinociception. **[A]** Optimal dose of anti-CXCL10 (2 µg) chosen from preliminary experiments was i.pl. administered on EA treated rats at 96 h post CFA. Paw pressure threshold (PPT) was determined before (BL) and 5, 15, 45 min and 2, 3, 24 h post injection. **[B]** Changes of PPT were also daily accessed before repeated injection (i.pl.) of 2 µg anti-CXCL10 at 0, 24, 48, 72, 96 h. All data were presented as mean ± SEM (n = 6 per group, *p < 0.05, **p < 0.01, CFA + EA + 2 µg anti-CXCL10 versus CFA + EA + IgG; two way RM ANOVA, Student-Newman-Keuls) (Figure and legend were modified from [51]).

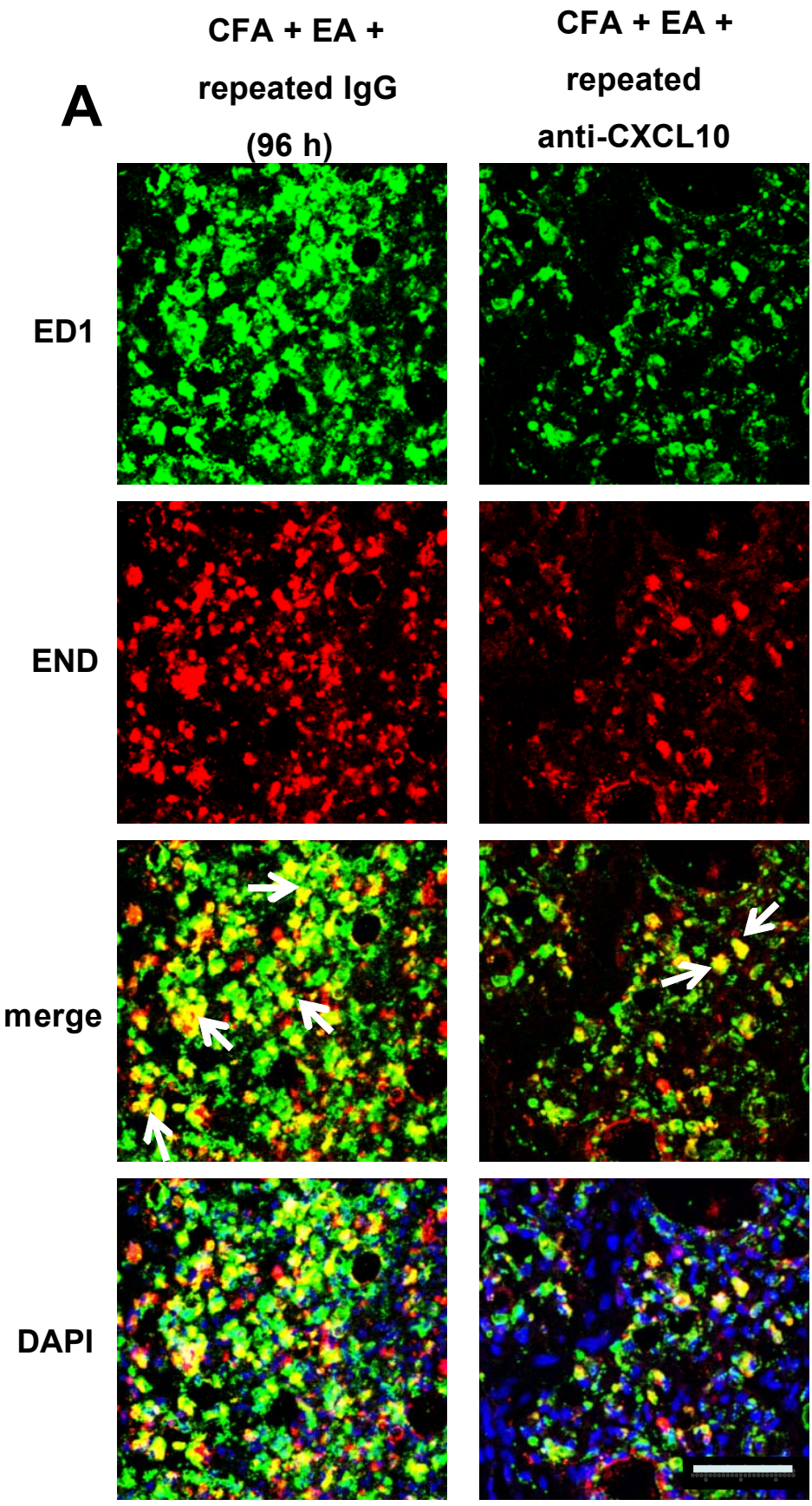
A
CFA + EA +
repeated IgG
(96 h)
CFA + EA +
repeated
anti-CXCL10
ED1
END
merge
DAPI

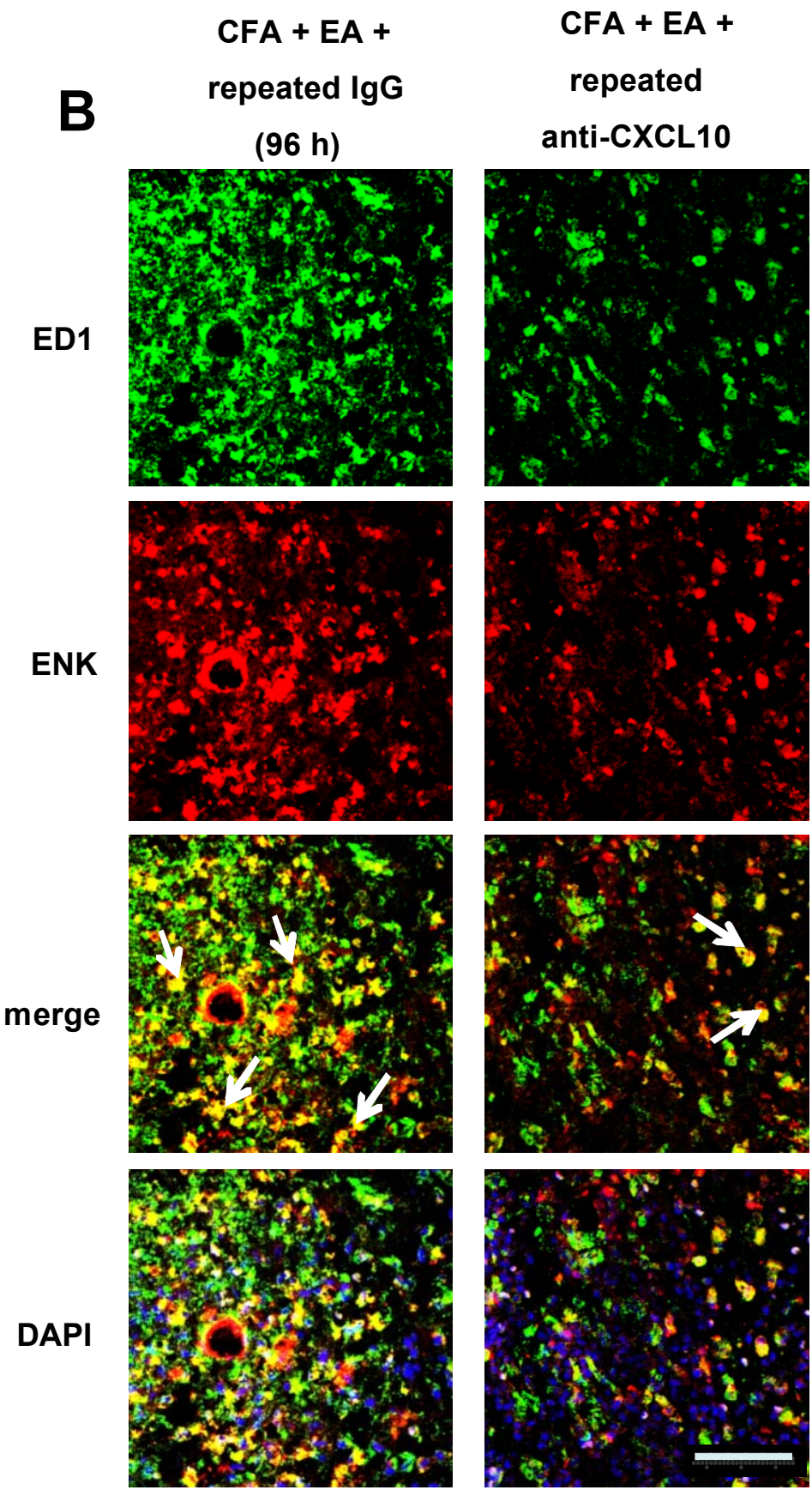
B
CFA + EA +
repeated IgG
(96 h)
CFA + EA +
repeated
anti-CXCL10
ED1
ENK
merge
DAPI

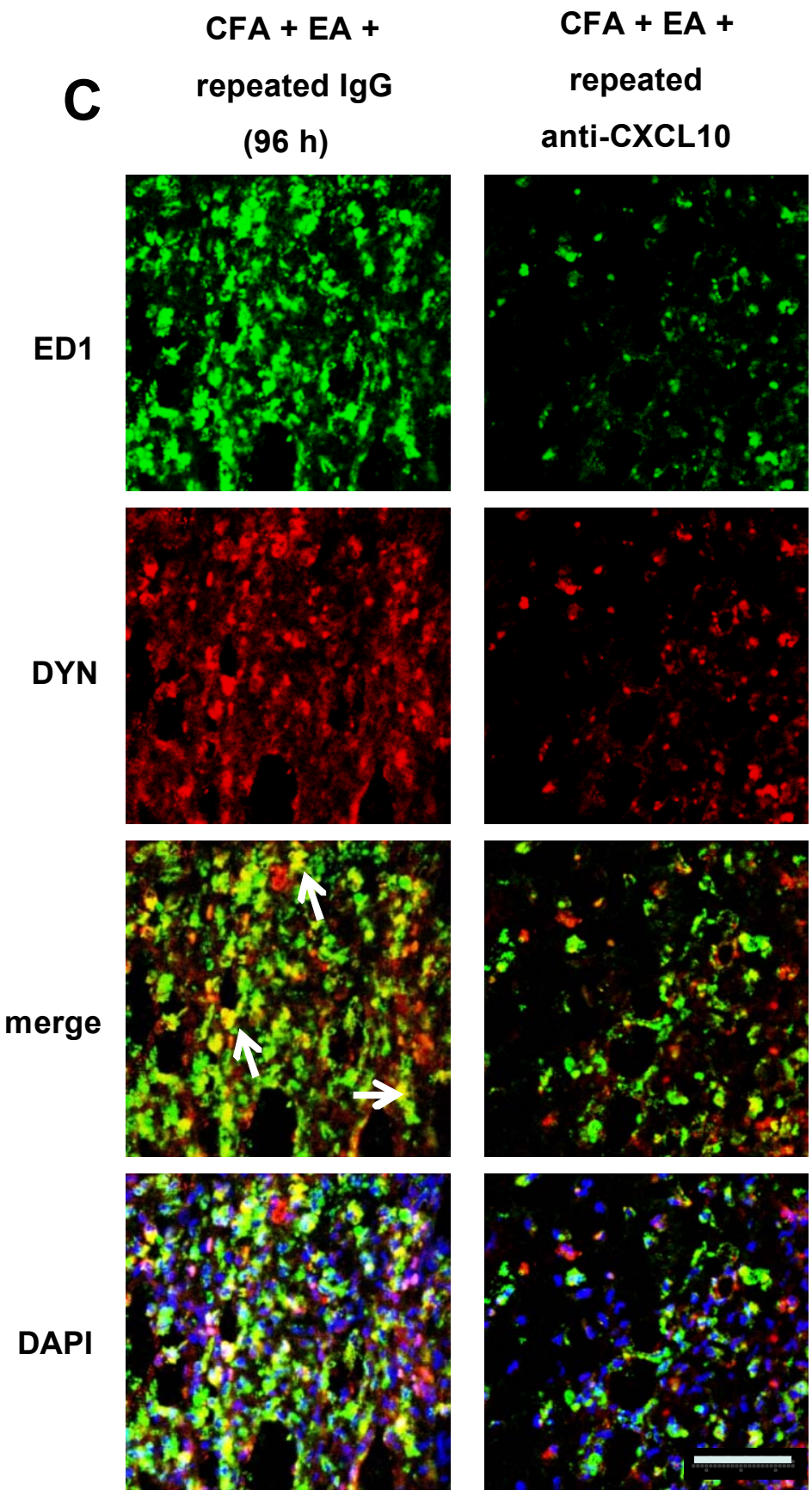
C
CFA + EA +
repeated IgG
(96 h)
CFA + EA +
repeated
anti-CXCL10
ED1
DYN
merge
DAPI

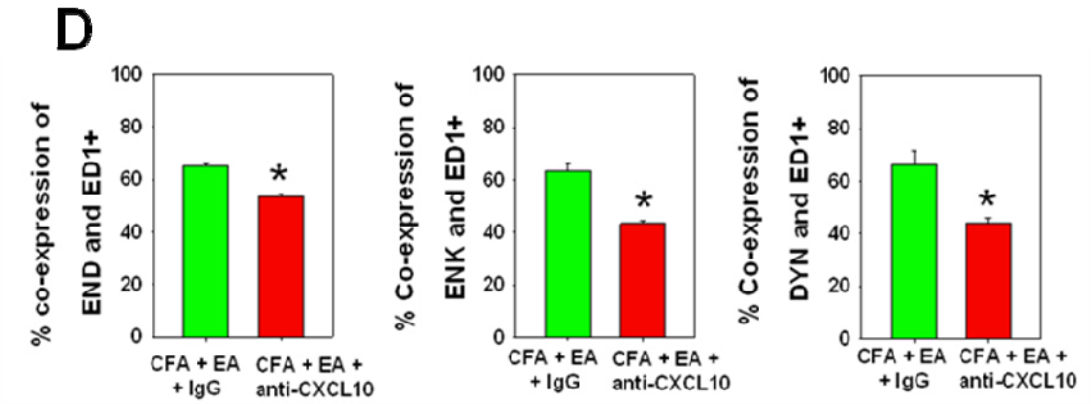

Fig. 24: Inhibitor of CXCL10 suppressed expression of opioid peptides on monocytes/macrophages. Rats with CFA inflammation and treated by EA were repeatedly administered (i.pl., 5 times, daily from 0-96 h) with anti-CXCL10 Ab or IgG control solution. Slices from inflamed paw tissue sections were used for immune staining. [**A-C**] Double staining was performed with mouse anti-ED1 (CD68, recognizing monocytes/macrophages, green) and rabbit anti-END, anti-ENK or anti-DYN Abs respectively (red). DAPI (blue) was used to recognize cell nuclei. White arrows were pointing at double positive cells (Scale bar: 50 μm). [**D**] Quantification analysis displayed the ratio (%) of double positive ED1 marked monocytes/macrophages in total amount of $ED1^+$ cells. Data were presented as mean ± SEM (n = 3 per group, *$p < 0.05$, CFA + EA + anti-CXCL10 versus CFA + EA + IgG; t-test) (Figure and legend were modified from [51]).

3.11 Expression of opioid receptors was not altered by EA

Peripheral analgesia is not only determined on the synthesis and expression of opioid peptides on immune cells, but also determined by the amount of opioid receptors produced transporting from dorsal root ganglion to nociceptive neurons on nerve terminals [55-57]. In the presented data, the protein level of opioid receptors in EA or CFA treated inflamed paw was dramatically upregulated in comparison to non-inflamed paw (contralateral) which was in complete accordance with previous results. As in the previous study we announced opioid receptor antagonist NLX and NTI could reverse EA evoked antinociception at 96 h [5], we therefore further questioned whether expression levels of opioid receptors in paw tissue were changed

by EA. From the presented data, protein levels of DOR and KOR detected by immunoblotting were not apparently affected by EA (**Fig. 25**) in comparison to CFA control. Due to the cross-reactivity of second Ab (anti-mouse Ab, GE Healthcare) for MOR reported from our laboratory, data from MOR was excluded.

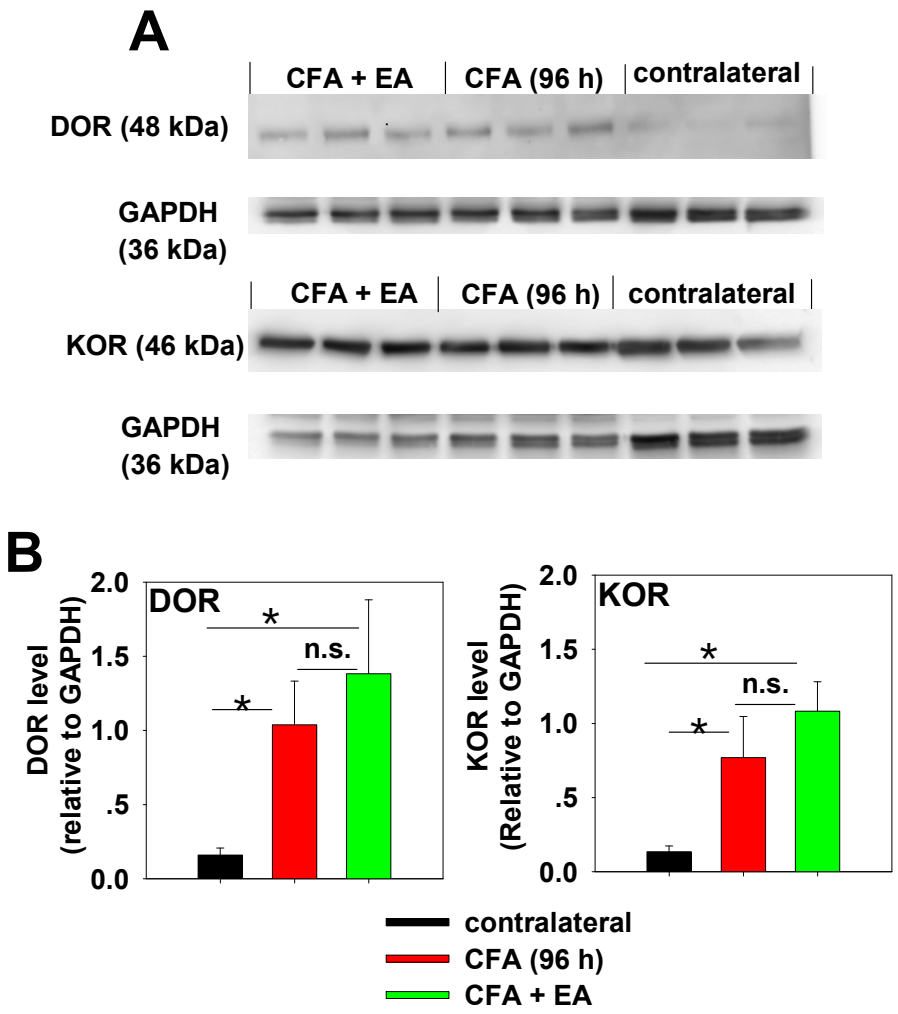

Fig. 25: Expression of opioid receptors at inflammation site was not affected by EA at late phase (96 h) of CFA. [**A**] Protein level of DOR and KOR in inflamed or non-inflamed paw tissue was evaluated by WB. [**B**] IDV values normalized to GAPDH were calculated within one blot. Protein levels of two receptors were upregulated in CFA + EA or CFA treated inflamed paw in comparison to non-inflamed paw (contralateral). No difference was seen between CFA + EA and CFA control (n = 6 per group, *p < 0.05, CFA + EA versus CFA versus contralateral, one way ANOVA, Holm-Sidak method).

4. Discussion

In this thesis, a standard EA treatment was established by modeling a 3D visualized image on fully free-moving rats with CFA-induced hind paw inflammatory pain. This thesis has furthered current understanding of electroacupuncture evoked analgesia with:

1. Two treatments (at 0 and 24 h post CFA) of optimal EA parameters (frequency: 100 Hz, intensity: 2-3 mA, pulse wide: 0.1 ms, duration: 20 min) on bilateral acupoints GB-30 Huantiao produced sustained thermal and mechanical antinociception.
2. Tonic antinociception produced by EA at a late phase (96 h) of CFA was mediated by peripheral opioid receptors and peptides.
3. Regulation of certain pro- and anti-inflammatory cytokines could arguably illustrate anti-inflammatory effects of EA.
4. Enhanced expression of CXCR3 and opioid peptides on macrophages in inflamed paw might be associated with EA induced antinociception, but the level of opioid receptors in inflamed paw were unchanged.
5. Upregulation of chemokine CXCL10 by EA may validly account for EA induced antinociception in an opioid peptide-dependent manner.

4.1 3D modeled acupuncture needling and EA treatment on conscious fully free-moving rats

According to TCM theory, the meridian systems theoretically existed in all biological organisms. However these meridian systems were thought to be restricted by diverse size and anatomical structures in non-human organisms, meaning that not all the

acupoints on humans could be successfully projected onto other species. Current obscure descriptions of acupoint locations on animals urged us to instigate a clear approach to better clarify the positioning and needling on the selected acupoint GB-30 Huantiao for this study and more importantly to pave a way for future reproducible research. Computer-developed 3D modeling is one of the useful tools used to describe intricate anatomical structures in a 3D space which is much more vivid than 2D presentations. 3D modeling is therefore broadly applied in medical research [58-60]. On the basis of the anatomical features of Wistar rats, a computer-based 3D rat skeleton model highlighting the bony symbols and needling approach on GB-30 Huantiao was set up (**Fig. 8**). However, it is worth noting that the 3D model could only provide a guidance for understanding the theoretical essentials of acupoint location as well as needling patterns, and the technical gist of accurate performance on experimental animals required apperception and considerable practice from experimenters.

In TCM theory, “Qi” stands for a beam of energy that circulates in meridians. Meridians refer to routes that transport “Qi” and blood, regulate “Yin” and “Yang”, connect Zang-Fu organs and associate the upper and lower, and exterior and interior, of the body [1]. “Qi” sensation is a frequently discussed theme in TCM as well as in acupuncture. Needle insertion will unavoidably evoke a needle sensation that is influenced by a number of factors. Nevertheless, an optimal effect can only be achieved when “Qi” arrives simultaneously by means of appropriate needling manipulations, the so-called “De Qi” sensation. The feeling of “De Qi” can be vividly characterized as soreness, numbness, heaviness, distension and aching which can be felt by both the patient and practitioner. Unfortunately, “De Qi” sensations from acupuncture can of course hardly be well expressed by animals, and in addition an invasive needling approach easily evokes a stressful response in terms of uncooperative behaviors. Stress-induced analgesia was therefore deemed as a contributing reason that accounted for acupuncture-produced analgesia [13].

Anesthetics or restrainers were therefore commonly applied on animals during acupuncture for the purpose of relieving the suffering and preventing the bias from stress-induced antinociception [20-22] (**Fig. 3**). Nevertheless, anesthetics or restrainers might potentially interfere with molecular signaling processing and/or biological or psychological conditions. Because the 'De Qi' sensation elicited by stimulation of the deep tissue underneath the acupoint is the pivotal premise for patients achieving the optimal effect of AA [4], an intact sensory system in local tissue was critical. Interestingly, EA treatment on conscious rats in a semi-free plastic restrainer was shown by other researchers to cause little stress to rats [3,16] (**Fig. 2**). Nevertheless, semi-free restrainers are still less optimal and also not in line with animal welfare principles. As a matter of fact, EA treatment on fully free-moving rats has been successfully trialed by previous investigator [61]. Therefore, we instituted EA treatment on a fully conscious rat allowed free mobility precluding any anesthesia or restrainer.

4.2 Characteristics of acupuncture-induced analgesic and anti-inflammatory mechanisms

4.2.1 Characteristics of endogenous opioids associated analgesic mechanisms in AA

Involvement of central opioid peptides and receptors in acupuncture analgesia has been intensively addressed [3,4,14-17,19,62,63]. Initial studies indicated frequency-determined central opioid-related AA by radioimmunoassay assessment of perfusate of the subarachnoid space of the spinal cord and further manifested that low frequency (2 Hz) EA potentiated the release of ENK, END and endomorphin (EM), while that of high frequency (100 Hz) selectively increased the release of DYN. An alternatively changed frequency of 2/100 Hz could elicit a simultaneous release of all

phenotypes of the four opioid peptides, leading to an optimal therapeutic action [15]. It was also demonstrated that extensive opioid receptors (MOR, DOR and KOR) mediated 10 Hz EA-induced antinociception in the central level [49]. Subsequent investigations extended this knowledge by identifying the involvement of peripheral opioid receptors and peptides in EA-triggered antinociception in different pain models [17-19]. Our initial study revealed involvement of peripheral opioid peptide receptors in CFA induced inflammatory pain as well as in EA-induced antinociception [5], although the expression levels of the opioid receptors were not affected by EA treatment (**Fig. 25**). Consistent with a recent study expounding repeated low frequency (2 Hz) EA treatment dramatically upregulated opioid peptide END expression on ED1 labeled monocytes/macrophages [3]. This thesis expanded this conclusion that two treatments of high frequency (100 Hz) EA promoted the expressive content of extensive opioid peptide (END, ENK and DYN) expression on ED1 positive monocytes/macrophages (**Fig. 19**). T cells constituted only a negligible rate (< 5%) among the total number of CD45 marked hematopoietic cells at 96 h CFA inflamed paw (**Fig. 17D**), validly supporting earlier investigations [26,64].

Corresponding to previous studies, peripheral opioid peptides mediated analgesia at an early stage (0-6 h) of CFA. This was due to the release of opioid peptides from neutrophils while monocytes/macrophages are considered as mainly responsible for the late phase (96 h) of CFA inflammation [26,45,65]. In earlier investigations, it was discovered that opioid peptide release did not only occur after cold water swim stress or exogenous stimulations but also was present under basal conditions depending on bacterial products via formyl peptide receptor stimulation [29]. The present study furthered current knowledge by illuminating the involvement of local opioid receptors and peptides on tonic antinociception of EA via post-EA application of opioid receptor antagonists (**Fig. 12**) or opioid peptide Abs (**Fig. 13**).

4.2.2 Endogenous cytokines-related anti-inflammatory properties of acupuncture

The effects of acupuncture against inflammation have been well documented [8-10,48,66]. It was suggested that lower frequencies (2 or 10 Hz) rather than higher frequencies EA (100 Hz) could attenuate inflammatory swelling, despite the fact that both patterns could produce comparable antinociceptive effects [48,66]. However in present study, elevated temperature and volume of the inflamed paws were distinctly depressed by high frequency EA (100 Hz) at 72 and 144 h post CFA (**Fig. 11**), although the anti-inflammatory effects of EA seemed less pronounced than the antinociceptive effects (**Fig. 10**). This might suggest that the anti-inflammatory action of EA was not so much determined by frequency but rather the appropriate parameter settings and individual performance was more relevant.

Cytokines were for a long time suggested to be involved in acupuncture elicited effects including anti-inflammatory action. The alleviated inflammation related cytokine changed by acupuncture has been extensively addressed [10,22,48,67]. Cumulative studies put forward the distinctive role of modulating cytokine expression by acupuncture, which was suggested to be balancing the T helper 1(T_h1)-and T helper 2 (T_h2) subtype immune cells-released cytokines [67-70]. In the presented data, EA significantly attenuated the level of pro-inflammatory molecule TNF-alpha and IL-1beta (**Fig. 15A, C**), which was in line with the previous research [10]. In addition, increased T_h1 cell type cytokine IFN-gamma (**Fig. 15F**) as well as T_h2 cytokines IL-13 (**Fig. 15E**) might also suggest interacted signaling of a subtype of cytokines, including at least T_h1 and 2, is involved in the mechanism scheme.

4.2.3 Potential placebo effect underlying verum acupuncture requires sham acupuncture control

Several lines of evidence from randomized controlled trials proposed the specific curative effect of verum acupuncture in comparison to sham acupuncture in pain management [71,72]. The existing studies however have also advocated the same superior effect produced by sham acupuncture, implying potential placebo effects behind verum acupuncture [73-76]. The question remains in clinical research which sham control would be optimal to exclude the bias from acupuncture skepticism [77-81]. Of note, the analgesic effect of sham treatment was overwhelmingly reported in patients. Analogical cases from animals were scantly mentioned, which allowed the author to suspect the possible involvement of technical deviations between different practitioners as well as the psychological factors among the patients [82-84]. In the present study, invasive sham-EA elicited slight antinociception at given time points (96 h CFA) (**Fig. 10)**, this may again suggest the described "minimal needling" of sham-EA was not sufficiently minimal. However, the increased mechanical threshold of sham-EA treated rats was barely affected by administration of an identical dose of NLX (**Fig. 12C)**, this would be an implication that the sham treatment triggered tonic anti-hyperalgesic effect might not depend on peripheral opioid receptors, partially in concordance with the distinct activation property of MOR in verum and sham acupuncture in earlier publication [85].

4.3 Tangled interaction between IFN-gamma and CXCL10 in immune responses and potential association in attenuating inflammatory pain by EA

The IFNs family was classified into type I and type II according to receptor specificity and sequence homology. IFN-gamma is so far the only known member of type II IFN,

which was believed to be produced by lymphocytes, T cells, NK cells, monocytes/macrophages, and dendritic cells [86-88]. Both types of IFN possess antiviral and immune-modulatory activities in early infectious stage [89-91]. Augmenting the immune system response to increased immune system sensitivity and in response to pathogens is suggested to be an important function of IFN-gamma during infection, one of the key means by which it modulates and trafficks specific immune cells to sites of inflammation through upregulating expression of adhesion molecules and chemokines [92].

Chemokines are a family of cytokines that play an important role in the recruitment of leukocytes to inflammatory sites. They have been subdivided into families on the basis of the relative position of their cysteine residue. The subtype alpha-chemokines (CXC-chemokines) which generally contain CXCL8 (interleukin-8, IL-8), CXCL10, and CXCL9 (monokine induced by interferon-gamma, MIG) are mainly chemotactic for neutrophils and T lymphocytes whereas the beta-chemokines (C-C-chemokines) including CCL2 (monocyte chemoattractant protein-1, MCP-1), CCL7 (monocyte chemoattractant protein-3, MCP-3) and CCL3 (macrophage inflammatory protein-1alpha, MIP-1alpha) selectively attract monocytes/macrophages, eosinophils, basophils, and T lymphocyte [93]. Chemokine receptors belong to the large family of seven transmembrane domain receptors which couple to heterotrimeric G-coupled receptor proteins [94,95]. CXCL10 was initially identified from human IFN-gamma-inducible protein of 10 kDa (IP-10) as an early response gene induced by IFN-gamma in monocytes-like U937 cells line [96]. Early studies dominantly identified the enlargement of the pathogenic role of CXCL10 and its so far sole known receptor CXCR3 in diverse immune system disorders involving the trafficking of inflammatory immune cells, on T cells, NK cells, dendritic cells (the majority of which were T cells), which potentiated CXCL10-CXCR3 for a long time to be an essential putative therapeutic target due to their pathogenesis development [97-101].

A broad set of investigations manifested that CXCL10 expression can be strongly induced in a variety of cell types e.g. endothelial cells, keratinocytes, fibroblasts, mesangial cells, astrocytes, monocytes, and neutrophils by stimulation with IFN-alpha, IFN-beta, IFN-gamma or lipopolysaccharide (LPS) [102-104]. Administration of exogenous IFN-gamma reversed the repression of CXCL10 on recruited exudative macrophages in CXCR3-silent rats and reflected again the causal connection between IFN-gamma and CXCL10, and the neutralization of virus-induced IFN-alpha/beta resulted in the downregulation of CXCL10 expression. IFN-alpha or IFN-gamma was found to directly promoted CXCL10 mRNA expression [105,106]. On the other hand, accumulating evidence supports the possibility that a positive feedback loop exists between IFN-gamma, CXCL10 and CXCR3, e.g. IFN-gamma levels as well as the number of $CXCR3^{+}CD4^{+}$ T cells were markedly reduced in both the lung and peripheral lymph node following CXCL10 neutralization [107]. CXCR3-null mice also in return impaired the production of IFN-gamma and CXCL10 [108]. These evidences supported that CXCL10 is an alternative marker of IFN-gamma in clinical diagnosis [109].

In line with previous investigations we observed a consistent upregulation of CXCR3 on macrophages (**Fig. 18**) as well as CXCL10 in the inflamed paw (**Fig. 16**) by EA, providing potential receptor availability for its ligand CXCL10, although the quantification level of CXCR3 and exact role in CXCL10 mediated antinociception might still need to be evaluated and understood. Additionally the distinctive upregulation of IFN-gamma (**Fig. 15F**) concomitant with CXCL10 (**Fig. 16**) by EA among the targeted cytokines validly confirmed the causal correlation between them, which was illustrated by earlier researchers, and implied another alternative target for investigating the signaling pathway of CXCL10 in EA.

4.4 Bilateral role of chemokines in regulating pain and novel antinociceptive property of CXCL10 in relieving inflammatory pain by EA

So far known cytokines and chemokines played a bilateral role in mediating both hyperalgesic and anti-hyperalgesic effects in inflammatory pain, e.g. as previously illustrated hyperalgesia-inducing mediators [32,33], TNF-alpha and IL-1beta themselves were also able to evoke considerable antinociception, which could be abolished by opioid antagonists [25,28]. Chemokine CXCL2/3 plays an important role in neutrophils recruitment and opioid release in the local inflammatory microenvironment [27]. Another chemokine CCL2 as well as its receptor C-C-chemokine receptor type 2 (CCR2) on monocytes/macrophages were considered as the key mediators for inducing inflammatory hyperalgesia as well as chronic pain [46,110].

Similarly, despite the promotion in pathogenesis development, increasing investigations also indicated that CXCL10 and CXCR3 exhibited an advantageous property in specific immune responses. It was manifested that systemic levels of CXCL10 are beneficial in controlling the allergic response, possibly by regulating cellular trafficking in the lymph node, whereas local administration of exogenous CXCL10 during an allergic response may be detrimental [111]. CXCR3 (-/-) mice had more severe chronic disease with increased demyelination and axonal damage [112]. CXCL10 (-/-) mice showed decreased luminal plaque, increased aortic size, worse morphological grades of aneurysms as well as a higher incidence of death due to aortic rupture, indicating a protective role against aneurysm formation and rupture in atherosclerotic plaque development [113]. In other words, the role of CXCL10 in the immune response has not been clearly understood. The currently conflicting results among diverse inflammatory models imply the complex and multiple roles of CXCL10 and CXCR3 in the specific inflammatory or autoimmune diseases [114], which might

be dependent on different stages and perspectives of immune response in different models. In the current study, we found application (i.pl.) of the anti-CXCL10 Ab could time- and dose-dependently inhibited EA elicited antinociception at 96 h CFA (**Fig. 23A**) and repeated administration (i.pl.) of anti-CXCL10 Ab could greatly abolish the daily pain threshold baseline of EA (**Fig. 23B**) and largely suppress opioid peptide expression (**Fig. 24**), indicating a direct correlation between CXCL10 and opioid peptides-expressing monocytes/macrophages.

In the meantime, the majority researchers agree that CXCL10-CXCR3 mediated T cell trafficking, the expression and regulation of CXCL10 and CXCR3 by macrophages, was for a long time poorly put forward. In the present study, we firstly confirmed the early theory for the predominately analgesic role of monocytes/macrophages in contributing to opioid peptide release at 96 h CFA by observing the dominant expression of monocytes/macrophages as opposed to T cells (**Fig. 17**), which was in line with earlier report [45]. Addionally, the majority of macrophages expressed CXCR3 (**Fig. 18**) as well as upregulation of CXCL10 (**Fig. 16**) consistently backed up the possibility of the CXCL10-CXCR3 axis in modulating macrophages trafficking and opioid peptides expression.

During inflammation, large amount of pro-inflammatory and pro-algesic mediators were secreted by immune cells trafficked to the inflammatory site, which sensitized nociceptor on nerve terminals and induced pain [115]. Immune cells e.g. neutrophils could also continuously release considerable amounts of opioid peptides to attenuate pain, triggering by calcium influx via activated PI3K due to mycobacterial components formyl peptides binding to FPR [29]. In recent studies, a hyperalgesic role of chemokine-receptor axis CCL2-CCR2 was suggested to be necessary for monocytes/macrophages-evoked hyperalgesia in CFA inflammation [46]. The hyperalgesic property of specific chemokines in neuropathic and other pain models was addressed by other researchers [110,116,117]. Nevertheless, from a controversial angle,

in earlier publications we also indicated that the chemokine-receptor alliance CXCL2/3 and CXCR1/2 alleviated inflammatory pain through chemotaxis to neutrophils, whereby opioid peptides were released depending on intracellular calcium mobilization as well as PI3K cascade [27]. Notably, local injection of CXCL1 or CXCL2/3 in non-inflamed tissue could only recruit neutrophils without inducing hyperalgesia [118]. This increasing evidence facilitated the novel concept that chemokines and their receptors processed bi-directional natures in mediating the inflammatory response, as announced by earlier researchers [119,120].

Inflammatory rat peritoneal macrophages have been commonly used as differentiated monocytic cells in our previous *in vitro* investigations [46]. In this study, CXCL10 did not stimulate END secretion from inflammatory peritoneal rat macrophages (**Fig. 22**) *in vitro* even though the content of opioid expressing-monocytes/macrophages were intensively increased by repeated treatments of CXCL10 (**Fig. 21**), which was not in complete line with the opioid peptide-dependent anti-hyperalgesia of CXCL10 *in vivo* (**Fig. 20**). However, CXC-chemokines in earlier studies played an dual role in neutrophils migration and opioid peptide release (END and ENK) at an early period of CFA (2 h) [27]. Additionally this secretion of opioid peptide from CXC-chemokine was dose-dependent and intracellular Ca^{2+} level determined [27]. Notably, we previously experienced mycobacterial component *Mycobacterium butyricum* stimulation on neutrophils but not monocytes could directly trigger opioid peptide (END and ENK) release [29]. Similarly, our new study [121] explored subtypes of macrophages and discovered that neither pro-inflammatory M1 macrophages nor anti-inflammatory M2 macrophages favored the secretion of opioid peptide except exposing to ionomycin or toll like receptor (TLR) 2/4 ligand LPS, although the robust expression of TLR 4 on both subpopulations of macrophages was observed. Tracing back all the documents, unlike neutrophils, monocytes/macrophages are a group of cell-type dull to extra stimuli. Therefore, finding out potential molecular targets for macrophages activation would be pivotal to illustrate the subcellular pathway of

CXC-chemokine mediated opioid peptide secretion from macrophages, and optimal stimulation duration and mode as well as the dose of CXCL10 would also needed to be well established *in vitro* in further studies.

The majority of references emphasized the critical role of CXCL10 in cell infiltration which tempted the secretion of pro-inflammatory cytokine from immune cells, however in the presented data, the upregulation of CXCL10 was not accompanied with the upregulation, but selective downregulation of hyperalgesic pro-inflammatory cytokine TNF-alpha and IL-1beta, indicating the co-existence of analgesic and anti-inflammatory properties by EA. These data constitutively support the specific advantages of CXCL10 by EA, which might be involved in independent specific cellular pathways in interacting with peripheral opioid peptide-containing immune cells. It is also predictable that, at least in a given phase (96 h) of peripheral inflammatory pain, CXCL10 is presented to be the key analgesic mediator, thus neutralization of CXCL10 as a therapeutic approach at this phase would undoubtedly impair the predominantly beneficial effects as opposed to increasing the possibly detrimental effects.

In summary, this thesis extends the current understanding on electroacupuncture induced analgesia at a late stage (96 h) of CFA induced inflammation and puts forward new information, predominantly with chemokine CXCL10 mediated EA produced tonic antinociception via peripheral opioid peptides and modulated the expression of opioid peptide on monocytes/macrophages. Partial restoration of certain local cytokines expression by EA may be relevant to both anti-inflammation and anti-hyperalgesia properties of EA. Intensified upregulation of CXCL10 as well as CXCR3 expression on macrophages at inflammation site might be associated with the antinociceptive property of CXCL10 in EA and need to be clarified further.

Laying a solid foundation on the 3D modeled acupoint position and acupuncture needling approach in this thesis, the results point towards elucidation of the possible signaling pathways involved in both opioid and non-opioid mechanisms. Future intensive, rigorous and quantitative acupuncture research needs to be directed towards determining the correlation between cytokines/chemokines and acupuncture induced analgesia.

5. References

1. Cheng X, editor (1999) Chinese Acupuncture and Moxibustion. Revised Edition ed. Beijing: Foreign Languages Press.
2. Goldman N, Chen M, Fujita T, Xu Q, Peng W, Liu W, Jensen TK, Pei Y, Wang F, Han X, Chen JF, Schnermann J, Takano T, Bekar L, Tieu K, Nedergaard M (2010) Adenosine A1 receptors mediate local anti-nociceptive effects of acupuncture. Nat Neurosci 13: 883-888.
3. Su TF, Zhang LH, Peng M, Wu CH, Pan W, Tian B, Shi J, Pan HL, Li M (2011) Cannabinoid CB2 receptors contribute to upregulation of beta-endorphin in inflamed skin tissues by electroacupuncture. Mol Pain 7: 98-128.
4. Zhao ZQ (2008) Neural mechanism underlying acupuncture analgesia. Prog Neurobiol 85: 355-375.
5. Wang Y, Hackel D, Peng F, Rittner HL (2013) Long-term antinociception by electroacupuncture is mediated via peripheral opioid receptors in free-moving rats with inflammatory hyperalgesia. Eur J Pain 17:1447-1457
6. Shiue HS, Lee YS, Tsai CN, Hsueh YM, Sheu JR, Chang HH (2008) DNA microarray analysis of the effect on inflammation in patients treated with acupuncture for allergic rhinitis. J Altern Complement Med 14: 689-698.
7. Gondim DV, Araujo JC, Cavalcante AL, Havt A, Quetz Jda S, Brito GA, Ribeiro Rde A, Lima Vale M (2012) CB1 and CB2 contribute to antinociceptive and anti-inflammatory effects of electroacupuncture on experimental arthritis of the rat temporomandibular joint. Can J Physiol Pharmacol 90: 1479-1489.
8. Kuai L, Jin RF, Gao M, Yang HY (2009) Fuzzy cluster analysis of therapeutic effects of electro-acupuncture at different parameters. Zhong Xi Yi Jie He Xue Bao (= Journal of Chinese integrative medicine) 7: 478-481.
9. Li WM, Cui KM, Li N, Gu QB, Schwarz W, Ding GH, Wu GC (2005) Analgesic effect of electroacupuncture on complete Freund's adjuvant-induced inflammatory pain in mice: a model of antipain treatment by acupuncture in mice. Jpn J Physiol 55: 339-344.
10. Su TF, Zhao YQ, Zhang LH, Peng M, Wu CH, Pei L, Tian B, Zhang J, Shi J, Pan HL, Li M (2012) Electroacupuncture reduces the expression of proinflammatory cytokines in inflamed skin tissues through activation of cannabinoid CB2 receptors. Eur J Pain 16: 624-635.
11. Ha H, Tan EC, Fukunaga H, Aochi O (1981) Naloxone reversal of acupuncture analgesia in the monkey. Exp Neur 73: 298-303.

12. Shen E, Wu, W.Y., Du, H.J., Wei, J.Y., Zhu, D.X (1973) Electromyographic activity produced locally by acupuncture manipulation. Chin Med J 9: 532–535.
13. Pomeranz B (1986) Relation of stress-induced analgesia to acupuncture analgesia. Ann N Y Acad Sci 467: 444-447.
14. Mayer DJ, Price DD, Rafii A (1977) Antagonism of acupuncture analgesia in man by narcotic-antagonist naloxone. Brain Res 121: 368-372.
15. Han JS (2004) Acupuncture and endorphins. Neurosci Lett 361: 258-261.
16. Lao L, Zhang RX, Zhang G, Wang X, Berman BM, Ren K (2004) A parametric study of electroacupuncture on persistent hyperalgesia and Fos protein expression in rats. Brain Res 1020: 18-29.
17. Zhang GG, Yu C, Lee W, Lao L, Ren K, Berman BM (2005) Involvement of peripheral opioid mechanisms in electroacupuncture analgesia. Explore (NY) 1: 365-371.
18. Ceccherelli F, Gagliardi G, Ruzzante L, Giron G (2002) Acupuncture modulation of capsaicin-induced inflammation: effect of intraperitoneal and local administration of naloxone in rats. A blinded controlled study. J Altern Complement Med 8: 341-349.
19. Taguchi R, Taguchi T, Kitakoji H (2010) Involvement of peripheral opioid receptors in electroacupuncture analgesia for carrageenan-induced hyperalgesia. Brain Res 1355: 97-103.
20. Kung HH, Hsu SF, Hung YC, Chen KB, Chen JY, Wen YR, Sun WZ (2011) Electroacupuncture analgesia, stress responses, and variations in sensitivity in rats anesthetized with different sub-MAC anesthetics. Eur J Pain 15: 600-607.
21. Niu C, Hao H, Lu J, Li L, Han Z, Tu Y (2011) A novel uni-acupoint electroacupuncture stimulation method for pain relief. Evid Based Complement Alternat Med 2011: 209879.
22. Xin Fu Y-QW, Gen-Cheng Wu (2006) Involvement of nociceptin/orphanin FQ and its receptor in electroacupuncture-produced anti-hyperalgesia in rats with peripheral inflammation. Brain Res 1078: 212-218.
23. Zou R, Xu Y, Zhang HX (2009) Evaluation on analgesic effect of electroacupuncture combined with acupoint-injection in treating lumbar intervertebral disc herniation. Zhongguo Gu Shang (= China journal of orthopaedics and traumatology) 22: 759-761.
24. Zhang J, Chen L, Su TF, Cao FY, Meng XF, Pei L, Shi J, Pan HL, Li M (2010) Electroacupuncture increases CB2 receptor expression on keratinocytes and infiltrating inflammatory cells in inflamed skin tissues of rats. J Pain 11: 1250-1258.

25. Czlonkowski A, Stein C, Herz A (1993) Peripheral mechanisms of opioid antinociception in inflammation: involvement of cytokines. Eur J Pharmacol 242: 229-235.
26. Rittner HL, Brack A, Machelska H, Mousa SA, Bauer M, Schäfer M, Stein C (2001) Opioid peptide-expressing leukocytes: identification, recruitment, and simultaneously increasing inhibition of inflammatory pain. Anesthesiology 95: 500-508.
27. Rittner HL, Labuz D, Schaefer M, Mousa SA, Schulz S, Schäfer M, Stein C, Brack A (2006) Pain control by CXCR2 ligands through Ca2(+)-regulated release of opioid peptides from polymorphonuclear cells. FASEB J 20: 2627-2629.
28. Schäfer M, Carter L, Stein C (1994) Interleukin 1 beta and corticotropin-releasing factor inhibit pain by releasing opioids from immune cells in inflamed tissue. Proc Natl Acad Sci U S A 91: 4219-4223.
29. Rittner HL, Hackel D, Voigt P, Mousa S, Stolz A, Labuz D, Schäfer M, Schaefer M, Stein C, Brack A (2009) Mycobacteria attenuate nociceptive responses by formyl peptide receptor triggered opioid peptide release from neutrophils. PLoS Pathog 5: e1000362.
30. Stein C, Hassan AH, Lehrberger K, Giefing J, Yassouridis A (1993) Local analgesic effect of endogenous opioid peptides. Lancet 342: 321-324.
31. Sitte N, Busch M, Mousa SA, Labuz D, Rittner H, Gore C, Krause H, Stein C, Schäfer M (2007) Lymphocytes upregulate signal sequence-encoding proopiomelanocortin mRNA and beta-endorphin during painful inflammation in vivo. J Neuroimmunol 183: 133-145.
32. Ferreira SH, Lorenzetti BB, Bristow AF, Poole S (1988) Interleukin-1-beta as a potent hyperalgesic agent antagonized by a tripeptide analog. Nature 334: 698-701.
33. Cunha FQ, Poole S, Lorenzetti BB, Ferreira SH (1992) The pivotal role of tumour necrosis factor alpha in the development of inflammatory hyperalgesia. Br J Pharmacol 107: 660-664.
34. Schäfer M, Svensson CI, Sommer C, Sorkin LS (2003) Tumor necrosis factor-alpha induces mechanical allodynia after spinal nerve ligation by activation of p38 MAPK in primary sensory neurons. J Neurosci 23: 2517-2521.
35. Cunha FQ, Poole S, Lorenzetti BB, Veiga FH, Ferreira SH (1999) Cytokine-mediated inflammatory hyperalgesia limited by interleukin-4. Br J Pharmacol 126: 45-50.

36. Lorenzetti BB, Poole S, Veiga FH, Cunha FQ, Ferreira SH (2001) Cytokine-mediated inflammatory hyperalgesia limited by interleukin-13. Eur Cytokine Netw 12: 260-267.
37. Poole S, Cunha FQ, Selkirk S, Lorenzetti BB, Ferreira SH (1995) Cytokine-mediated inflammatory hyperalgesia limited by interleukin-10. Br J Pharmacol 115: 684-688.
38. Benard A, Cavailles P, Boue J, Chapey E, Bayry J, Blanpied C, Meyer N, Lamant L, Kaveri SV, Brousset P, Dietrich G (2010) Mu-opioid receptor is induced by IL-13 within lymph nodes from patients with Sezary syndrome. J Invest Dermatol 130: 1337-1344.
39. Bianchi M, Panerai AE (1995) CRH and the noradrenergic system mediate the antinociceptive effect of central interleukin-1 alpha in the rat. Brain Res Bull 36: 113-117.
40. Zimmermann M (1983) Ethical guidelines for investigations of experimental pain in conscious animals. Pain 16: 109-110.
41. Stein C, Millan MJ, Herz A (1988) Unilateral inflammation of the hindpaw in rats as a model of prolonged noxious-stimulation - alterations in behavior and nociceptive thresholds. J Pharmacol Exp Ther 31: 445-451.
42. Schreiter A, Gore C, Labuz D, Fournie-Zaluski MC, Roques BP, Stein C, Machelska H (2012) Pain inhibition by blocking leukocytic and neuronal opioid peptidases in peripheral inflamed tissue. FASEB J 26: 5161-5171.
43. Kohli DR, Li Y, Khasabov SG, Gupta P, Kehl LJ, Ericson ME, Nguyen J, Gupta V, Hebbel RP, Simone DA, Gupta K (2010) Pain-related behaviors and neurochemical alterations in mice expressing sickle hemoglobin: modulation by cannabinoids. Blood 116: 456-465.
44. Schmitt TK, Mousa SA, Brack A, Schmidt DK, Rittner HL, Welte M, Schäfer M, Stein C (2003) Modulation of peripheral endogenous opioid analgesia by central afferent blockade. Anesthesiology 98: 195-202.
45. Brack A, Labuz D, Schiltz A, Rittner HL, Machelska H, Schäfer M, Reszka R, Stein C (2004) Tissue monocytes/macrophages in inflammation: hyperalgesia versus opioid-mediated peripheral antinociception. Anesthesiology 101: 204-211.
46. Pflücke D, Hackel D, Mousa SA, Partheil A, Neumann A, Brack A, Rittner HL (2013) The molecular link between C-C-chemokine ligand 2-induced leukocyte recruitment and hyperalgesia. J Pain 15: 1-14.
47. Kintz P, Cirimele V, Ludes B (2002) Blood investigation in a fatality involving the veterinary drug T-61. J Anal Toxicol 26: 529-531.

48. Zhang RX, Lao LX, Wang X, Fan A, Wang L, Ren K, Berman BM (2005) Electroacupuncture attenuates inflammation in a rat model. J Altern Complement Med 11: 135-142.
49. Zhang RX, Lao LX, Wang LB, Liu B, Wang XY, Ren K, Berman BM (2004) Involvement of opioid receptors in electroacupuncture-produced anti-hyperalgesia in rats with peripheral inflammation. Brain Res 1020: 12-17.
50. Huang C, Hu ZP, Long H, Shi YS, Han JS, Wan Y (2004) Attenuation of mechanical but not thermal hyperalgesia by electroacupuncture with the involvement of opioids in rat model of chronic inflammatory pain. Brain Res Bull 63: 99-103.
51. Y. Wang, R. Gehringer, S. A. Mousa, D. Hackel, A. Brack, H. L. Rittner (2014) CXCL10 controls inflammatory pain via opioid peptide-containing macrophages in electroacupuncture. PLoS ONE. (Accepted)
52. Taub DD, Lloyd AR, Conlon K, Wang JM, Ortaldo JR, Harada A, Matsushima K, Kelvin DJ, Oppenheim JJ (1993) Recombinant human interferon-inducible protein 10 is a chemoattractant for human monocytes and T lymphocytes and promotes T cell adhesion to endothelial cells. J Exp Med 177: 1809-1814.
53. Booth V, Keizer DW, Kamphuis MB, Clark-Lewis I, Sykes BD (2002) The CXCR3 binding chemokine IP-10/CXCL10: structure and receptor interactions. Biochemistry 41: 10418-10425.
54. Rittenhouse SE, Horne WC (1984) Ionomycin can elevate intraplatelet Ca2+ and activate phospholipase A without activating phospholipase C. Biochem Biophys Res Commun 123: 393-397.
55. Stein C, Millan MJ, Shippenberg TS, Peter K, Herz A (1989) Peripheral opioid receptors mediating antinociception in inflammation. Evidence for involvement of mu, delta and kappa receptors. J Pharmacol Exp Ther 248: 1269-1275.
56. Hassan AH, Ableitner A, Stein C, Herz A (1993) Inflammation of the rat paw enhances axonal-transport of opioid receptors in the sciatic-nerve and increases their density in the inflamed tissue. Neuroscience 55: 185-195.
57. Mousa SA, Zhang Q, Sitte N, Ji R, Stein C (2001) Beta-endorphin-containing memory-cells and mu-opioid receptors undergo transport to peripheral inflamed tissue. J Neuroimmunol 115: 8.
58. Bolliger MJ, Buck U, Thali MJ, Bolliger SA (2012) Reconstruction and 3D visualisation based on objective real 3D based documentation. Forensic Sci Med Pathol 8: 208-217.
59. Davies JC, Fattah A, Ravichandiran M, Agur AM (2012) Clinically relevant landmarks of the frontotemporal branch of the facial nerve: a three-dimensional study. Clin Anat 25: 858-865.

60. Wang R, Yang D, Li S (2012) Three-dimensional virtual model and animation of penile lengthening surgery. J Plast Reconstr Aesthet Surg 65: e281-285.
61. Iwa M, Matsushima M, Nakade Y, Pappas TN, Fujimiya M, Takahashi T (2006) Electroacupuncture at ST-36 accelerates colonic motility and transit in freely moving conscious rats. Am J Physiol 290: G285-G292.
62. Clement-Jones V, McLoughlin L, Tomlin S, Besser GM, Rees LH, Wen HL (1980) Increased beta-endorphin but not met-enkephalin levels in human cerebrospinal fluid after acupuncture for recurrent pain. Lancet 2: 946-949.
63. Kiser RS, Khatami MJ, Gatchel RJ, Huang XY, Bhatia K, Altshuler KZ (1983) Acupuncture relief of chronic pain syndrome correlates with increased plasma met-enkephalin concentrations. Lancet 2: 1394-1396.
64. Brack A, Rittner HL, Machelska H, Leder K, Mousa SA, Schäfer M, Stein C (2004) Control of inflammatory pain by chemokine-mediated recruitment of opioid-containing polymorphonuclear cells. Pain 112: 229-238.
65. Hackel D, Stolz A, Mousa SA, Brack A, Rittner HL (2011) Recruitment of opioid peptide-containing neutrophils is independent of formyl peptide receptors. J Neuroimmunol 230: 65-73.
66. Hahm TS (2007) The effect of 2 Hz and 100 Hz electrical stimulation of acupoint on ankle sprain in rats. J Korean Med Sci 22: 347-351.
67. Song C, Halbreich U, Han C, Leonard BE, Luo H (2009) Imbalance between pro- and anti-inflammatory cytokines, and between Th1 and Th2 cytokines in depressed patients: the effect of electroacupuncture or fluoxetine treatment. Pharmacopsychiatry 42: 182-188.
68. Wang K, Wu HX, Wang GN, Li MM, Zhang ZD, Gu G (2009) The effects of electroacupuncture on Th1/Th2 cytokine mRNA expression and mitogen-activated protein kinase signaling pathways in the splenic T cells of traumatized rats. Anesth Analg 109: 1666-1673.
69. Carneiro ER, Xavier RA, De Castro MA, Do Nascimento CM, Silveira VL (2010) Electroacupuncture promotes a decrease in inflammatory response associated with Th1/Th2 cytokines, nitric oxide and leukotriene B4 modulation in experimental asthma. Cytokine 50: 335-340.
70. Gui J, Xiong F, Li J, Huang G (2012) Effects of acupuncture on Th1, th2 cytokines in rats of implantation failure. Evid Based Complement Alternat Med 2012: 893023.
71. Molsberger AF, Schneider T, Gotthardt H, Drabik A (2010) German Randomized Acupuncture Trial for chronic shoulder pain (GRASP) - a pragmatic, controlled, patient-blinded, multi-centre trial in an outpatient care environment. Pain 151: 146-154.

72. Witt C, Brinkhaus B, Jena S, Linde K, Streng A, Wagenpfeil S, Hummelsberger J, Walther HU, Melchart D, Willich SN (2005) Acupuncture in patients with osteoarthritis of the knee: a randomised trial. Lancet 366: 136-143.
73. Brinkhaus B, Witt CM, Jena S, Linde K, Streng A, Wagenpfeil S, Irnich D, Walther HU, Melchart D, Willich SN (2006) Acupuncture in patients with chronic low back pain: a randomized controlled trial. Arch Intern Med 166: 450-457.
74. Dincer F, Linde K (2003) Sham interventions in randomized clinical trials of acupuncture - a review. Complement Ther Med 11: 235-242.
75. Hutchinson AJ, Ball S, Andrews JC, Jones GG (2012) The effectiveness of acupuncture in treating chronic non-specific low back pain: a systematic review of the literature. J Orthop Surg Res 7: 36-49.
76. Rossberg E, Larsson PG, Birkeflet O, Soholt LE, Stavem K (2005) Comparison of traditional Chinese acupuncture, minimal acupuncture at non-acupoints and conventional treatment for chronic sinusitis. Complement Ther Med 13: 4-10.
77. Bender T, Geher P, Balint G (2001) Minimal acupuncture may not always minimize specific effects of needling. Clin J Pain 17: 278-278.
78. Lund I, Naslund J, Lundeberg T (2009) Minimal acupuncture is not a valid placebo control in randomised controlled trials of acupuncture: a physiologist's perspective. Chin Med 4: 1-8.
79. Lundeberg T, Lund I, Sing A, Naslund J (2011) Is placebo acupuncture what it is intended to be? Evid Based Complement Alternat Med 2011: 1-5.
80. Streitberger K, Kleinhenz J (1998) Introducing a placebo needle into acupuncture research. Lancet 352: 364-365.
81. Yamashita H, Tsukayama H (2001) Minimal acupuncture may not always minimize specific effects of needling. Clin J Pain 17: 277-277.
82. Kong J, Fufa DT, Gerber AJ, Rosman AS, Vangel MG, Gracely RH, Gollub RL (2005) Psychophysical outcomes from a randomized pilot study of manual, electro, and sham acupuncture treatment on experimentally induced thermal pain. J Pain 6: 55-64.
83. Kong J, Kaptchuk TJ, Polich G, Kirsch I, Vangel M, Zyloney C, Rosen B, Gollub RL (2009) An fMRI study on the interaction and dissociation between expectation of pain relief and acupuncture treatment. Neuroimage 47: 1066-1076.
84. Shi GX, Yang XM, Liu CZ, Wang LP (2012) Factors contributing to therapeutic effects evaluated in acupuncture clinical trials. Trials 13: 42-46.
85. Harris RE, Zubieta JK, Scott DJ, Napadow V, Gracely RH, Clauw DJ (2009) Traditional Chinese acupuncture and placebo (sham) acupuncture are

differentiated by their effects on mu-opioid receptors (MORs). Neuroimage 47: 1077-1085.

86. Frucht DM, Fukao T, Bogdan C, Schindler H, O'Shea JJ, Koyasu S (2001) IFN-gamma production by antigen-presenting cells: mechanisms emerge. Trends Immunol 22: 556-560.
87. Yoshimoto T, Takeda K, Tanaka T, Ohkusu K, Kashiwamura S, Okamura H, Akira S, Nakanishi K (1998) IL-12 up-regulates IL-18 receptor expression on T cells, Th1 cells, and B cells: synergism with IL-18 for IFN-gamma production. J Immunol 161: 3400-3407.
88. Flaishon L, Lantner F, Hershkoviz R, Levo Y, Shachar I (2001) Low levels of IFN-gamma down-regulate the integrin-dependent adhesion of B cells by activating a pathway that interferes with cytoskeleton rearrangement. J Biol Chem 276: 46701-46706.
89. Isaacs A, Lindenmann J, Valentine RC (1957) Virus interference. II. Some properties of interferon. Proc R Soc Lond B Biol Sci 147: 268-273.
90. Müller U, Steinhoff U, Reis LF, Hemmi S, Pavlovic J, Zinkernagel RM, Aguet M (1994) Functional role of type I and type II interferons in antiviral defense. Science 264: 1918-1921.
91. Biron CA (2001) Interferons alpha and beta as immune regulators - A new look. Immunity 14: 661-664.
92. Schroder K, Hertzog PJ, Ravasi T, Hume DA (2004) Interferon-gamma: an overview of signals, mechanisms and functions. J Leukoc Biol 75: 163-189.
93. Zlotnik A, Yoshie O (2000) Chemokines: a new classification system and their role in immunity. Immunity 12: 121-127.
94. Murphy PM, Baggiolini M, Charo IF, Hebert CA, Horuk R, Matsushima K, Miller LH, Oppenheim JJ, Power CA (2000) International union of pharmacology. XXII. Nomenclature for chemokine receptors. Pharmacol Rev 52: 145-176.
95. Murphy PM (2002) International Union of Pharmacology. XXX. Update on chemokine receptor nomenclature. Pharmacol Rev 54: 227-229.
96. Luster AD, Unkeless JC, Ravetch JV (1985) Gamma-interferon transcriptionally regulates an early-response gene containing homology to platelet proteins. Nature 315: 672-676.
97. Lasagni L, Francalanci M, Annunziato F, Lazzeri E, Giannini S, Cosmi L, Sagrinati C, Mazzinghi B, Orlando C, Maggi E, Marra F, Romagnani S, Serio M, Romagnani P (2003) An alternatively spliced variant of CXCR3 mediates the inhibition of endothelial cell growth induced by IP-10, Mig, and I-TAC, and acts as functional receptor for platelet factor 4. J Exp Med 197: 1537-1549.

98. Shields PL, Morland CM, Salmon M, Qin S, Hubscher SG, Adams DH (1999) Chemokine and chemokine receptor interactions provide a mechanism for selective T cell recruitment to specific liver compartments within hepatitis C-infected liver. J Immunol 163: 6236-6243.
99. Moser B, Loetscher P (2001) Lymphocyte traffic control by chemokines. Nat Immunol 2: 123-128.
100. Christensen JE, de Lemos C, Moos T, Christensen JP, Thomsen AR (2006) CXCL10 is the key ligand for CXCR3 on CD8(+) effector T cells involved in immune surveillance of the lymphocytic choriomeningitis virus-infected central nervous system. J Immunol 176: 4235-4243.
101. Kohler RE, Comerford I, Townley S, Haylock-Jacobs S, Clark-Lewis I, McColl SR (2008) Antagonism of the chemokine receptors CXCR3 and CXCR4 reduces the pathology of experimental autoimmune encephalomyelitis. Brain Pathol 18: 504-516.
102. Luster AD, Ravetch JV (1987) Biochemical characterization of a gamma interferon-inducible cytokine (IP-10). J Exp Med 166: 1084-1097.
103. Vanguri P, Farber JM (1990) Identification of CRG-2. An interferon-inducible mRNA predicted to encode a murine monokine. J Biol Chem 265: 15049-15057.
104. Ohmori Y, Hamilton TA (1990) A macrophage LPS-inducible early gene encodes the murine homologue of IP-10. Biochem Biophys Res Commun 168: 1261-1267.
105. Tighe RM, Liang JR, Liu NS, Jung Y, Jiang DH, Gunn MD, Noble PW (2011) Recruited exudative macrophages selectively produce CXCL10 following noninfectious lung injury. Am J Respir Cell Mol Biol 45: 781-788.
106. Matikainen S, Pirhonen J, Miettinen M, Lehtonen A, Govenius-Vintola C, Sareneva T, Julkunen I (2000) Influenza A and sendai viruses induce differential chemokine gene expression and transcription factor activation in human macrophages. Virology 276: 138-147.
107. Dufour JH, Dziejman M, Liu MT, Leung JH, Lane TE, Luster AD (2002) IFN-gamma-inducible protein 10 (IP-10; CXCL10)-deficient mice reveal a role for IP-10 in effector T cell generation and trafficking. J Immunol 168: 3195-3204.
108. Jiang D, Liang J, Hodge J, Lu B, Zhu Z, Yu S, Fan J, Gao Y, Yin Z, Homer R, Gerard C, Noble PW (2004) Regulation of pulmonary fibrosis by chemokine receptor CXCR3. J Clin Invest 114: 291-299.

109. Ruhwald M, Aabye MG, Ravn P (2012) IP-10 release assays in the diagnosis of tuberculosis infection: current status and future directions. Expert Rev Mol Diagn 12: 175-187.
110. Abbadie C, Bhangoo S, De Koninck Y, Malcangio M, Melik-Parsadaniantz S, White FA (2009) Chemokines and pain mechanisms. Brain Res Rev 60: 125-134.
111. Thomas MS, Kunkel SL, Lukacs NW (2002) Differential role of IFN-gamma-inducible protein 10 kDa in a cockroach antigen-induced model of allergic airway hyperreactivity: systemic versus local effects. J Immunol 169: 7045-7053.
112. Müller M, Carter SL, Hofer MJ, Manders P, Getts DR, Getts MT, Dreykluft A, Lu B, Gerard C, King NJ, Campbell IL (2007) CXCR3 signaling reduces the severity of experimental autoimmune encephalomyelitis by controlling the parenchymal distribution of effector and regulatory T cells in the central nervous system. J Immunol 179: 2774-2786.
113. King VL, Lin AY, Kristo F, Anderson TJ, Ahluwalia N, Hardy GJ, Owens AP 3rd, Howatt DA, Shen D, Tager AM, Luster AD, Daugherty A, Gerszten RE (2009) Interferon-gamma and the interferon-inducible chemokine CXCL10 protect against aneurysm formation and rupture. Circulation 119: 426-435.
114. Liu L, Callahan MK, Huang D, Ransohoff RM (2005) Chemokine receptor CXCR3: an unexpected enigma. Curr Top Dev Biol 68: 149-181.
115. Hua S, Cabot PJ (2010) Mechanisms of peripheral immune-cell-mediated analgesia in inflammation: clinical and therapeutic implications. Trends Pharmacol Sci 31: 427-433.
116. Akimoto N, Honda K, Uta D, Beppu K, Ushijima Y, Matsuzaki Y, Nakashima S, Kido MA, Imoto K, Takano Y, Noda M (2013) CCL-1 in the spinal cord contributes to neuropathic pain induced by nerve injury. Cell Death Dis 4: e679.
117. Miller RE, Tran PB, Das R, Ghoreishi-Haack N, Ren D, Miller RJ, Malfait AM (2012) CCR2 chemokine receptor signaling mediates pain in experimental osteoarthritis. Proc Natl Acad Sci U S A 109: 20602-20607.
118. Rittner HL, Mousa SA, Labuz D, Beschmann K, Schäfer M, Stein C, Brack A (2006) Selective local PMN recruitment by CXCL1 or CXCL2/3 injection does not cause inflammatory pain. J Leukoc Biol 79: 1022-1032.
119. Moser B, Wolf M, Walz A, Loetscher P (2004) Chemokines: multiple levels of leukocyte migration control. Trends Immunol 25: 75-84.
120. Moser B, Willimann K (2004) Chemokines: role in inflammation and immune surveillance. Ann Rheum Dis 63 Suppl 2: ii84-ii89.

121. RS Sauer, D Hackel, L. Morshel, H. Helbach, Y. Wang, S. A. Mousa, N. Roewer, A. Brack, H. L. Rittner (2014) Toll like receptor (TLR)-4 as a regulator of peripheral endogenous opioid-mediated analgesia in inflammation. Mol Pain 10: doi:10.1186/1744-8069-10-10

Curriculum vitae

Personal details

First and last name	Ying Wang
E-Mail	y.w.acu16@gmail.com

Educations

09. 2010 - (Ph.D.)	Department of Anesthesiology, University Hospital of Würzburg, Würzburg, Germany (Thesis: Immune and peripheral endogenous opioid mechanisms of electroacupuncture analgesia)
09. 2007 - 07. 2010 (Master)	Acupuncture and Moxibustion College, Beijing University of Chinese Medicine, Peking, China (Thesis: Experimental and clinical research of Balance Acupuncture for pain relief on LDH (lumbar disc herniation) rats and SP (scapulohumeral periarthritis) rabbits)
09. 2001 - 07. 2006 (Bachelor) (American MD equivalent)	Department of Acupuncture, Moxibustion and Tuina, Xinjiang Medical University, China (Thesis: Review on clinical acupuncture-related treatment for frozen shoulder)

Practical experiences

12. 2013 - 1. 2014	Assistant Anesthesiologist, Xijing Hospital, China
08. 2008 - 10. 2008	Physical therapist, Clinic of Olympic Village, Beijing 2008 Olympic Games
07. 2005 - 08. 2007	Acupuncturist, Affiliated Hospital of Shaanxi College of Traditional Chinese Medicine, China

Skills

Experimental skills	ELISA, FACS, immune staining, Western Blot, RT-PCR, MACS, cell culture, pain measurements (Thermal and mechanical behavioral test)
Language level	Excellent writing and speaking in English
Computer skills	Microsoft Office, Photoshop, EndNote, Statistical software (SAS, SPSS, Sigma plot), Experimental software (NIH Image J, CellQuest, Tecan)
Medical identities	Licensed TCM Practitioner (China); Approved candidate of Diplomate in Acupuncture (NCCAOM®) (America)

Research projects attendance

2007 - 2010	Balance acupuncture in treating frozen shoulder and Lumbar Disc Herniation (LDH)
2010 - 2011	Resolvin D1 and chemerin attenuate inflammatory pain through peripheral opioid action
2011 - 2013	Peripheral analgesic mechanism of electroacupuncture

International/National congresses/meetings attendance

10. 2013	8th EFIC® Pain in Europe Congress" (Florence, Italy) (Poster presentation: "CXCL10 mediates peripheral acupuncture analgesia via opioid peptide-containing macrophages")
10. 2012	7th International Symposium organized by GSLS, University of Würzburg (Poster presentation: "Peripheral mechanism of electroacupuncture in relieving inflammatory pain")
10. 2011	6th International Symposium organized by GSLS, University of Würzburg (Poster presentation: "Resolvin D1 and chemerin attenuate inflammatory pain through peripheral opioid action")

2009 and 2010	Annual National Congress of national key projects (Peking, China)

Reviewer experiences

1. 2014	Reviewer for <Journal of Acupuncture and Meridian Studies> (peer-reviewed Journal, Elsevier)
6. 2013 - 8. 2013	Reviewer for <Life Sciences> (peer-reviewed Journal, Elsevier) (Twice)

Würzburg, 12-3-2014

(Ying Wang)

Publications

2014 **Y. Wang**, R. Gehringer, S. A. Mousa, D. Hackel, A. Brack, H. L. Rittner. CXCL10 controls inflammatory pain via opioid peptide-containing macrophages in acupuncture. PLoS ONE. 2014 (Shared corresponding author with H. Rittner) (Accepted)

2014 RS Sauer, D. Hackel, L. Morshel, H. Helbach, **Y. Wang**, S. A. Mousa, N. Roewer, A. Brack, H. L. Rittner. Toll like receptor (TLR)-4 as a regulator of peripheral endogenous opioid-mediated analgesia in inflammation. Molecular Pain 2014 10:10 doi:10.1186/1744-8069-10-10

2013 **Y. Wang**, D. Hackel, F. Peng, H. Rittner. Long-term antinociception by electroacupuncture is mediated via peripheral opioid receptors in free-moving rats with inflammatory hyperalgesia. European Journal of Pain 2013 17: 1447-1457. (Shared corresponding author with H. Rittner)

2010 Wang JS, Wei WT, **Wang Y**. History review and summary of periarthritis of shoulder treated by Balance Acupuncture in clinic. Zhong Hua Zhong Yi Yao Za Zhi (= Chinese Medicine) 2010 25:1451-1455. (Article in Chinese) (corresponding author)

2010 Yuan H, Chen R, Huang DP, **Wang Y**, Wang WY. Analgesic and anti-inflammatory effects of balance acupuncture on experimental scapulohumeral periarthritis in rabbits. Zhongguo Zhen Jiu (= Chinese Acupuncture) 2011 31: 1106-1110. (Article in Chinese) (PMID: 22256649)

2009 **Wang Y**, Yuan H, Danni X. Balance Acupuncture: An Experimental Study on the Effectiveness of Treating Radicular Pain in a Lumbar Disc Herniation Rat Model. Deutsche Zeitschrift für Akupunktur (= German Journal of Acupuncture) 2009 52: 18-32 (corresponding author)

Abstract

Y. Wang, R. Gehringer, S. A. Mousa, D. Hackel, A. Brack, H. L. Rittner. 8th EFIC® Pain in Europe Congress", Florence, 2013. CXCL10 mediates peripheral acupuncture analgesia via opioid peptide-containing macrophages.

Appendix

Units

°C	degrees Celsius
cm	centimeter
g	gram
h	hour
M	molar
µg	microgram
µl	microliter
µm	micrometer
mA	milliampere
min	minute
mg	milligram
ml	milliliter
mm	millimetre
mM	millimolar
ng	nanogram
nm	nanometer
pg	picogram
rpm	rotations per minute
s	second
V	volt

Copyright Licenses

Of

2013 **Y. Wang**, D. Hackel, F. Peng, H. Rittner. Long-term antinociception by electroacupuncture is mediated via peripheral opioid receptors in free-moving rats with inflammatory hyperalgesia. Eur J Pain. 2013 17: 1447-1457. (Shared corresponding author with H. Rittner)

(Author contributions: Y. Wang performed the experiments; Y. Wang, D. Hackel, H. Rittner designed the experiments; Y. Wang, F. Peng designed 3D rat model; Y. Wang drafted the manuscript, H. Rittner revised the manuscript, Y. Wang cooperated with the revision)

2014 **Y. Wang**, R. Gehringer, S. A. Mousa, D. Hackel, A. Brack, H. L. Rittner. CXCL10 controls inflammatory pain via opioid peptide-containing macrophages in acupuncture. PLoS ONE. 2014 (Shared corresponding author with H. Rittner) (Accepted)

(Author contributions: Y. Wang, R. Gehringer, S. A. Mousa performed experiments; Y. Wang, D. Hackel, H. Rittner designed the experiments; Y. Wang drafted the manuscript, H. Rittner and A. Brack revised the manuscript, Y. Wang cooperated with the revision)

JOHN WILEY AND SONS LICENSE TERMS AND CONDITIONS

Feb 26, 2014

This is a License Agreement between Ying Wang ("You") and John Wiley and Sons ("John Wiley and Sons") provided by Copyright Clearance Center ("CCC"). The license consists of your order details, the terms and conditions provided by John Wiley and Sons, and the payment terms and conditions.

All payments must be made in full to CCC. For payment instructions, please see information listed at the bottom of this form.

License Number	3336761168859
License date	Feb 26, 2014
Licensed content publisher	John Wiley and Sons
Licensed content publication	European Journal of Pain
Licensed content title	Long-term antinociception by electroacupuncture is mediated via peripheral opioid receptors in free-moving rats with inflammatory hyperalgesia
Licensed copyright line	© 2013 European Federation of International Association for the Study of Pain Chapters
Licensed content author	Y. Wang,D. Hackel,F. Peng,H. L. Rittner
Licensed content date	May 6, 2013
Start page	1447
End page	1457
Type of use	Dissertation/Thesis
Requestor type	Author of this Wiley article
Format	Print and electronic
Portion	Full article
Will you be translating?	No
Title of your thesis / dissertation	Immune and peripheral endogenous opioid mechanisms of electroacupuncture analgesia
Expected completion date	Mar 2014
Expected size (number of pages)	120
Total	0.00 USD
Terms and Conditions	

TERMS AND CONDITIONS

This copyrighted material is owned by or exclusively licensed to John Wiley & Sons, Inc. or one of its group companies (each a "Wiley Company") or a society for whom a Wiley Company has exclusive publishing rights in relation to a particular journal (collectively "WILEY"). By clicking "accept" in connection with completing this licensing transaction, you

agree that the following terms and conditions apply to this transaction (along with the billing and payment terms and conditions established by the Copyright Clearance Center Inc., ("CCC's Billing and Payment terms and conditions"), at the time that you opened your RightsLink account (these are available at any time at http://myaccount.copyright.com).

Terms and Conditions

1. The materials you have requested permission to reproduce (the "Materials") are protected by copyright.

2.You are hereby granted a personal, non-exclusive, non-sublicensable, non-transferable, worldwide, limited license to reproduce the Materials for the purpose specified in the licensing process. This license is for a one-time use only with a maximum distribution equal to the number that you identified in the licensing process. Any form of republication granted by this license must be completed within two years of the date of the grant of this license (although copies prepared before may be distributed thereafter). The Materials shall not be used in any other manner or for any other purpose. Permission is granted subject to an appropriate acknowledgement given to the author, title of the material/book/journal and the publisher. You shall also duplicate the copyright notice that appears in the Wiley publication in your use of the Material. Permission is also granted on the understanding that nowhere in the text is a previously published source acknowledged for all or part of this Material. Any third party material is expressly excluded from this permission.

3. With respect to the Materials, all rights are reserved. Except as expressly granted by the terms of the license, no part of the Materials may be copied, modified, adapted (except for minor reformatting required by the new Publication), translated, reproduced, transferred or distributed, in any form or by any means, and no derivative works may be made based on the Materials without the prior permission of the respective copyright owner. You may not alter, remove or suppress in any manner any copyright, trademark or other notices displayed by the Materials. You may not license, rent, sell, loan, lease, pledge, offer as security, transfer or assign the Materials, or any of the rights granted to you hereunder to any other person.

4. The Materials and all of the intellectual property rights therein shall at all times remain the exclusive property of John Wiley & Sons Inc or one of its related companies (WILEY) or their respective licensors, and your interest therein is only that of having possession of and the right to reproduce the Materials pursuant to Section 2 herein during the continuance of this Agreement. You agree that you own no right, title or interest in or to the Materials or any of the intellectual property rights therein. You shall have no rights hereunder other than the license as provided for above in Section 2. No right, license or interest to any trademark, trade name, service mark or other branding ("Marks") of WILEY or its licensors is granted hereunder, and you agree that you shall not assert any such right, license or interest with respect thereto.

5. NEITHER WILEY NOR ITS LICENSORS MAKES ANY WARRANTY OR REPRESENTATION OF

ANY KIND TO YOU OR ANY THIRD PARTY, EXPRESS, IMPLIED OR STATUTORY, WITH RESPECT TO THE MATERIALS OR THE ACCURACY OF ANY INFORMATION CONTAINED IN THE MATERIALS, INCLUDING, WITHOUT LIMITATION, ANY IMPLIED WARRANTY OF MERCHANTABILITY, ACCURACY, SATISFACTORY QUALITY, FITNESS FOR A PARTICULAR PURPOSE, USABILITY, INTEGRATION OR NON-INFRINGEMENT AND ALL SUCH WARRANTIES ARE HEREBY EXCLUDED BY WILEY AND ITS LICENSORS AND WAIVED BY YOU.

6. WILEY shall have the right to terminate this Agreement immediately upon breach of this Agreement by you.

7. You shall indemnify, defend and hold harmless WILEY, its Licensors and their respective directors, officers, agents and employees, from and against any actual or threatened claims, demands, causes of action or proceedings arising from any breach of this Agreement by you.

8. IN NO EVENT SHALL WILEY OR ITS LICENSORS BE LIABLE TO YOU OR ANY OTHER PARTY OR ANY OTHER PERSON OR ENTITY FOR ANY SPECIAL, CONSEQUENTIAL, INCIDENTAL, INDIRECT, EXEMPLARY OR PUNITIVE DAMAGES, HOWEVER CAUSED, ARISING OUT OF OR IN CONNECTION WITH THE DOWNLOADING, PROVISIONING, VIEWING OR USE OF THE MATERIALS REGARDLESS OF THE FORM OF ACTION, WHETHER FOR BREACH OF CONTRACT, BREACH OF WARRANTY, TORT, NEGLIGENCE, INFRINGEMENT OR OTHERWISE (INCLUDING, WITHOUT LIMITATION, DAMAGES BASED ON LOSS OF PROFITS, DATA, FILES, USE, BUSINESS OPPORTUNITY OR CLAIMS OF THIRD PARTIES), AND WHETHER OR NOT THE PARTY HAS BEEN ADVISED OF THE POSSIBILITY OF SUCH DAMAGES. THIS LIMITATION SHALL APPLY NOTWITHSTANDING ANY FAILURE OF ESSENTIAL PURPOSE OF ANY LIMITED REMEDY PROVIDED HEREIN.

9. Should any provision of this Agreement be held by a court of competent jurisdiction to be illegal, invalid, or unenforceable, that provision shall be deemed amended to achieve as nearly as possible the same economic effect as the original provision, and the legality, validity and enforceability of the remaining provisions of this Agreement shall not be affected or impaired thereby.

10. The failure of either party to enforce any term or condition of this Agreement shall not constitute a waiver of either party's right to enforce each and every term and condition of this Agreement. No breach under this agreement shall be deemed waived or excused by either party unless such waiver or consent is in writing signed by the party granting such waiver or consent. The waiver by or consent of a party to a breach of any provision of this Agreement shall not operate or be construed as a waiver of or consent to any other or subsequent breach by such other party.

11. This Agreement may not be assigned (including by operation of law or otherwise) by you without WILEY's prior written consent.

12. Any fee required for this permission shall be non-refundable after thirty (30) days from receipt

13. These terms and conditions together with CCC's Billing and Payment terms and conditions (which are incorporated herein) form the entire agreement between you and WILEY concerning this licensing transaction and (in the absence of fraud) supersedes all prior agreements and representations of the parties, oral or written. This Agreement may not be

amended except in writing signed by both parties. This Agreement shall be binding upon and inure to the benefit of the parties' successors, legal representatives, and authorized assigns.

14. In the event of any conflict between your obligations established by these terms and conditions and those established by CCC's Billing and Payment terms and conditions, these terms and conditions shall prevail.

15. WILEY expressly reserves all rights not specifically granted in the combination of (i) the license details provided by you and accepted in the course of this licensing transaction, (ii) these terms and conditions and (iii) CCC's Billing and Payment terms and conditions.

16. This Agreement will be void if the Type of Use, Format, Circulation, or Requestor Type was misrepresented during the licensing process.

17. This Agreement shall be governed by and construed in accordance with the laws of the State of New York, USA, without regards to such state's conflict of law rules. Any legal action, suit or proceeding arising out of or relating to these Terms and Conditions or the breach thereof shall be instituted in a court of competent jurisdiction in New York County in the State of New York in the United States of America and each party hereby consents and submits to the personal jurisdiction of such court, waives any objection to venue in such court and consents to service of process by registered or certified mail, return receipt requested, at the last known address of such party.

Wiley Open Access Terms and Conditions

Wiley publishes Open Access articles in both its Wiley Open Access Journals program [http://www.wileyopenaccess.com/view/index.html] and as Online Open articles in its subscription journals. The majority of Wiley Open Access Journals have adopted the Creative Commons Attribution License (CC BY) which permits the unrestricted use, distribution, reproduction, adaptation and commercial exploitation of the article in any medium. No permission is required to use the article in this way provided that the article is properly cited and other license terms are observed. A small number of Wiley Open Access journals have retained the Creative Commons Attribution Non Commercial License (CC BY-NC), which permits use, distribution and reproduction in any medium, provided the original work is properly cited and is not used for commercial purposes.

Online Open articles - Authors selecting Online Open are, unless particular exceptions apply, offered a choice of Creative Commons licenses. They may therefore select from the CC BY, the CC BY-NC and the Attribution-NoDerivatives (CC BY-NC-ND). The CC BY-NC-ND is more restrictive than the CC BY-NC as it does not permit adaptations or modifications without rights holder consent.

Wiley Open Access articles are protected by copyright and are posted to repositories and websites in accordance with the terms of the applicable Creative Commons license referenced on the article. At the time of deposit, Wiley Open Access articles include all changes made during peer review, copyediting, and publishing. Repositories and websites that host the article are responsible for incorporating any publisher-supplied

amendments or retractions issued subsequently.
Wiley Open Access articles are also available without charge on Wiley's publishing platform, Wiley Online Library or any successor sites.

Conditions applicable to all Wiley Open Access articles:

- The authors' moral rights must not be compromised. These rights include the right of "paternity" (also known as "attribution" - the right for the author to be identified as such) and "integrity" (the right for the author not to have the work altered in such a way that the author's reputation or integrity may be damaged).

- Where content in the article is identified as belonging to a third party, it is the obligation of the user to ensure that any reuse complies with the copyright policies of the owner of that content.

- If article content is copied, downloaded or otherwise reused for research and other purposes as permitted, a link to the appropriate bibliographic citation (authors, journal, article title, volume, issue, page numbers, DOI and the link to the definitive published version on Wiley Online Library) should be maintained. Copyright notices and disclaimers must not be deleted.
    - Creative Commons licenses are copyright licenses and do not confer any other rights, including but not limited to trademark or patent rights.

- Any translations, for which a prior translation agreement with Wiley has not been agreed, must prominently display the statement: "This is an unofficial translation of an article that appeared in a Wiley publication. The publisher has not endorsed this translation."

Conditions applicable to non-commercial licenses (CC BY-NC and CC BY-NC-ND)

For non-commercial and non-promotional purposes individual non-commercial users may access, download, copy, display and redistribute to colleagues Wiley Open Access articles. In addition, articles adopting the CC BY-NC may be adapted, translated, and text- and data-mined subject to the conditions above.

Use by commercial "for-profit" organizations

Use of non-commercial Wiley Open Access articles for commercial, promotional, or marketing purposes requires further explicit permission from Wiley and will be subject to a fee. Commercial purposes include:

- Copying or downloading of articles, or linking to such articles for further redistribution, sale or licensing;

- Copying, downloading or posting by a site or service that incorporates advertising with such content;

- The inclusion or incorporation of article content in other works or services (other than normal quotations with an appropriate citation) that is then available for sale or licensing, for a fee (for example, a compilation produced for marketing purposes, inclusion in a sales pack)

- Use of article content (other than normal quotations with appropriate citation) by for-profit organizations for promotional purposes

- Linking to article content in e-mails redistributed for promotional, marketing or educational purposes;

- Use for the purposes of monetary reward by means of sale, resale, license, loan, transfer or other form of commercial exploitation such as marketing products

- Print reprints of Wiley Open Access articles can be purchased from: corporatesales@wiley.com

The modification or adaptation for any purpose of an article referencing the CC BY-NC-ND License requires consent which can be requested from RightsLink@wiley.com .

Other Terms and Conditions:

BY CLICKING ON THE "I AGREE..." BOX, YOU ACKNOWLEDGE THAT YOU HAVE READ AND FULLY UNDERSTAND EACH OF THE SECTIONS OF AND PROVISIONS SET FORTH IN THIS AGREEMENT AND THAT YOU ARE IN AGREEMENT WITH AND ARE WILLING TO ACCEPT ALL OF YOUR OBLIGATIONS AS SET FORTH IN THIS AGREEMENT.

v1.8

If you would like to pay for this license now, please remit this license along with your payment made payable to "COPYRIGHT CLEARANCE CENTER" otherwise you will be invoiced within 48 hours of the license date. Payment should be in the form of a check or money order referencing your account number and this invoice number RLNK501236957. Once you receive your invoice for this order, you may pay your invoice by credit card. Please follow instructions provided at that time.

Make Payment To:
Copyright Clearance Center
Dept 001
P.O. Box 843006
Boston, MA 02284-3006

For suggestions or comments regarding this order, contact RightsLink Customer Support: customercare@copyright.com or +1-877-622-5543 (toll free in the US) or +1-978-646-2777.

Gratis licenses (referencing $0 in the Total field) are free. Please retain this printable license for your reference. No payment is required.